JAIST Repository
https://dspace.jaist.ac.jp/

Title	微量の反応性官能基を有するポリプロピレンの複合材料への応用
Author(s)	Kurahashi, Eiji
Citation	
Issue Date	2020-03-25
Type	Thesis or Dissertation
Text version	ETD
URL	http://hdl.handle.net/10119/16664
Rights	
Description	Supervisor:谷池　俊明，先端科学技術研究科，博士

JAIST
JAPAN
ADVANCED INSTITUTE OF
SCIENCE AND TECHNOLOGY

Japan Advanced Institute of Science and Technology

Application of Functionalized Polypropylene with a Trace Amount of Reactive Functional Groups for Composite Materials

EIJI KURAHASHI

Japan Advanced Institute of Science and Technology

Doctoral Dissertation

Application of Functionalized Polypropylene with a Trace Amount of Reactive Functional Groups for Composite Materials

Eiji Kurahashi

Supervisor: Dr. Toshiaki Taniike

Graduate School of Advanced Science and Technology

Japan Advanced Institute of Science and Technology

[Materials Science]

March 2020

Referee-in-chief: **Associate Professor Dr. Toshiaki Taniike**
Japan Advanced Institute of Science and Technology

Referees: **Associate Professor Dr. Kazuaki Matsumura**
Japan Advanced Institute of Science and Technology

Associate Professor Dr. Eijiro Miyako
Japan Advanced Institute of Science and Technology

Associate Professor Dr. Ken-ichi Shinohara
Japan Advanced Institute of Science and Technology

Group Leader Dr. Junji Mizukado
National Institute of Advanced Industrial Science and Technology

Preface

The present dissertation is the result of studies under the direction of Associate Professor Dr. Toshiaki Taniike during FY2017-FY2019. The purpose of this dissertation is to investigate the synthesis of functionalized polypropylene with a trace amount of reactive functional groups and its application for composite materials.

The first chapter shows a general introduction based on the purpose of this dissertation. Chapter 2 describes the synthesis of polypropylene functionalized with a trace amount of silicon alkoxy groups based on copolymerization using a Ziegler-Natta catalyst. Chapter 3 describes the utilization of polypropylene functionalized with a trace amount of silicon trimethoxy groups in graft-type nanocomposites. Chapter 4 describes the design of graft-type PP/elastomer/SiO_2 ternary nanocomposites for balanced toughness and stiffness. The last chapter concludes this dissertation.

Eiji Kurahashi

Taniike Laboratory,

Graduate School of Advanced Science and Technology,

Japan Advanced Institute of Science and Technology

March 2020

Contents

Chapter 1

General Introduction

1.1. Polypropylene

380 million tons of plastics are now produced worldwide over the year [1]. Plastics are classified from commodity plastics to super engineering plastics according to their heat resistance, and various types of polymers are industrially synthesized and used for various applications. Polypropylene (PP) is the second most produced plastic, and its advantages are found in a good balance between mechanical properties and processability, excellent chemical resistance, lightest among the commodity plastics, etc. The ability to produce PP with a wide range of melt flowability enables various molding processes, while the consumption by injection molding is the largest among them (Fig. 1). The examples of injection-molded products include automobile parts such as bumpers and instrument panels. PP and its composites are used in a large number of interior and exterior parts. The use of PP in automobile parts reduces the total weight of the car and contributes to the environment and users. About 50% of plastics used in automobiles correspond to PP.

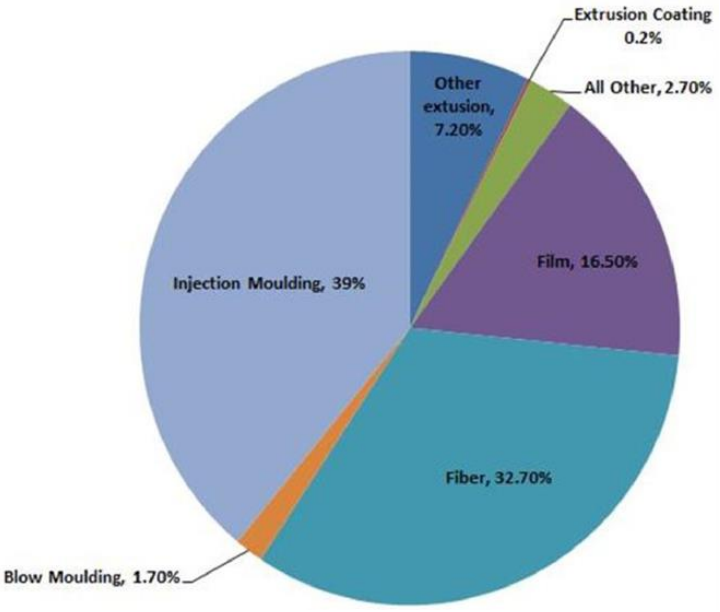

Fig. 1. Global consumption of polypropylene by end use application [2]

1.1.1. Structure of Polypropylene

PP, a crystalline polymer, has a characteristic hierarchical structure: skin-core structure, spherulites, lamellae, and crystals, in decreasing order of size. The crystals are mainly dominated by molecular chain tacticity. These morphologies greatly affect the physical properties of the final product, therefore, each of these morphologies is described in this section.

1.1.1.1. Tacticity

PP is classified into three types based on the relative configuration of adjacent chiral center. A stereostructure in which all adjacent tertiary carbons have the same chirality is called isotactic, an alternating case syndiotactic, and a random case atactic (Fig. 2). Such stereoregularity is called tacticity. Generally, PP used in industry is isotactic PP, and the isotactic PP with higher tacticity expresses higher crystallinity, melting point, and elastic modulus [3]. The term “stereoblock” refers to an alternating structure in which a high isotactic sequence is partially replaced by an incomplete isotactic or syndiotactic sequence, and the presence of the defects into isotactic PP inhibits crystallization. Syndiotactic PP is also a crystalline polymer that is tougher than isotactic PP, whereas atactic PP does not form crystals.

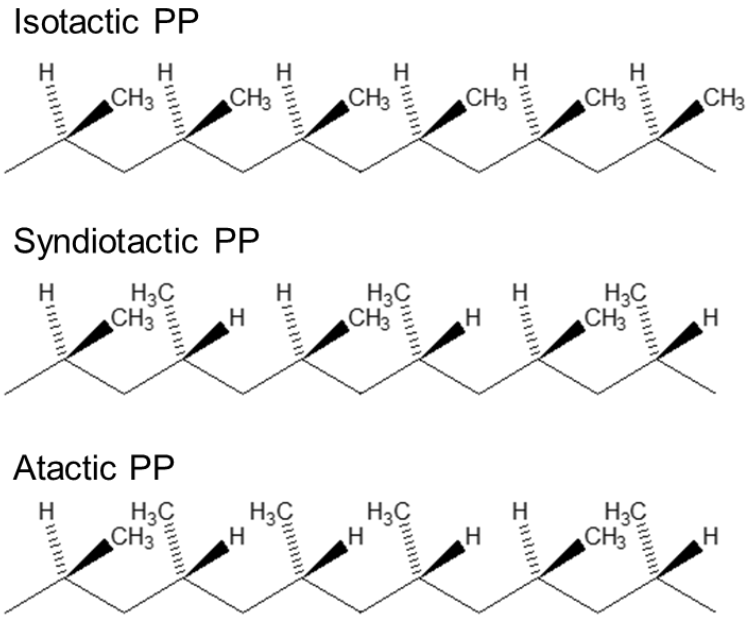

Fig. 2. Stereo configuration of polypropylene.

1.1.1.2. Crystalline Structure

PP crystals are formed by regularly arranging molecular chains with high tacticity. Although both isotactic and syndiotactic PP have crystal structures, this section describes about isotactic PP as an example. It is known that the crystals of an isotactic PP form a crystal structure of α-, β-, and γ-form and mesophase on the basis of 3_1 helix structure that constitutes one pitch of a helix with three monomers. Among them, only α- and β-form are widely observed, while γ-form is observed only under specific processing conditions or material modifications. The most common crystal structure is a monoclinic α-form, which is composed of 6.6 × 20.8 × 6.5 Å unit cells. The β-form, which is a trigonal lattice, is observed under specific processing conditions such as temperature gradients [4] and shear stress field [5] or using a specific nucleating agents [6]. Although it has lower

tensile strength than α-form PP, it exhibits higher impact strength and toughness. Mesophase is an intermediate ordered state between crystal and amorphous, and is often observed in processes under rapid cooling conditions.

1.1.1.3. Lamella

When PP is cooled, the polymer chains (including crystals) form a regular folded structure. The lamella thickness is related to the melting point as shown in the following equation,

$$T_{\mathrm{m}} = {T_{\mathrm{m}}}^{0}\left\{1 - \left(\frac{2\sigma_{\mathrm{e}}}{\Delta {h_{\mathrm{f}}}^{0} l}\right)\right\} \quad \text{Eq. (1),}$$

where T_{m}, ${T_{\mathrm{m}}}^{0}$, σ_{e}, $\Delta {h_{\mathrm{f}}}^{0}$, and l are the melting point from measurement, theoretical equilibrium melting point (the melting point of an infinitely large crystal without defects), interfacial energy of folding surface, heat of fusion per unit volume of crystal, and lamella thickness, respectively [7]. The distance between lamellae is called as “long period”, the value is around 100–300 Å. The gap is an amorphous part, and the lamellae are connected by several tie chains. As shown in Fig. 3, in addition to tie chains, there would be loop chains where the molecular ends are connected to the same crystal plane, cilia chains where only one molecular end is connected to the crystal plane, and floating chains where an entire molecular chain exists in the amorphous phase. Among them, the presence of tie chains will greatly affect the mechanical properties of PP by transmitting a stress applied during deformation to lamellae [8].

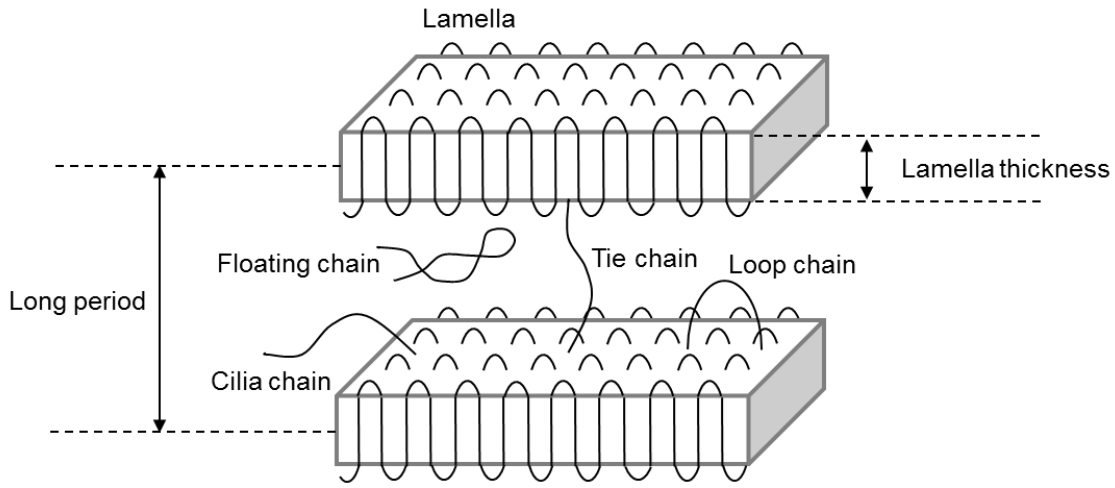

Fig. 3. Schematic diagram of lamellae structure.

1.1.1.4. Spherulite

The plate-like structure is called a lamella. As a characteristic property of α-form, it tends to form a structure of cross hatch in which a daughter lamellar grows in the tangential direction almost perpendicular to the mother lamellar formed in the radial direction. Spherulites are composed of lamellar crystals. The spherulite size strongly depends on the crystallization temperature and cooling process, and large spherulites can be observed when the crystallization temperature is high or when the cooling rate is slow. Although the normal spherulite size is about 1–50 μm, it grows to mm order under specific conditions. An increase in the number of crystal nuclei by adding nucleating agents or other effects results in a small spherulite size and improves transparency and impact resistance [9]. Fillers such as a talc and silica are also capable of nucleation and lead to similar effects.

1.1.1.5. Nucleation and Crystallization Behavior

The generation of PP crystal is triggered by the formation of primary nuclei by aggregation of several molecular chains. Subsequently, molecular chains adsorbed on the surface of primary nuclei generate secondary nuclei, and the crystal continuously grows. Crystallization is completed when the growing crystal collides with the neighboring ones and all the crystallizable space are consumed. The crystallization rate determined by the nucleation ability and growth speed is dependent on the crystallization temperature. In the case of isothermal crystallization, the crystallization rate at a high temperature is governed by the nucleation ability that is relatively slow at a high temperature, and increases with a decrease in temperature. On the other hand, the crystallization rate at a low temperature is governed by diffusion of macromolecules. As a result, the temperature at which the crystallization rate is maximized is called the crystallization temperature and this also depends on the cooling rate. Any nucleating agent used in industry has the role of increasing nuclei during crystallization and affects the physical and optical properties of the product [10].

In general, it is recognized that the nucleation in α-form is faster than that in β-form, crystal, while the growth speed is faster in the β-form. In addition, it is reported that, when α- and β-forms are mixed, the growth speed of α-form spherulites is faster when the crystallization temperature is lower than 90 °C or higher than 133 °C, whereas that of β-form spherulites is faster when the crystallization temperature is between 90 °C–133 °C [11].

1.1.1.6 Branch Structure

PP mostly indicate a linear chain with stereochemically aligned metyl groups as shortest side chains. Partial disappearance of the methyl groups or replacement with longer side chains inhibits the crystallization and greatly affect the physical properties. In addition, it varies greatly depending on its length and number. Among them, PP having long side chains (called as long-chain branced PP: LCBPP) has very attacted attention in both academic and industrial fields because of its unique characteristics. LCBPP can be prepared by two methods. One is the method in which a macromonomer is incorporated into the main chain during chain growth using a specific metallocene catalyst. The other is the method of converting linear PP to LCBPP by post-treatment such as an electron beam irradiation in inert atmosphere [12,13], reaction extrusion using peroxide [5,14], grafting [15,16], and so on. From a rheological point of view, the branch length required to function as a long chain branch should be $2M_e$ (M_e = critical molecular weight for entanglement: 6900 g/mol for isotactic PP) [15-17]. The long chain branch makes it possible to change the characteristics greatly with only one or two branches per main chain. It affects many properties such as crystallization behavior, mechanical properties, and rheological properties. In particular, the melt strength and elongational viscosity are greatly improved. The strain-hardening behavior given by LCBPP makes it possible to apply PP to foam molding and blow molding where high melt tension is required [18,19].

1.2. Catalysts for Olefin Polymerization

The structure and performance of polyolefins greatly depend on the employed catalysts. A wide variety of polyolefins are produced with various types of catalysts. Table 1 summarizes the types and characteristics of catalysts for polyolefins. Polyolefin catalysts can be categorized into two types: solid and molecular catalysts. ZN and Phillips catalysts are solid catalysts. They are featured with multi-site nature because they have different kinds of active sites. The presence of different active sites generates polymers having different molecular weights, resulting into a broad molecular weight distribution (MWD) as compared to the molecular catalyst. Since the discovery of ZN catalyst in the 1950s, it has been continuously improved and is still the most used catalyst for polyolefins today [20]. The obtained polymer is linear polyolefins with a high molecular weight and a relatively wide MWD. The Phillips catalyst used for PE gives a broader MWD than a ZN catalyst, producing polymers having short and long chain branching [21,22]. On the other hand, the molecular catalysts (*e.g.*, metallocene catalysts) have a single type of active sites, thereby producing polymers with a narrow MWD and chemical composition distribution of copolymers with α-olefins [23]. They are also called as single-site catalysts. In addition to isotactic PP, syndiotactic PP having different stereoregularity can be synthesized. Isotactic PP synthesized with a metallocene catalyst has a heterogeneous bond such as 1,3-insertion that cannot be found with a solid catalyst. Therefore, it has low melting point and low stiffness, although it has high isotacticity. As molecular catalysts other than metallocene catalysts, constrained geometry catalyst (CGC) exhibiting high copolymerization ability with bulky comonomer [24], Brookhart catalyst for higher molecular weight [25], Phenoxy-Imine (FI) catalysts capable of producing various types of polyolefins with higher activity [26], etc. have been developed. Note that these

molecular catalysts are more difficult to handle because of its sensitivity to moisture than ZN catalysts, which results in higher costs. The following sections specifically focus on the catalyst for PP production.

Table 1. Types and characteristics of catalysts for polyolefins.

Type	Catalyst		Characteristic
Solid catalyst (Multi-site)	ZN	$TiCl_4/MgCl_2$/donor + $AlEt_3$	・Non-branching ・Broad MWD (M_w/M_n = 3–6)
	Phillips	CrO_x/SiO_2	・Short/long-chain branching ・Broad MWD (M_w/M_n = 6–30)
Molecular catalyst (Single-site)	Metallocene	Cyclopentadienyl-Ti(IV) Trichloride + MAO	・Narrow MWD (M_w/M_n = 2–3) ・Narrow composition distribution for copolymer with α-olefin
	Post-metallocene	A: CGC	A・Effective for copolymerization with bulky α-olefin ・Short/long-chain branching
		B: Brookhart catalyst	B・High molecular weight ・Linear to hyperbranch
		C: FI catalyst	C・Remarkable catalytic activity ・High living performance

1.2.1. Propylene Polymerization Catalyst

A ZN catalyst is most generally used as a polymerization catalyst for propylene. ZN-derived isotactic PP has a relatively long continuous defectless sequence in a polymer chain due to the concentration of stereo or regiochemical defects in a certain part of polymer, thereby exhibiting a relatively high crystallinity, melting point (163–167 °C), and elastic modulus. In addition to the excellent physical properties, due to the good processability (wide MWD) and high cost performance, the ZN-derived isotactic

PP is widely used in the industry.

On the other hand, PP synthesized with a metallocene catalyst has a lower melting point (150–160 °C) and elastic modulus compared to that given by ZN catalysts because a small amount of defects are randomly distributed throughout the chains. Since it is easier to design the molecular structure of a single site catalyst, metallocene catalysts are used for specific PP such as syndiotactic PP or branched PP. Hereafter, the ZN catalyst used in this study is mentioned in more detail.

1.2.2. History of Ziegler-Natta Catalyst

Karl Ziegler first discovered that a titanium tetrachloride ($TiCl_4$)/alkylaluminum (AlR_3) mixture had an ability to polymerize ethylene. After that, in 1954, Giulio Natta succeeded in synthesizing isotactic PP for the first time using a different catalyst system based on a similar concept [27]. At this time, the content of isotactic polymer (defined as isotactic index) was only 30–40%, but Natta immediately improved the isotactic index to 90% using a $TiCl_3/AlR_2Cl$ catalyst. Thereafter, the activity was further improved using aluminum-reduced $TiCl_3$ (including its mixture with aluminum: $TiCl_3 \cdot 0.33AlCl_3$). This catalyst is considered as the first generation ZN catalyst. PP synthesized by the first generation ZN catalyst required removal of catalyst residues and separation of atactic polymer due to its low activity and stereoregularity, leading to a complex production process accompanied by a high cost.

In the early 1970s, Solvay developed a porous $TiCl_3$ catalyst with a high specific surface area (Solvay $TiCl_3$) [28]. This catalyst was obtained by treating aluminum-reduced $TiCl_3$ with isoamyl ether and $TiCl_4$. The increment in the specific surface area resulted in the exposure of more Ti atoms on the crystal surface, thus

improving the activity about five times over the first generation aluminum-reduced $TiCl_3$ catalyst. Moreover, the isotactic index of produced PP reached 95%. The second generation catalysts such as Solvay $TiCl_3$ are featured with a large surface area, small crystal size, and a small amount of $AlCl_3$ co-crystallized with $TiCl_3$, and hence they also known as a "low aluminum catalyst".

Following the invention of the second generation catalysts, supported catalysts using silica or alumina have been developed. The support materials generally have a high surface area and functional groups those can be chemically bonded to a transition metal compound on the surface. The development of the supported catalysts began in the 1960s, and it soon became clear that only $MgCl_2$-supported catalysts have excellent activity for PP. However, the stereoregularity of the obtained polymer was very low. This situation was improved by the introduction of a Lewis base (defined as an internal donor: D_i). The catalysts obtained by co-grinding of $MgCl_2$, $TiCl_4$, and D_i are usually used with a trialkylaluminum as a co-catalyst and a second Lewis base called an external donor (D_e). The catalyst developed by Montedison in 1978 used ethyl benzoate as D_i and methyl-*p*-toluate as D_e. Such a $MgCl_2$-supported catalyst with donors is called the third generation catalysts. Its high activity eliminated the removal of the catalyst residue. However, the low stereoregularity had been still an issue where 10% or less of atactic polymer carried over to the final product.

A catalyst possessed a well-balanced activity and stereospecificity was discovered in the early 1980s. This catalyst, called the fourth generation catalyst, was achieved by a different donor combination compared to the third generation catalysts. Specifically, it had alkyl phthalate as D_i and alkoxysilane as D_e. The obtained PP exhibited an isotactic index of at least 95%, thus eliminating the process for the removal of atactic polymer.

In the late 1980s, a catalyst with 1,3-diether as D_i was developed. The advantage of this catalyst was an extremely high activity and isotacticity without the necessity of D_e addition. Further, the catalyst exhibited excellent hydrogen response, and the obtained PP has a very narrow MWD among ZN catalysts. This type of catalysts is called the fifth generation catalyst and has been used in industry along with the current mainstream, the fourth generation catalyst. In 1999, a catalyst with succinate as D_i and alkoxysilane as D_e was developed. In addition to the high stereospecificity, it has become possible to cope with the demand for PP having a very wide MWD.

ZN catalysts have been investigated to mainly pursue better productivity and stereospecificity, and at the present time, a variety types of PP that can be used for various application is manufactured and supplied at much more reasonable price than in the past. In this study, the fifth generation $TiCl_4/MgCl_2$/diether catalyst was selected due to its excellent activity and stereospecificity.

1.2.3. Propylene Polymerization Mechanism with Ziegler-Natta Catalyst

The polymerization of propylene is classified into three stages; initiation, propagation, and termination. The initiation (activation) begins with the formation of Ti-C bonds as a result of alkylation of $TiCl_4$ by AlR_3 as a co-catalyst. The Ti-Cl bond of $TiCl_4$ is dissociated upon contacting with alkylaluminum to form a radical trivalent species (Eq. 2), and then the Ti species alkylates with alkylaluminum by transalkylation (Eq. 3). This alkylated trivalent species is considered as the active species in polymerization.

Activation

$TiCl_4 + AlR_3 \rightarrow TiCl_3\cdot + AlR_3Cl\cdot$ Eq. (2)

$TiCl_3\cdot + AlR_3 \rightarrow TiCl_2R\cdot + AlR_2Cl$ Eq. (3)

The growth reaction (propagation) proceeds in two steps. In the first step, the C=C bond of a propylene monomer is π-coordinated to the vacancy site of the Ti species. In the next step, the monomer is inserted into the Ti-C bond, and a vacant site forms again. The repetition of this process proceeds the polymer chain growth (Eq. 4 and Scheme 1) [29]. In the step for coordination of propylene, its orientation (position of methyl group) is controlled by the steric hinderance of the active site, which determines the stereoregularity of the growing polymer chain. There are four types of the coordination forms as shown in Fig. 4. The case where β-carbon of propylene (carbon with the methyl group) positions towards the growing chain is defined as 1,2-insertion, and when the position of carbon is opposite, it is called as 2,1-insertion. Stereoregularity is determined by the choice of the coordination plane, and isotactic PP is generated when the coordination always occurs on the same plane.

Propagation

$Ti\text{-}P + C_3H_6 \rightarrow Ti\text{-}P\cdot \cdot C_3H_6 \rightarrow Ti\text{-}C_3H_6\text{-}P$ Eq. (4)

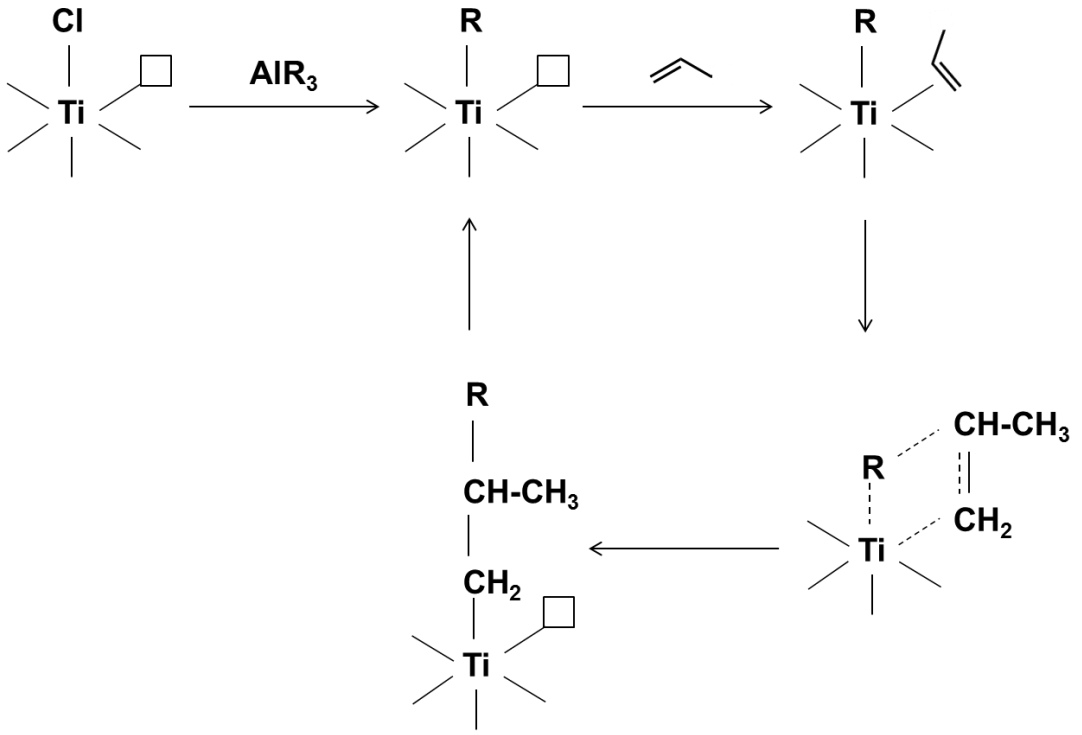

Scheme 1. Propylene polymerization mechanism (Cossee model).

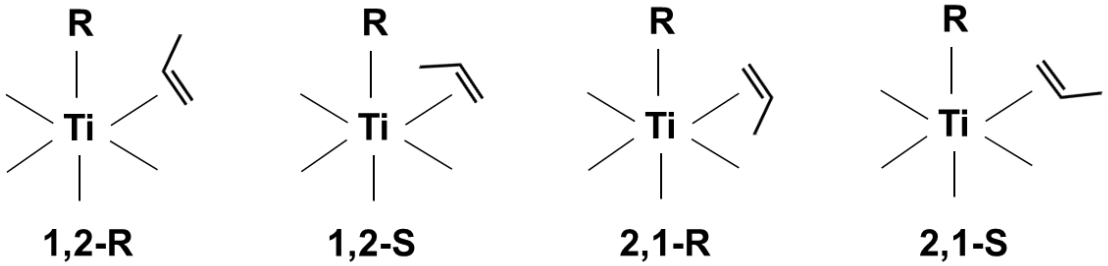

Fig. 4. Propylene coordination model.

Several pathways can be involved in the termination of polymer chain growth. The dominant termination route is chain transfer to monomers (Eq. 5), co-catalysts (Eq. 6), and hydrogen (Eq. 7) if it is introduced. The termination by β-hydrogen elimination can also occur (Eq. 8), but it does not play a major role in propylene polymerization with a $MgCl_2$-supported ZN catalyst at normal polymerization temperature. Among them, chain transfer to hydrogen is the most efficient termination process and is widely used to control the molecular weight of PP in the industry. Other termination reactions include the formation of inactive (dormant) sites. This happens when a propylene monomer is inserted into the growing polymer chain in the 2,1-insertion manner in a supported ZN catalyst, resulting in a temporary loss of the activity due to the steric hindrance caused by the methyl group of the inserted propylene prohibits the accessibility of the monomer to the vacant coordination site. This temporary restriction is recoverd by chain transfer to hydrogen. Note that the addition of hydrogen also improves the activity in many catalyst systems including a $TiCl_4/MgCl_2$/diether catalyst.

The above termination releases the growing polymer chain from the active site, while the active site keeps alive. Further reducing the Ti species from trivalent to divalent completely deactivates the Ti species for α-olefins, and the activity can not be recovered without specific oxidation agents such as organic halides. Other possible pathways for the over reduction have been proposed but it has not reached a general consensus [30].

Termination (chain transfer)

$Ti\text{-}CH_2\text{-}CH(CH_3)\text{-}P + CH_2{=}CH(CH_3) \rightarrow Ti\text{-}CH_2\text{-}CH_2\text{-}CH_3 + CH_2{=}C(CH_3)\text{-}P$ Eq. (5)

$Ti\text{-}CH_2\text{-}CH(CH_3)\text{-}P + AlR_3 \rightarrow Ti\text{-}R + R_2Al\text{-}CH_2\text{-}CH(CH_3)\text{-}P$ Eq. (6)

$Ti\text{-}CH_2\text{-}CH(CH_3)\text{-}P + H_2 \rightarrow Ti\text{-}H + CH_3\text{-}CH(CH_3)\text{-}P$ Eq. (7)

$Ti\text{-}CH_2\text{-}CH(CH_3)\text{-}P \rightarrow Ti\text{-}H + CH_2{=}C(CH_3)\text{-}P$ Eq. (8)

1.2.4. Components of $MgCl_2$-Supported Ziegler-Natta Catalyst and Their Roles

A ZN catalyst is generally composed of a main transition metal (*e.g.*, $TiCl_4$), a support material (*e.g.*, $MgCl_2$), an activator called a co-catalyst (*e.g.*, alkylaluminium), and donors (Lewis base). Here, the co-catalyst and donors are briefly described.

As described in the polymerization mechanism in the previous Section 1.2.3., the co-catalyst is essential for activating the active sites. In addition, the co-catalyst is involved in the chain transfer reaction, and it also induces the loss of the activity by extracting donors from the catalyst. The co-catalyst used in the $MgCl_2$-supported catalyst is always a trialkylaluminum, among which triethylaluminum (TEA) or triisobutylaluminum (TIBA) is most common.

The main purpose for addition of donors is to improve the stereospecificity of the catalyst. Donors are classified into D_i which is added during the catalyst preparation and D_e which is added together with a cocatalyst during polymerization. It is expected that D_i adsorbs on the $MgCl_2$ surface in the vicinity of the Ti species to equip an appropriate steric hindrance to the active site. However, as mentioned above, some D_is are extracted from the catalyst surface by a co-catalyst, resulting in deterioration of the stereospecificity. Addition of D_e would suppress the extraction by forming a complex

with the co-catalyst, or covering the vacant adsorption site, which is previously covered by D_i in order to maintain or further improve the stereospecificity. The type of effective D_e depends on the type of D_i. For example, when aromatic monoester such as ethyl benzoate is adopted as D_i, the same type of ester compounds such as methyl-*p*-toluate is usually required. On the other hand, alkoxysilanes as D_e are an effective for phthalate and diether as D_i.

1.3. Functionalization of Polypropylene

PP is composed of simple carbon-carbon and carbon-hydrogen single bonds. Although this feature affords major advantages of PP, the absence of functional groups that can interact with polar groups restricts the use of PP in terms of adhesion, paintability, printability, compatibility with polar polymers, and affinity for fillers. Many studies on the functionalization of PP have been conducted to release the restrictions on the use of PP [31-52]. There are four main strategies to functionalize PP: i) copolymerization, ii) reactive intermediate, iii) chain transfer reaction, and iv) post-treatment. The following part describes each method and feature.

1.3.1. Copolymerization

The copolymerization strategy utilizes a comonomer or macromonomer having a target functional group directly copolymerized with propylene. Functionalized PP having side functional groups or graft chains can be prepared by copolymerization with a comonomer or macromonomer, respectively. In general, PP is synthesized by a ZN catalyst or metallocene catalyst using group 4 transition metals. If these catalysts could be used to copolymerize with a comonomer having a functional group, it would be very simple and cost-effective. However, early transition metals, which are Lewis acids, form complexes with unshared electron pairs of heteroatoms such as N, O, and halides, which greatly inactivate the catalyst. As a result, it is actually difficult to obtain functionalized PP with sufficient quantity and quality. It has been reported that this problem can be partly alleviated by using a comonomer with a long spacer between the vinyl group and the polar group, and using a large amount of alkylaluminum in the copolymerization of

propylene with a hydroxyl group containing comonomer using a metallocene catalyst [34-36]. In addition, there is an example in which ethylene and a polar monomer are directly copolymerized by using a less oxophilic late transition metal catalyst such as Ni-diimine catalysts [37,38]. However, it is highly challenging to apply the copolymerization strategy in the production of highly stereoregular PP.

1.3.2. Reactive Intermediate

The second strategy is to utilize a reactive intermediate. First, a copolymer of propylene and a comonomer that contains a reactive but less poisonous functional group is synthesized. Thereafter, the side-functionalized PP is obtained by converting the reactive group into a desired functional group. Methods for temporarily protecting a polar functional group with a non-polar group are also included in this category because this method requires subsequent conversion of the protecting group back to the initial functional group. In general, protecting groups provide a steric shielding or/and an electronic neutralization of Lewis base functional groups [39], which weaken the interaction between the catalyst and the functional groups. Unfortunately, it is not possible to ensure complete activity, and some decrease in activity is inevitable. In addition, electronic protection also reduces the molecular weight as well as the polymer yield by reducing the solubility of the propagating polymer chain.

As the reactive functional group, borane group [31,40], tolyl group [32,41], etc., which are copolymerizable with propylene and can be converted to other functional groups are selected. A side-functionalized PP having a polar functional group such as OH, COOH, NH_2, or halide can be synthesized by converting these reactive groups with specific chemicals. For example, a borane group incorporated into PP chains by a ZN or

metallocene catalyst could be converted into halides, OH, and NH_2 groups, and an oxidation of C-B bond by H_2O_2/NaOH produced side-functionalized PP with OH groups (Scheme 2). On the other hand, the tolyl group produced by copolymerization of *p*-methylstyrene and propylene could be converted to functional groups such as COOH, halides, and maleic anhydride to give side-functionalized PP (Scheme 3). Furthermore, these reactive functional groups could be converted into radical or anionic initiators to become (polymerization) initiation points, and as a result, PP having other functional groups or grafted chains can be prepared. In addition, PP containing a C=C double bond in the side chain obtained by copolymerization propylene with dienes such as divinylbenzene and methyl-1,4-hexadiene could be also used for a cross-linking reaction and functionalization [32]. The preparation of functionalized PP using these reactive intermediates is advantageous because it can be applied to various types of functional groups by many techniques, whereas high technology and labor are required to obtain only the target functionalized PP with high accuracy.

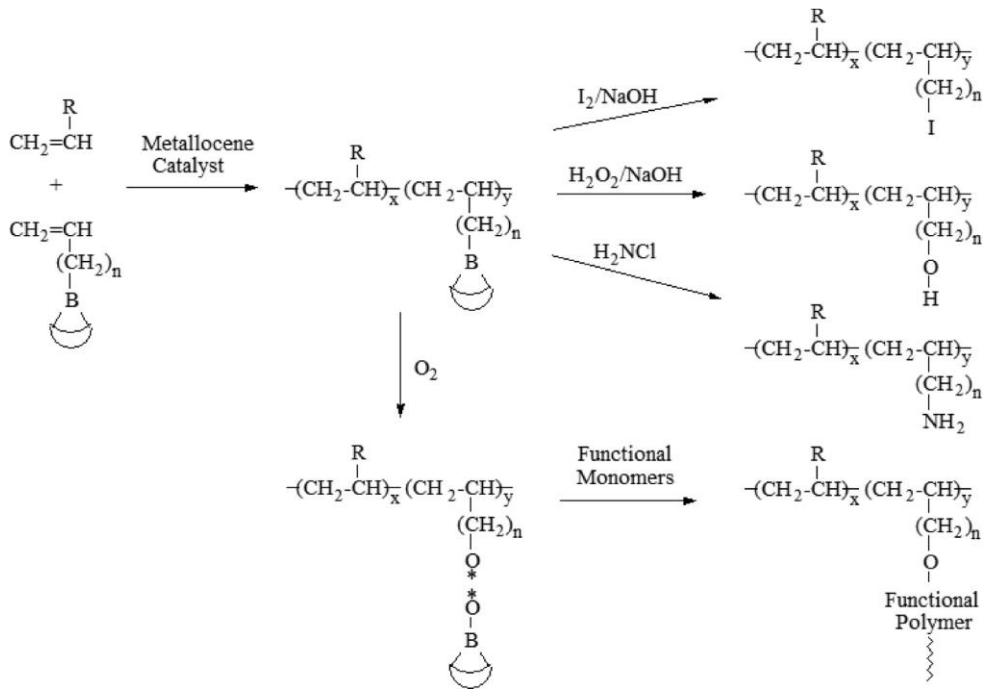

Scheme 2. Functionalization of polyolefin using a borane intermediate [31].

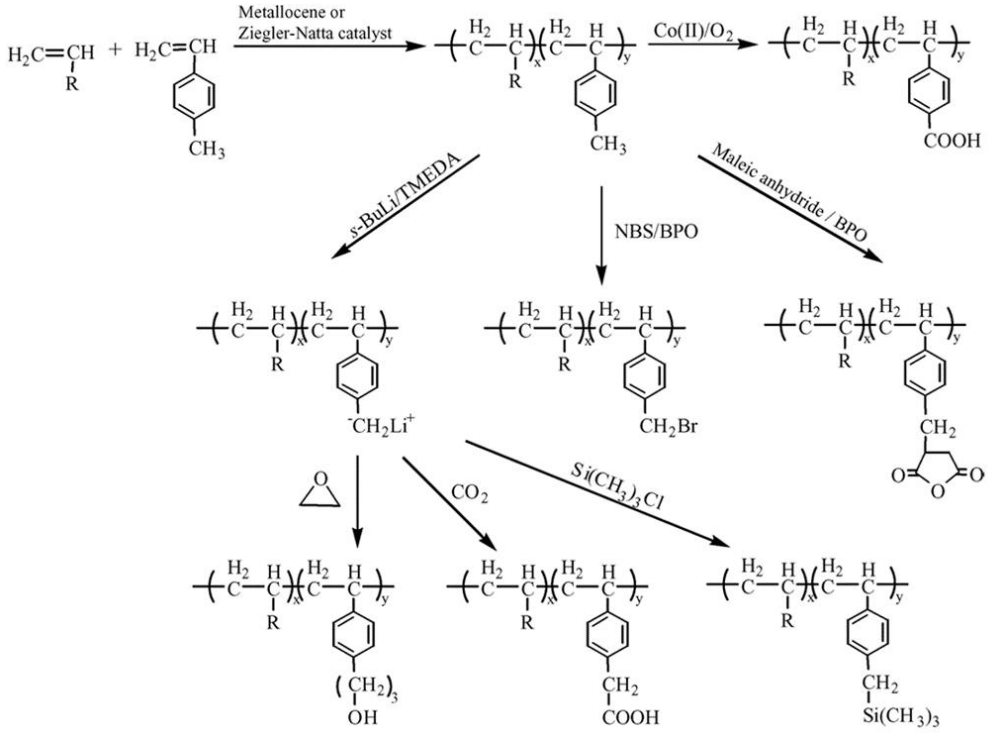

Scheme 3. Functionalization of polyolefin using a tolyl intermediate [32].

1.3.3. Chain Transfer Reaction

The third strategy uses a chain transfer reaction during propylene polymerization. Utilizing a terminal double bond such as vinylidene or terminal PP-metal bond generated by β-hydrogen elimination or chain transfer reaction to monomer, co-catalyst, etc., desired functional groups are introduced from there. By the way, double bonds can also be formed in a thermal degradation of PP using peroxide. In the chain transfer method, it is very useful that a reactive functional group can be selectively introduced into the chain end, and it can be converted into an end-functionalized PP, which is applicable to multisegment polymer. However, it is difficult to introduce a functional group into each molecular chain. In addition, the fact that the chain transfer reaction must be controlled limits the polymerization conditions and makes it difficult to cope with a wide range of molecular weights. Depending on the choice of chain transfer agents, various types of functionalized PP such as terminal silane [42], borane [43,44], Al [45,46], and Zn [47,48] could be obtained. It is possible to transform these to other functional groups such as a hydroxyl group by further reactions with specific chemicals.

1.3.4. Post-Treatment

The fourth strategy is to decompose PP by chemical post-treatment using radicals generated by organic peroxides or thermal decomposition to form free radicals in the PP chain [49-52]. When PP is attacked by free radicals, H atoms are extracted to form stable tertiary carbon radicals. Side-functionalized PP can be prepared by reacting these radicals with a vinyl monomer having functional groups (Scheme 4). An example of a typical side-functionalized PP prepared by this method is maleic anhydride modified PP

(PP-*g*-MA) [49-51]. The anhydride group is very reactive and becomes an efficient coupling agent for both fillers such as glass fiber and polymers having a polar group such as polyamide. Moreover, it can be prepared at a realistic cost for industry. However, since this method is often executed at the same time as a processing process, it is difficult to control the reaction, *i.e.* the chemical structure and the degree of functionalization are difficult to be turned. Furthermore, as shown in Scheme 4, a molecular weight changes due to two undesired side reactions: β-cleavage (decrease molecular weight) and cross-linking (increase molecular weight), both of which can cause a significant effect on physical properties and processability. In general, the β-cleavage reaction is faster than the functionalization reaction. So that the molecular weight tends to be lowered along with the degree of functionalization. Therefore, PP prepared in this way is also called vis-breaking PP because the viscosity is reduced by degradation. Polypropylene having a low molecular weight by the β-cleavage reaction adversely affects physical properties such as adhesive strength and impact strength. Therefore, the balance between the graft amount and the molecular weight is very important in terms of physical properties.

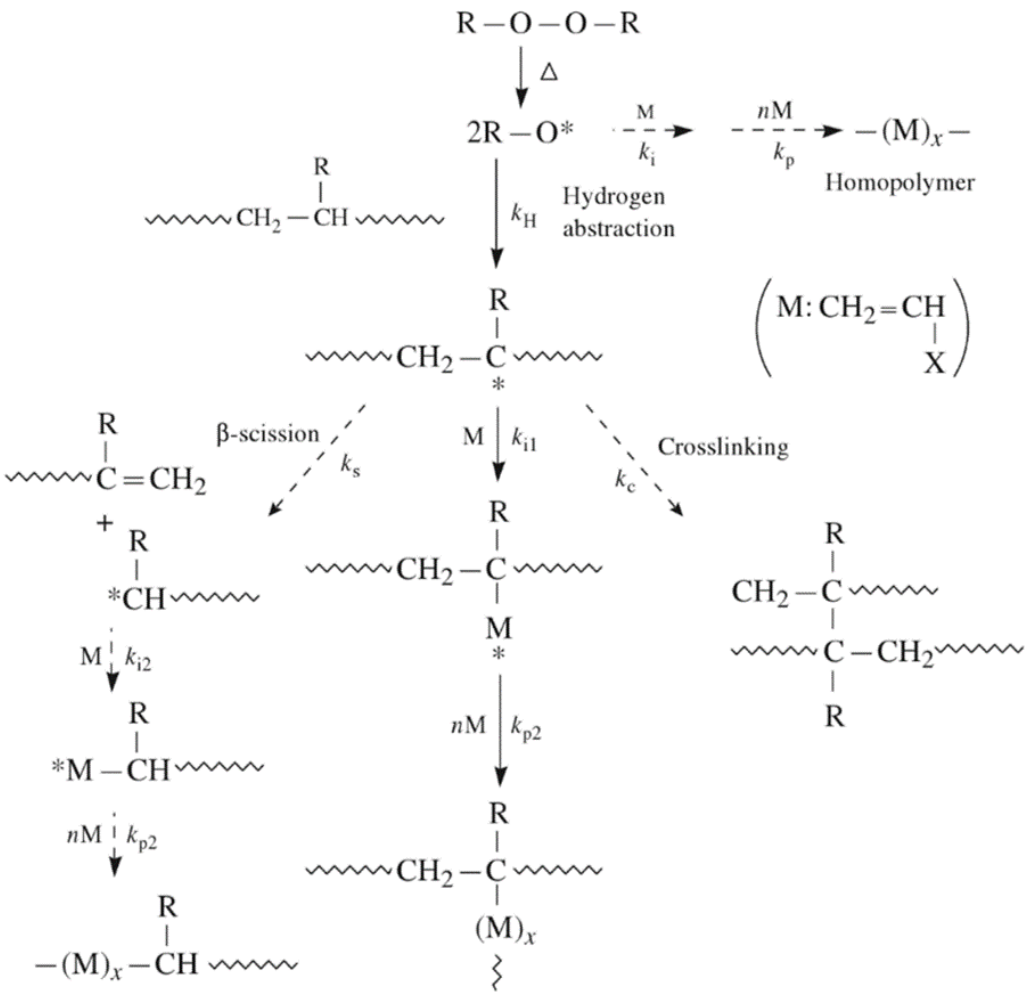

Scheme 4. Functionalization of polyolefin using a free radical [31].

In order to improve the wettability (adhesiveness), the surface of molded products is sometimes treated with plasma [53], corona [54], ultraviolet [55], gamma ray [56], etc., and a functional group is introduced to the surface. Unlike the modification of the PP chain itself, these are intended to modify only the surface, so details are omitted in this dissertation.

1.4. Polypropylene Composite Materials

Although PP exhibits many advantage, it is easy to imagine that it is not the best material for every application. For example, it is inferior to engineering plastics in terms of mechanical strength and heat resistance. In some cases, higher impact strength is required. Therefore, various materials, both organic and inorganic, have been compounded with PP in order to improve mechanical properties and/or impart new functions [57-64]. This compounding significantly expanded the use of PP, and other plastics have been replaced by PP composite materials, sometimes even engineering plastics. PP is superior to other plastics in its light weight, processability, recyclability, etc., which intensifies further demands from relevant fields. Inorganic micro-sized fillers such as a glass fiber [61], talc [62,63], calcium carbonate [64], etc are often used for the purpose of improving the stiffness and heat resistance (heat deflection temperature, HDT) of PP. Among them, a talc is the most used filler because of the balance between a price and the degree of improvement in stiffness. As shown in Fig. 5, the reinforcement of the flexural modulus is larger for fillers with a larger aspect ratio (glass fiber > talc > calcium carbonate). However, a large aspect ratio leads to anisotropy problems, resulting in deformation and warping of a molded product. Therefore, it is necessary to select a filler according to an application. It is noted that coupling agents (compatibility agents) such as a maleic anhydride modified PP (PP-*g*-MA) are often used to improve the adhesion between the matrix and fillers [65]. On the other hand, an elastomer represented by ethylene-propylene rubber (EPR) is added to enhance an impact strength [66-68].

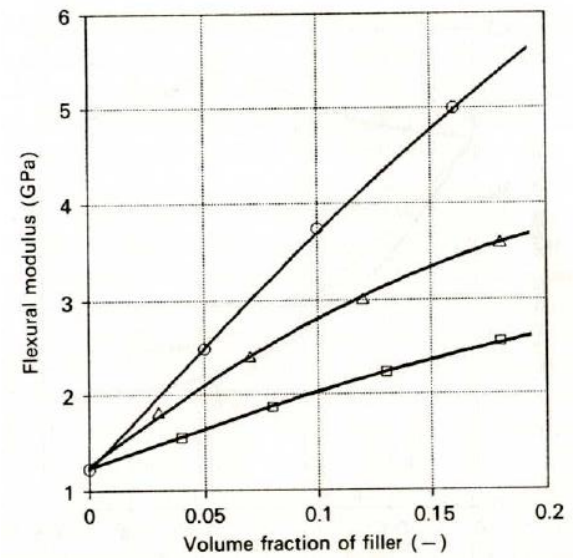

Fig. 5 . Relationship between the volume fraction of filler with different aspect ratio and flexural modulus : (○) glass fiber, (Δ) talc, and (□) $CaCO_3$ [60].

1.4.1. Polypropylene Composites with Elastomer

While the matrix PP can be strengthened by adding fillers, there is a limit to the improvement of its properties by simply mixing one kind of fillers. In particular, an impact strength at low temperatures, which is a drawback of PP, cannot be improved by simply adding fillers, but rather deteriorates. Hence, various attempts have been made to prepare multi-component PP, and among them, the most widely used method is a ternary system of PP/filler/elastomer blend [69,70]. In this system, it is possible to improve the impact strength by the elastomer and at the same time improve the stiffness by the filler. As a method for preparing such an elastomer-containing composite materials, a combination of the following two techniques has become the mainstream. The first techniques is preparing a thermoplastic elastomer in a reactor, called reactor blending technology [71]. In this method, PP is produced in multiple steps. Firstly, PP is

synthesized in the first stage, and elastomer (mainly EPR) is prepared in the second stage in the presence of ethylene gas. While this technique can highly disperse the elastomer, it is difficult to ensure the high fraction of the elastomer, and the impact strength at low temperatures is often insufficient. Therefore, a method of externally adding a thermoplastic elastomer during the pelletizing process is also used. The dispersion of a rubber is most important factors in these elastomer composite materials. Although PP and elastomers are generally incompatible, they can be finely dispersed to some extent by melt mixing (shearing force). The dispersion size of rubber (D_R) in melt mixing is given by the following equation,

$$D = \frac{4\sigma}{\eta_M \dot{\gamma}} \left(\frac{\eta_R}{\eta_M}\right)^{0.84} \quad (\eta_R > \eta_M), \qquad D = \frac{4\sigma}{\eta_M \dot{\gamma}} \left(\frac{\eta_R}{\eta_M}\right)^{-0.84} \quad (\eta_R < \eta_M) \qquad \text{Eq. (9),}$$

where σ, η_i, and $\dot{\gamma}$ are the interfacial tension, viscosity of matrix (M) and rubber (R), and shear rate [72]. This equation shows that the rubber size is the smallest when the viscosity ratio between the rubber and matrix is about 1 ($\eta_R/\eta_M \approx 1$). Faster shear rates ($\dot{\gamma}$) also give a fine dispersion. The smaller the dispersion size is, the greater the improvement is. It has also been reported that the Izod impact strength increases rapidly at a specific interparticle distance as shown in Fig. 6.

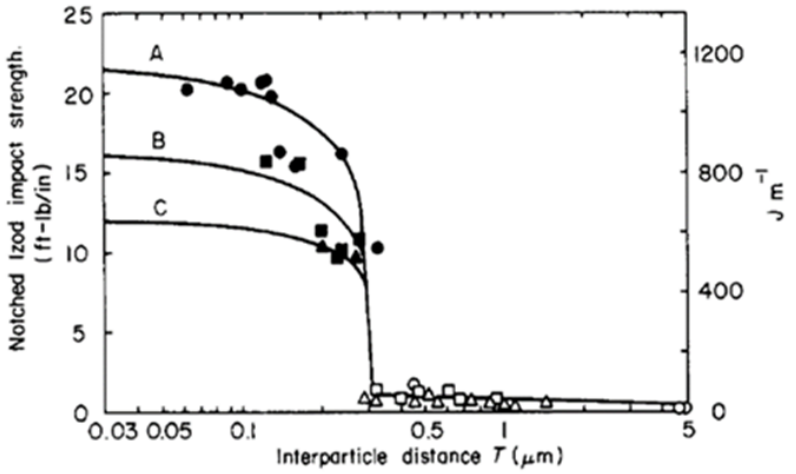

Fig. 6. Effect of interparticle distance on Izod impact strength in nylon-rubber blends: (A) 10 wt%, (B) 15 wt%, and (C) 25 wt% of rubber [67].

1.4.2. Polymer-Based Nanocomposites

As described in the previous sub-chapter, micro-sized fillers have been used to enhance the stiffness of PP. However, it is necessary to add several tens of percents of fillers in order to embody sufficient effects. As a result, the density of the material is increased. In current material development, weight reduction is very important, so that there is a demand for a method that provides a high effect at a small amount of fillers. Therefore, research on polymer nanocomposites has been actively conducted. A polymer nanocomposite is a composite material in which nano-sized fillers such as clay (represented by montmorillonite) [73-78], carbon nanotube (CNT) [79-82], and nano-silica [83-98] is added to a polymer matrix instead of micro-sized fillers such as talc and glass fiber described above. Since Usuki et al. in Toyota Central R&D Labs. succeeded in dramatically improving the elastic modulus and HDT by adding nano-clay to PA in 1990s [76], research on various nanocomposites has been conducted. The high

reinforcing effect in nanocomposites comes from the fact that the specific surface area is dramatically improved compared to micro-sized fillers, which makes load transfer more efficient. In addition, an increase in the number of particles shortens the distance between adjacent fillers, leading to the stronger interaction between fillers. These effects are expected to reduce the required filler amount of 10 wt% or more in the micro-sized filler below 1–5 wt%. Nanocomposite materials are expected not only in physical properties but also in functional aspects. As mentioned earlier, nanocomposites enhance the interaction between fillers, thereby it is expected to have a significant effect on properties that use the interactions such as electrical conductivity and heat transfer. In terms of electrical conductivity, carbon-based fillers such as carbon black [81], CNT [80,81], graphene [99], etc. are mainly studied. In particular, CNT and graphene are easier to form a conductive path because of their high aspect ratio, and various studies have been conducted. From the viewpoint of thermal conductivity, in addition to the carbon-based fillers [82], a wide range of fillers such as alumina nanoparticles and alumina whiskers have been studied [100,101]. In order to fully enhance these properties, it is important to control the dispersion state of the fillers and to improve the matrix/filler interface interaction.

1.4.3. Polypropylene-Based Nanocomposites

In order to achieve a dramatic improvement in mechanical properties of polymer-based nanocomposites, it is essential to uniformly disperse nanofillers. However, the lack of polarity of PP causes poor dispersion of polar fillers, and large aggregates of fillers are formed. Therefore, various methods have been reported to improve this poor dispersion. The first approach is the addition of a compatibilizing

agent. A maleic anhydride-grafted PP (PP-*g*-MA) is mainly used as a compatibilizing agent, and it is well known that the dispersion of nanofillers can be improved by adding it [74,86]. Nevertheless, the addition of the compatibilizing agent has not been very effective in terms of physical properties. This is because PP-*g*-MA has a relatively low molecular weight and soft material due to radical treatment. Furthermore, it covers the filler surface to inhibit the load transfer to the filler. The second approach is surface modification of fillers. Its aim is to improve the matrix/filler compatibility by hydrophobizing the hydrophilic filler surfaces. Actually, the ion exchange of a clay with octadecylammonium [77] or the treatment of a silica surface with a silane coupling agent having an aminopropyl group [89] improved their dispersion. However, the reinforcement was not as-expected due to the insufficient interfacial strength between the matrix and fillers. As other approaches, an *in-situ* polymerization method for synthesizing a polymer in the presence of a filler [78] and an *in-situ* sol-gel method for synthesizing a filler [88,102] in a polymer have been developed, but it is insufficient in terms of interfacial strength.

1.4.4. Polypropylene/SiO_2 Nanocomposites

A typical nanofiller used in nanocomposites includes spherical silica nanoparticles because they are inexpensive, non-toxic, abundant in particle size, and easily modifiable, and so on. In addition, the absence of anisotropy can be usefully used as a model filler. In order to overcome the obstacles between PP and fillers as described in the previous section, many research for PP/SiO_2 nanocomposites has been conducted on the use of compatibilizers [86], organic surface modifications of SiO_2 surface [86,87,89-91], *in-situ* methods for fillers or polymers [88], polymer grafting [93-98], etc. Among them,

Taniike *et al*. have realized a strong interface in addition to uniform dispersion by using PP chains as graft chains [97]. Table 2 summarizes the reinforcement of PP/SiO_2 nanocomposite systems. As shown in Table 2, although the degree of improvement varies depending on the method, the maximum improvement of Young's modulus has been confirmed to be *ca.* +30%, but that of strength remains below +20%. Surprisingly, grafting PP chains enabled *ca.* +30% reinforcement in both strength and modulus. It was considered that the significant improvement in strength is due to the strong interfacial bonding between the matrix PP and grafted PP chains. These PP chains can be entangled with each other and co-crystallize during cooling process. As a result, physical crosslinks are formed by SiO_2 nanoparticles grafted with PP chains between lamellae, which contributes to the yielding during deformation. Since the length of the graft chain that is entangled and co-crystallized with the matrix chain is necessary, no significant reinforcement can be obtained either when the graft length is short or when the graft chain is not PP. Moreover, when the lengths of the graft chains are the same, the density of graft chains is also important [98]. Therefore, in PP-based nanocomposite, it is important to graft longer PP chains to fillers as many as possible. On the other hand, the improvement of Young's modulus is considered to be an effect of suppressing the formation of SiO_2 aggregates by the presence of grafted chains. A large amount of grafting and longer grafted chains are not required for improving the dispersion of SiO_2 nanoparticles because it is enough to wet the filler surfaces. From the above, it was concluded that the polymer grafting with long PP as graft chains is the most effective for simultaneous improvement for dispersion and interfacial bonding. However, the preparation of the end-functionalized PP for grafting used in the previous research is very laborious because the terminal modification by using chain transfer reaction is

inefficient and the reactivity of the end-functionalized PP with the filler is not sufficient. They decline the value of the excellent material in terms of cost, so that the nanocomposites are not yet used from an industrial use point of view. Therefore, in this dissertation, I focused on this issue and tried to solve it.

Table 2. Reinforcements of PP/SiO_2 nanocomposites in previous studies [97]

Sample [a]	Filler content [wt%]	Young's modulus [%]	Tensile strength [%]
PP/SiO_2	5.0	+7	+4
PP/MAPP/mSiO_2	5.3	+7	0
PP/MAPP/SiO_2	5.0	+31	+5
PP/colloidal SiO_2	4.5	+33	–5
PP/PVP-*g*-SiO_2	0.5	+8	+6
PP/PP-NH_2/PGMA-*g*-SiO_2	1.6	+30	+13
PP/PS-*g*-SiO_2	2.1	+18	+18
PP/PS-*g*-SiO_2	1.4	+15	+4
PP/PBA-*g*-SiO_2	1.1	+9	+7
PP/HBP-*g*-SiO_2	5.0	—	+11
PP/PMMA-*g*-SiO_2	0.2	—	+6
PP/PP-*g*-SiO_2	**5.0**	**+30**	**+27**

[a] MAPP: maleic anhydride grafted PP, mSiO_2: SiO_2 modified with short alkyl chains, PVP: poly(p-vinylphenylsulfonyl-hydrazide), PP-NH_2: PP with terminal amine, PGMA: poly(glycidylmethacrylate), PS: polystyrene, PBA: poly(butylacrylate), HBP: octadecyl isocyanate-grafted hyperbranched polyester (BoltornTM H_2O), PMMA: poly(methylmethacrylate).

[b] Reinforcement from pristine PP.

1.5. Purpose

As shown in the general introduction, very attractive characteristics of PP are evident from its production volume and its utilization in various products, and its wide range of uses can be attributed to the development of various techniques such as catalyst, functionalization, composite, and so on. In terms of catalysts, a ZN catalyst for commodity PP and a metallocene catalyst for high-performance PP are main drivers. Also, functionalization of PP has been carried out to improve the interaction of PP with other materials such as inorganic fillers. In this regard, functionalization of PP requires additional works other than polymerization, resulting in more elaborate preparation. Elaborate and expensive materials have a high value but lack versatility and ultimately limit their use. In this dissertation, I focused on a trace amount of functionalization in ZN catalyst. Studies of direct functionalization by the copolymerization using ZN catalysts have not been studied much because of their weakness of poisons from the polar groups. Of course, functionalized PP with a trace amount of functional groups is not suitable for applications that require large amounts of functional groups. However, if a functional group can be selectively present, there are many scenes that act very effectively such as for multisegment polymer and compounding. The purpose of this dissertation is to explore the possibility of synthesis of a functionalized PP with a trace amount of reactive functional groups by means of copolymerization of PP and a polar monomer using a ZN catalyst and its application to composite materials. Note that the word “a trace amount” in this thesis means less than one functional group per molecular chain.

In Chapter 2, I studied the synthesis of PP copolymers containing various types of alkoxysilanes in order to understand the possibility and mechanism of copolymerization

of propylene and polar vinyl comonomers using a ZN catalyst. The effects on the comonomer insertion and catalytic activity under the different polymerization conditions were investigated for PP-OTMS, which is a copolymer of propylene and (7-octen-1-yl) trimethoxysilane (OTMS). Subsequently, the thermal and mechanical properties of the PP-OTMS was further evaluated for a deeper understanding.

In Chapter 3, PP-OTMS containing one or less OTMS per molecular chain was synthesized, and the nanocomposite was prepared by melt mixing with PP-OTMS and nano-sized SiO_2. During melt mixing, the alkoxy groups of PP-OTMS were expected to react with silanol group on the SiO_2 surfaces to form *in-situ* grafted chains. The consumption of methoxy (OMe) groups in OTMS, melt viscoelasticity, dispersion of SiO_2 nanoparticles, crystallization behavior and mechanical properties were evaluated.

In Chapter 4, PP-OTMS/elastomer/SiO_2 nanocomposites were prepared to understand the effects of grafting on the stiffness and toughness in the ternary system. Two types of ethylene-octene copolymers (EOC) with different melt index were used as an impact modifier. The morphology of the ternary nanocomposites and the dispersion of SiO_2 nanoparticles were observed by SEM and TEM, respectively. Thereafter, the crystallization behavior, tensile properties, and impact strength were evaluated.

In Chapter 5, the synthesis of functionalized PP with a trace amount of reactive functional groups using a ZN catalyst and its application to composite materials were summarized and concluded.

The synthesis of functionalized PP with a trace amount of functional groups and the concept of application to composite materials in this study are expected to make many contributions to further PP prosperity.

References

[1] R. Geyer, J. R. Jambeck, K. L. Law, Sci. Adv. 3 (2017) 25–29.

[2] H. A. Maddah, Am. J. Polym. Sci. 6 (2016) 1–11.

[3] R. Paukkeri, A. Lehtinen, Polymer 34 (1993) 4075–4082.

[4] A. J. Lovinger, J. O. Chua, C. C. Gryte, J. Polym. Sci. Polym. Phys. Ed. 15 (1977) 641–656.

[5] S. Zhou, W. Wang, S. Zhao, Z. Xin, Y. Shi, Polym. Eng. Sci. 56 (2016) 240–247.

[6] M. Dong, Z. Guo, J. Yu, Z. Su, J. Polym. Sci. Part B: Polym. Phys. 46 (2008) 1725–1733.

[7] J. D. Hoffman, G. T. Davis, J. I. Lauritzen, N. B. Hannay (Ed.), Treatise on solid state Chemistry 3 (1976) 497–614.

[8] F. Coppola, R. Greco, E. Martuscelli, H. W. Kammer, C. Kummerlowe, Polymer 28 (1987) 47–56.

[9] J. L. Way, J. R. Atkinson, J. Nutting, J. Mater. Sci. 9 (1974) 293–299.

[10] T. Xu, H. Lei, C. S. Xie, Mater. Des. 24 (2003) 227–230.

[11] K. Nakamura, S. Shimizu, S. Umemoto, A. Thierry, B. Lotz, N. Okui, Polym. J. 40 (2008) 915–922.

[12] B. Krause, M. Stephan, S. Volkland, D. Voigt, L. Häußler, H. Dorschner, J. Appl. Polym. Sci. 99 (2006) 260–265.

[13] D. Auhl, J. Stange, H. Münstedt, B. Krause, D. Voigt, A. Lederer, U. Lappan, K. Lunkwitz, Macromolecules 37 (2004) 9465–9472.

[14] S. Zhou, W. Wang, Z. Xin, S. Zhao, Y. Shi, J. Mater. Sci. 51 (2016) 5598–5608.

[15] J. Tian, W. Yu, C. Zhou, Polymer 47 (2006) 7962–7969.

[16] J. Tian, W. Yu, C. Zhou, J. Appl. Polym. Sci. 104 (2007) 3592–3600.

[17] A. Eckstein, J. Suhm, C. Friedrich, R.-D. Maier, J. Sassmannshausen, M. Bochmann, R. Mülhaupt, Macromolecules 31 (1998) 1335–1340.

[18] S. Zhou, S. Zhao, Z. Xin, W. Wang, J. Macromol. Sci. Part B Phys. 53 (2014) 1695–1714.

[19] S. Zhou, S. Zhao, Z. Xin, Polym. Eng. Sci. 55 (2015) 251–259.

[20] H. Sinn, W. Kaminsky, Adv. Organomet. Chem. 18 (1980) 99–149.

[21] P. J. Deslauriers, M. P. McDaniel, J. Polym. Sci. Part A: Polym. Chem. 45 (2007) 3135–3149.

[22] M. P. McDaniel, D. C. Rohlfing, E. A. Benham, Polym. React. Eng. 11 (2003) 101–132.

[23] H. H. Brintzinger, D. Fischer, R. Mülhaupt, B. Rieger, R. M. Waymouth, Angew. Chemie Int. Ed. English. 34 (1995) 1143–1170.

[24] L. J. Irwin, J. H. Reibenspies, S. A. Miller, J. Am. Chem. Soc. 126 (2004) 16716–16717.

[25] L. K. Johnson, C. M. Killian, M. Brookhart, J. Am. Chem. Soc. 117 (1995) 6414–6415.

[26] S. Matsui, T. Fujita, Catal. Today. 66 (2001) 63–73.

[27] G. Natta, P. Pino, P. Corradini, F. Danusso, G. Moraglio, E. Mantica, G. Mazzanti, J. Am. Chem. Soc. 77 (1955) 1708–1710.

[28] J. P. Hermans, P. Henrioulle, US 3769233, 1973.

[29] P. Corradini, V. Barone, R. Fusco, G. Guerra, Eur. Polym. J. 15 (1979) 1133–1141.

[30] N. Bahri-Laleh, A. Correa, S. Mehdipour-Ataei, H. Arabi, M. N. Haghighi, G. Zohuri, L. Cavallo, Macromolecules 44 (2011) 778–783.

[31] T. C. M. Chung, Functionalization of polyolefins, Elsevier, 2002.

[32] J.-Y. Dong, Y. Hu, Coord. Chem. Rev. 250 (2006) 47–65.

[33] J. M. Santos, M. R. Ribeiro, M. F. Portela, S. G. Pereira, T. G. Nunes, A. Deffieux, Macromol. Chem. Phys. 202 (2001) 2195–2201.

[34] K. Hakala, B. Löfgren, T. Helaja, Eur. Polym. J. 34 (1998) 1093–1097.

[35] S. Paavola, B. Löfgren, J. V. Seppälä, Eur. Polym. J. 41 (2005) 2861–2866.

[36] P. Aaltonen, G. Fink, B. Löfgren, J. Seppälä, Macromolecules 29 (1996) 5255–5260.

[37] L. Zhong, G. Li, G. Liang, H. Gao, Q. Wu, Macromolecules 50 (2017) 2675–2682.

[38] L. Guo, W. Liu, C. Chen, Mater. Chem. Front. 1 (2017) 2487–2494.

[39] J. Imuta, Y. Toda, N. Kashiwa, Chem. Lett. 30 (2001) 710–711.

[40] T. C. Chung, D. Rhubright, Macromolecules 24 (1991) 970–972.

[41] H. L. Lu, T. C. Chung, J. Polym. Sci. Part A: Polym. Chem. 37 (1999) 4176–4183.

[42] P. F. Fu, T. J. Marks, J. Am. Chem. Soc. 117 (1995) 10747–10748.

[43] T. C. Chung, G. Xu, Y. Lu, Y. Hu, Macromolecules 34 (2001) 8040–8050.

[44] W. Lin, J. Dong, T. C. M. Chung, Macromolecules 41 (2008) 8452–8457.

[45] C.-L. Zhang, Y.-X. Wu, X. Xu, Y. Li, L. Feng, G.-Y. Wu, J. Polym. Sci. Part A: Polym. Chem. 46 (2008) 936–946.

[46] T. Shiono, K. Soga, Macromolecules 25 (1992) 3356–3361.

[47] T. Shiono, K. Yoshida, K. Soga, Makromol. Chem. Rapid Commun. 11 (1990) 169–175.

[48] T. Shiono, K. Hiroki, S. Kazuo, Macromol. Chem. Phys. 193 (1992) 2751–2761.

[49] B. De Roover, M. Sclavons, V. Carlier, J. Devaux, R. Legras, A. Momtaz, J. Polym. Sci. Part A: Polym. Chem. 33 (1995) 829–842.

[50] D. Shi, J. Yang, Z. Yao, Y. Wang, H. Huang, W. Jing, J. Yin, G. Costa, Polymer 42

(2001) 5549–5557.

[51] Z. M. Wang, H. Hong, T. C. Chung, Macromolecules 38 (2005) 8966–8970.

[52] M. F. Diop, J. M. Torkelson, Macromolecules 46 (2013) 7834–7844.

[53] N. V. Bhat, D. J. Upadhyay, J. Appl. Polym. Sci. 86 (2002) 925–936.

[54] S. Guimond, I. Radu, G. Czeremuszkin, D. J. Carlsson, M. R. Wertheimer, Plasmas Polym. 7 (2002) 71–88.

[55] L. F. Macmanus, M. J. Walzak, N. S. Mcintyre, J. Polym. Sci. Part A: Polym. Chem. 37 (1999) 2489–2501.

[56] J. K. Shim, H. S. Na, Y. M. Lee, H. Huh, Y. C. Nho, J. Memb. Sci. 190 (2001) 215–226.

[57] H. Ku, H. Wang, N. Pattarachaiyakoop, M. Trada, Compos. Part B Eng. 42 (2011) 856–873.

[58] N. M. Stark, R. E. Rowlands, Wood Fiber Sci. 35 (2003) 167–174.

[59] P. Toro, R. Quijada, M. Yazdani-Pedram, J. L. Arias, Mater. Lett. 61 (2007) 4347–4350.

[60] H.-P. Schlumpf, Kunststoffe 73 (1983) 511–515.

[61] S.-Y. Fu, B. Lauke, E. Mäder, C.-Y. Yue, X. Hu, Compos. Part: A Appl. Sci. Manuf. 31 (2000) 1117–1125.

[62] S. N. Maiti, K. K. Sharma, J. Mater. Sci. 27 (1992) 4605–4613.

[63] G. Guerrica-Echevarría, J. I. Eguiazábal, J. Nazábal, Eur. Polym. J. 34 (1998) 1213–1219.

[64] S. N. Maiti, P. K. Mahapatro, Int. J. Polym. Mater. Polym. Biomater. 14 (1990) 205–222.

[65] S. C. Tjong, S. A. Xu, R. K.-Y. Li, Y.-W. Mai, Compos. Sci. Technol. 62 (2002)

831–840.

[66] Y. Yokoyama, T. Ricco, Polymer 39 (1998) 3675–3681.

[67] S. Wu, Polymer 26 (1985) 1855–1863.

[68] T. McNally, P. McShane, G. M. Nally, W. R. Murphy, M. Cook, A. Miller, Polymer 43 (2002) 3785–3793.

[69] J. E. Stamhuis, Polym. Compos. 5 (1984) 202–207.

[70] M. Denac, V. Musil, I. Šmit, Compos. Part A: Appl. Sci. Manuf. 36 (2005) 1282–1290.

[71] Z.-Q. Fan, Y.-Q. Zhang, J.-T. Xu, H.-T. Wang, L.-X. Feng, Polymer 42 (2001) 5559–5566.

[72] T. Ogizawa, Nippon GOMU KYOKAISHI. 72 (1999) 519–525.

[73] E. Manias, A. Touny, L. Wu, K. Strawhecker, B. Lu, T. C. Chung, Chem. Mater. 13 (2001) 3516–3523.

[74] Q. Zhang, Q. Fu, L. Jiang, Y. Lei, Polym. Int. 49 (2000) 1561–1564.

[75] Z. M. Wang, H. Nakajima, E. Manias, T. C. Chung, Macromolecules 36 (2003) 8919–8922.

[76] Y. Kojima, A. Usuki, M. Kawasumi, A. Okada, Y. Fukushima, T. Kurauchi, O. Kamigaito, J. Mater. Res. 8 (1993) 1185–1189.

[77] Y. Tang, Y. Hu, L. Song, R. Zong, Z. Gui, Z. Chen, W. Fan, Polym. Degrad. Stab. 82 (2003) 127–131.

[78] Y. Fukushima, S. Inagaki, J. Incl. Phenom. 5 (1987) 473–482.

[79] M. A. L. Manchado, L. Valentini, J. Biagiotti, J. M. Kenny, Carbon N. Y. 43 (2005) 1499–1505.

[80] F. Du, R. C. Scogna, W. Zhou, S. Brand, J. E. Fischer, K. I. Winey, Macromolecules

37 (2004) 9048–9055.

[81] P.-C. Ma, M.-Y. Liu, H. Zhang, S.-Q. Wang, R. Wang, K. Wang, Y.-K. Wong, B.-Z. Tang, S.-H. Hong, K.-W. Paik, J.-K. Kim, ACS Appl. Mater. Interfaces. 1 (2009) 1090–1096.

[82] Z. Han, A. Fina, Prog. Polym. Sci. 36 (2011) 914–944.

[83] M. Garcia, G. V. Vliet, S. Jain, B. A. G. Schrauwen, A. Sarkissov, W. E. V. Zyl, B. Boukamp, Rev. Adv. Mater. Sci. 6 (2004) 169–175.

[84] M. Bailly, M. Kontopoulou, K. El Mabrouk, Polymer 51 (2010) 5506–5515.

[85] R. Watanabe, M. Kunioka, J. Mizukado, H. Suda, H. Hagihara, Polymer 99 (2016) 63–71.

[86] V. N. Dougnac, R. Alamillo, B. C. Peoples, R. Quijada, Polymer. 51 (2010) 2918–2926.

[87] D. N. Bikiaris, G. Z. Papageorgiou, E. Pavlidou, N. Vouroutzis, P. Palatzoglou, G. P. Karayannidis, J. Appl. Polym. Sci. 100 (2006) 2684–2696.

[88] E. Kluenker, J. Faymonville, K. Peter, M. Moeller, C. Hopmann, Polymer 55 (2014) 5370–5380.

[89] O. H. Lin, H. M. Akil, Z. A. M. Ishak, Polym. Compos. 32 (2011) 1568–1583.

[90] X. Li, Z. Cao, Z. Zhang, H. Dang, Appl. Surf. Sci. 252 (2006) 7856–7861.

[91] G. Z. Papageorgiou, D. S. Achilias, D. N. Bikiaris, G. P. Karayannidis, Thermochim. Acta. 427 (2005) 117–128.

[92] L. Xie, X. Liang, H. Huang, L. Yang, F. Zhang, X. Li, Z. Luo, RSC Adv. 9 (2019) 1123–1133.

[93] M. Z. Rong, M. Q. Zhang, S. L. Pan, K. Friedrich, (2003).

[94] W. Yuan, F. Wang, Z. Chen, C. Gao, P. Liu, Y. Ding, S. Zhang, M. Yang, Polymer

151 (2018) 242–249.

[95] P. Chammingkwan, M. Toyonaga, T. Wada, M. Terano, T. Taniike, Compos. Sci. Technol. 165 (2018) 183–189.

[96] Y. Fukuyama, T. Kawai, S. Kuroda, M. Toyonaga, T. Taniike, M. Terano, J. Therm. Anal. Calorim. 113 (2013) 1511–1519.

[97] T. Taniike, M. Toyonaga, M. Terano, Polymer 55 (2014) 1012–1019.

[98] M. Toyonaga, P. Chammingkwan, M. Terano, T. Taniike, Polymers 8 (2016) 300–312.

[99] H. Kim, Y. Miura, C. W. MacOsko, Chem. Mater. 22 (2010) 3441–3450.

[100] B. Maira, K. Takeuchi, P. Chammingkwan, M. Terano, T. Taniike, Compos. Sci. Technol. 165 (2018) 259–265.

[101] K. Sato, A. Ijuin, Y. Hotta, Ceram. Int. 41 (2015) 10314–10318.

[102] K. Kaneko, N. Yadav, K. Takeuchi, B. Maira, M. Terano, T. Taniike, Compos. Sci. Technol. 102 (2014) 120–125.

Chapter 2

Synthesis of Polypropylene Functionalized with a Trace Amount of Silicon Alkoxy Groups Based on Copolymerization using Ziegler-Natta Catalyst

Abstract

The functionalization of polypropylene (PP) by means of copolymerization with a polar comonomer using a Ziegler-Natta (ZN) catalyst is challenging due to the serious deactivation of the catalyst from heteroatoms. In this chapter, I propose a novel concept of a trace functionalization. Five alkoxysilanes having different alkoxy groups and spacer lengths were copolymerized with PP by means of copolymerization using a ZN catalyst. Subsequently, the effects of polymerization conditions on the catalytic activity and comonomer insertion were investigated, followed by the evaluation of physical properties of the obtained functionalized PP. It was found that a trace functionalization of PP was achieved using a comonomer having a long spacer and a non-bulky alkoxy groups, besides there was no significant deactivation when synthesized under the suitable polymerization conditions. The functionalized PP with a trace amount of reactive silicon alkoxy groups not only showed the similar melting point and crystallinity as homoPP, but also reacted with each other during melt mixing to generate a partial long-chain branched structure, resulting in enhanced strength and modulus.

2.1. Introduction

Polypropylene (PP), a crystalline polymer, is one of the most widely used plastics due to its low-cost, well-balanced properties and excellent moldability. On the other hand, the inertness of PP due to the absence of polar functional groups lead to poor adhesion and compatibility with other materials. To address this challenge, many research has been conducted on the introduction of polar functional groups into PP [1-13].

The strategies for introducing polar functional groups into PP include post-treatment using radicals [2,3], reactive intermediate [4-6], chain transfer reaction [7,8], and copolymerization [9-13]. In industry, post-treatment strategy is often adopted because of its simplicity. In fact, a maleic anhydride-grafted PP, which is particularly famous among functionalized PPs, is produced by this strategy. The strategy through reactive intermediate is a method in which a less poisonous functional group such as a borane group is temporarily introduced into PP chain and subsequently converted into a desired functional group [4,5]. There is also a method in which a polar functional group is covered with a temporary protecting group and a functionalized PP is obtained by subsequent deprotection treatment [6]. Although these methods have an advantage which can be applied to various functional groups, but they are not versatile because they require a plurality of steps. In the strategy using chain transfer reaction, it is necessary to limit the conditions in order to control the reaction, and as a result, the yield is extremely low [7]. On the other hand, a copolymerization strategy can be considered as one of the simple ways for PP functionalization in terms of ease. However, since the catalysts generally used in PP synthesis such as a Ziegler-Natta (ZN) catalyst are Lewis acid, the unshared electron pair of heteroatoms contained in a polar monomer becomes a catalyst poison, and it dramatically reduces the activity. Although direct

polymerization is possible with some post-metallocene catalysts such as Brookhart catalyst using a late transition metal [14], generally it results into poor stereospecificity and is difficult to apply for PP. Therefore, in terms of the stereoregularity and physical properties, it is very important to be able to cope with a ZN catalyst.

In the viewpoint of the physical properties of a polymer, a typical functionalized PP prepared by copolymerization or reactive intermediate strategy has multi-point functional groups in its side chain. They inhibit the crystallization, greatly reducing the melting point and crystallinity. Gupta *et al*. copolymerized propylene with undecenyloxytrimethylsilane using a ZN catalyst and treated with HCl to obtain side-functionalized PP. Unfortunately, the introduction of only 0.4 mol% functional groups has already caused deteriorations in melting point and crystallinity [11]. In the post-treatment strategy using radicals, the radicals also cause the main chain scission, leading to deteriorations in molecular weight and physical properties. Degradation of physical properties is sometimes a major problem because it expenses some of the advantages of PP. On the other hand, in the case of functionalization using a chain transfer reaction, the amount of the functional group is limited by selective introduction of the functional group at the terminal, inhibiting the deterioration of polymer, but the molecular weight is limited for the chain transfer reaction. Therefore, limiting the amount of the functional group can be effective way to maintain the physical properties of PP.

To overcome these issues, I propose a novel concept using a trace functionalization of PP. By limiting the amount of a polar monomer will simultaneously solve the catalyst deactivation in a copolymerization and degradation of physical properties [13]. In a sense, such a side-functionalized PP with a trace amount of functional groups can be

expected to behave like an end-functionalized PP. However, the functionalization using copolymerization in a ZN catalyst has not been studied well and is poorly understood due to the problem of deactivating active sites by polar groups. In this chapter, I investigated the possibility of copolymerization of propylene with polar monomers using a ZN catalyst, and discussed the mechanism. Specifically, five alkoxysilanes having two types of alkoxy groups and different spacer lengths between the olefinic double bond and alkoxy group were selected. These alkoxysilanes were used as comonomers and copolymerized with PP using a fifth generation ZN catalyst. Furthermore, the effect of polymerization conditions was investigated in a functionalized PP with a trace amount of silicon trimethoxy group that could incorporate into PP. Finally, the crystallization behavior and mechanical properties of the functionalized PP were investigated and the structure was discussed.

2.2. Experimental

2.2.1. Materials

Propylene of a polymerization grade was donated by Japan Polypropylene Corporation and used as delivered. Vinylmethyldimethoxysilane (VMDMS), (7-octen-1-yl)trimethoxysilane (OTMS), vinyltriethoxysilane (VTES), allyltriethoxysilane (ATES), and 5-hexenyltriethoxysilane (HTES) were used as comonomers without further purification. A $TiCl_4/MgCl_2$ Ziegler-Natta (ZN) catalyst containing diether as an internal donor was prepared based on our previous publication [15]. Triethylaluminum (TEA, donated by Tosoh Finechem Corporation) was used as an activator. *n*-Heptane as a polymerization solvent was dried over molecular sieve 4A. Octadecyl-3-(3,5-di-tert-butyl-4-hydroxyphenyl)propionate (AO-50, donated by ADEKA Corporation) was used as a stabilizer. Long-chain branched PP (LCBPP, MFI = 2.4 g/10 min at 230 °C/2.16 kg) was used after removing additives by reprecipitation (xylene/acetone).

2.2.2. Polymerization Test

PP-X copolymers (X is the comonomer) were synthesized by catalyzed polymerization of propylene with five types of comonomers with different alkoxy groups or/and spacers between double bond and silicon alkoxy groups. The polymerization was conducted in a 1 L stainless steel reactor using the ZN catalyst in a semi-batch mode. To the reactor that was exchanged with nitrogen, 500 mL of heptane, 15 mmol of TEA, and 10 mmol of a comonomer were introduced in this order. Subsequently, the solution was saturated with 0.5 MPa of propylene at 50 °C for 30 min. Followed by the introduction of 16 mmol of hydrogen (H_2), 50 mg of the catalyst was

injected to initiate the polymerization. The polymerization was continued for 60 min at 50 °C under the constant pressure of propylene, and terminated by depressurization. The supernatant of the reaction slurry was removed by decantation under nitrogen, and the remaining polymer powder was repetitively washed with ethanol and acetone. Thus obtained powder was finally purified by reprecipitation (xylene to acetone), followed by drying in *vacuo* at room temperature. As reference sample, homoPP was synthesized with 5 mmol of TEA (instead of 15 mmol) without a comonomer. Thereafter, in order to investigate the effect of polymerization conditions on catalytic performance for PP-OTMS synthsis, the polymerization conditions were changed as follow: Temperature (30–80 °C), TEA (5–45 mol), H_2 (0–33 mmol), and OTMS (5–45 mmol).

2.2.3. Film Preparation

PP-X copolymers (and homo PP) that were pre-impregnated with 1.0 wt% of AO-50 were melt-mixed using Micro Compounder MC5 (Xplore) at 185 °C and 100 rpm for 15 min under nitrogen atmosphere. The amount of sample was fixed at 3.675 g. During the melt mixing, the force value was recorded. After melt mixing, the extrudate was hot-pressed into films with a thickness of 200 μm at 230 °C under 20 MPa for 5 min, followed by quenching at 100 °C and subsequently at 0 °C. As reference sample, homoPP was melt-mixed in the presence of 1.0 wt% of LCBPP using the same procedure.

2.2.4. Characterizations

Impurities in the comonomers were analyzed by GC-MS (JEOL AccuTOF GCX) using a non-polar column (Agilent HP-5, 30 m × 0.32 mm × 0.25 μm) under helium gas flow

(99.9999% purity, 1.5 mL/min) at a sprit ratio of 10:1. Each comonomer was diluted with chloroform (infinity pure grade) and 2 μL of the solution was injected. The injection temperature was 250 °C, and the temperature of GC column was set at 50 °C for 2 min, subsequently raised to 300 °C at a rate of 10 °C/min, and held at 300 °C for 3 min. Ionization of the sample was treated by the chemical ionization (CI) method using methane as the reaction gas. Mass spectra were obtained in the range of m/z = 50–800 at a rate of 0.4 s per scan.

The primary structure of polymer samples was analyzed by NMR (Bruker 400 MHz) operated at 120 °C. About 60 mg of a polymer sample was dissolved in 0.2 mL of 1,1,2,2-tetrachloroethane-d_2 (internal lock and reference) and 0.5 mL of 1,2,4-trichlorobenzene (TCB) containing 0.006 wt% of 2,6-di-*tert*-butyl-4-methylphenol (BHT). The content of a comonomer was determined based on ^{1}H NMR (the number of scan = 1,000). The measurement for comonomers were performed using the same procedure, but 16 scans were accumulated instead of 1000.

Differential scanning calorimetry (DSC) measurements were performed on Mettler Toledo DSC 822 under nitrogen. About 8 mg of a film sample was placed in an aluminum pan, and heated to 230 °C at the heating rate of 20 °C/min. The melting temperature (T_m) and the crystallinity (X_c) were determined from the endotherm of the melting. After erasing the thermal history at 230 °C for 10 min, the sample was cooled down to 25 °C at the cooling rate of 20 °C/min for acquiring the crystallization temperature (T_c).

The crystalline structure of the film samples was evaluated by wide-angle x-ray diffraction (WAXD, Rigaku Smartlab). The Cu-Kα radiation was used at 40 kV and 30 mA. The measurements were performed in the range of 2θ = 5–45° with scan interval

0.02° at duration time 1 s. The fraction of β-form was determined using a standard equation [16]:

$$k = \frac{I_{(300)\beta}}{I_{(300)\beta} + I_{(110)\alpha} + I_{(040)\alpha} + I_{(130)\alpha}} \quad \text{Eq. (1),}$$

where $I_{(xyz)\sigma}$ is the intensity of a peak corresponding to the (x y z) plane of σ phase.

Tensile properties were measured using a tensile tester (Abecks Inc., Dat-100) at a crosshead speed of 1 mm/min at room temperature. Dumbbell-shaped specimens were cut out from a 200 μm-thick film. The listed data reported in this study correspond to the average over five or more specimens per sample.

2.3. Results and Discussion

In order to investigate the possibility of copolymerization of propylene with polar monomers using a ZN catalyst, five olefinic group containing alkoxysilanes were selected. The chemical structures of the alkoxysilanes are shown in Fig. 1. They can be broadly classified based on the kind of alkoxy groups, that are methoxy (OMe) and ethoxy (OEt) groups, respectively. Among each kind of alkoxysilane, the spacer length between the alkoxy groups and the olefinic bond was varied. Thus, with the selected comonomers, I tried to elucidate a general relationship between the structure of polar comonomers and polymerization performance of a ZN catalyst. According to the analysis by GC-MS (Figs. 2–6), the impurities in these alkoxysilanes were those in which the olefinic bond was replaced by a saturated bond (in VMDMS and VTES), those in which one of the substituents bonded to Si (including the olefinic bond) was replaced by a longer chain (in VMDMS and VTES), and/or those with different double bond positions (in OTMS and HTES). These impurities have a similar or lower level of poisoning effect than the main comonomers. Therefore, they were regarded as unimportant for the obtained results.

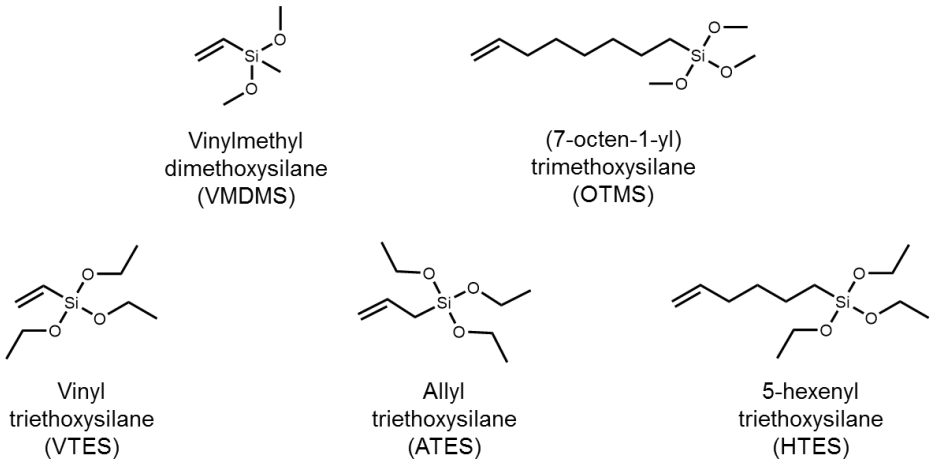

Fig. 1. Structure of comonomers.

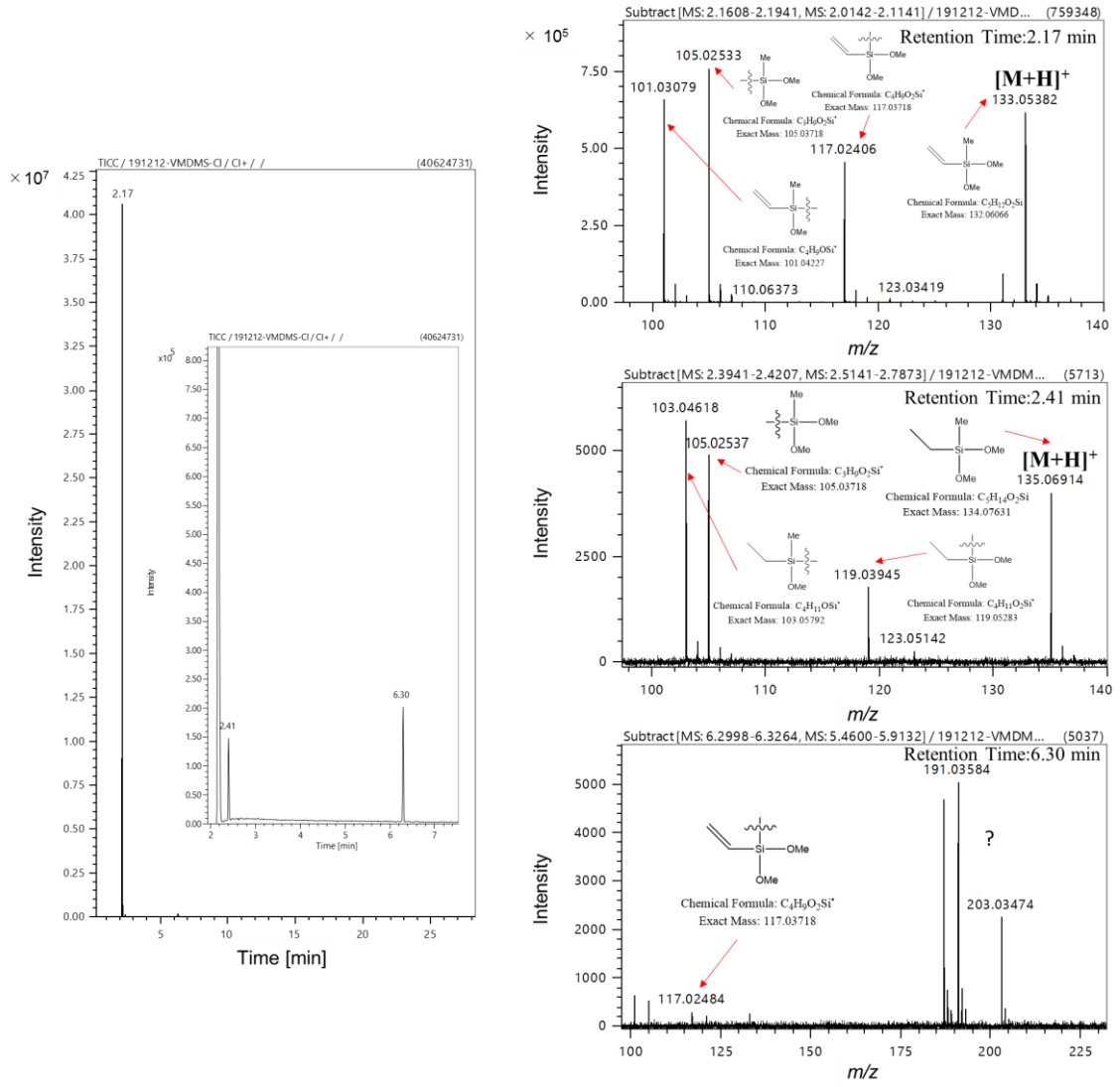

Fig. 2. GC chart of VMDMS and mass spectrum at each retention time. The expected structures were also shown. The impurity with a retention time of 6.30 min could not be analyzed, but its fragment pattern suggested that it has a longer chain instead of methyl group.

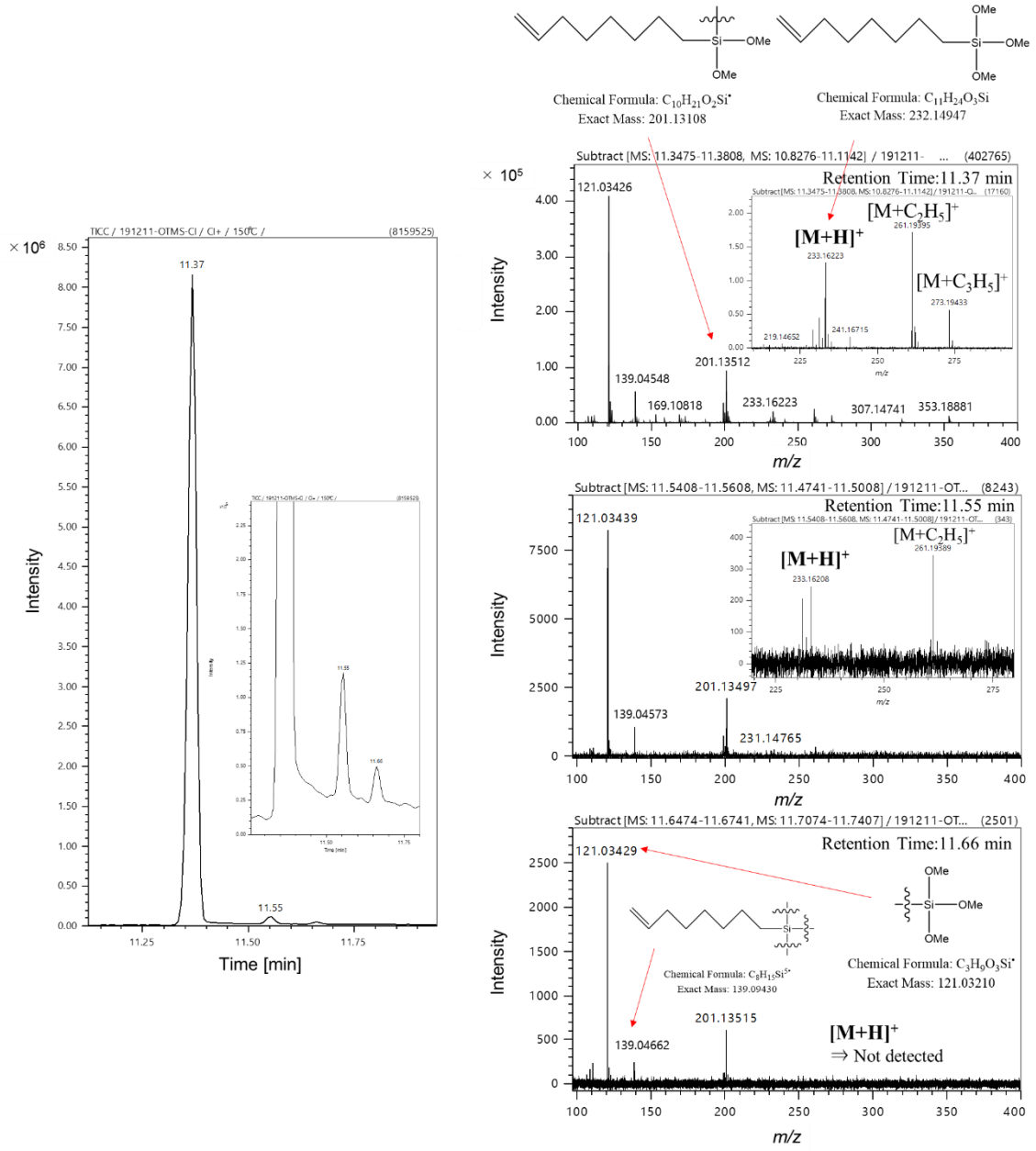

Fig. 3. GC chart of OTMS and mass spectrum at each retention time. The expected structures were also shown. It is presumed that the protonated molecular ions $[M+H]^+$ of the impurity with a retention time of 11.66 min was not detected due to its low content. The presence of the same mass molecular ion and fragment patterns at different retention time suggests that they are isomers with different double bond positions.

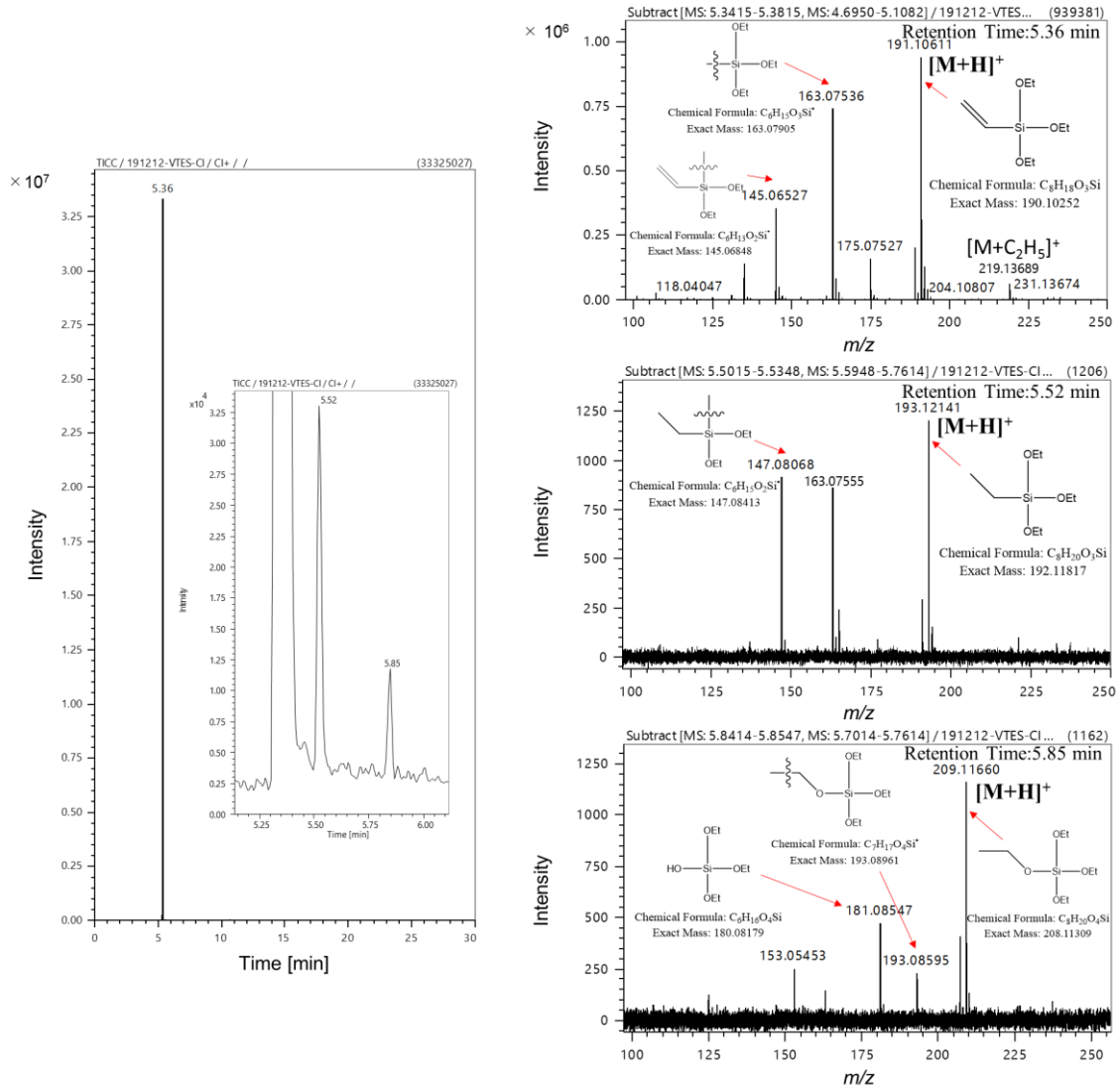

Fig. 4. GC chart of VTES and mass spectrum at each retention time. The expected structures were also shown.

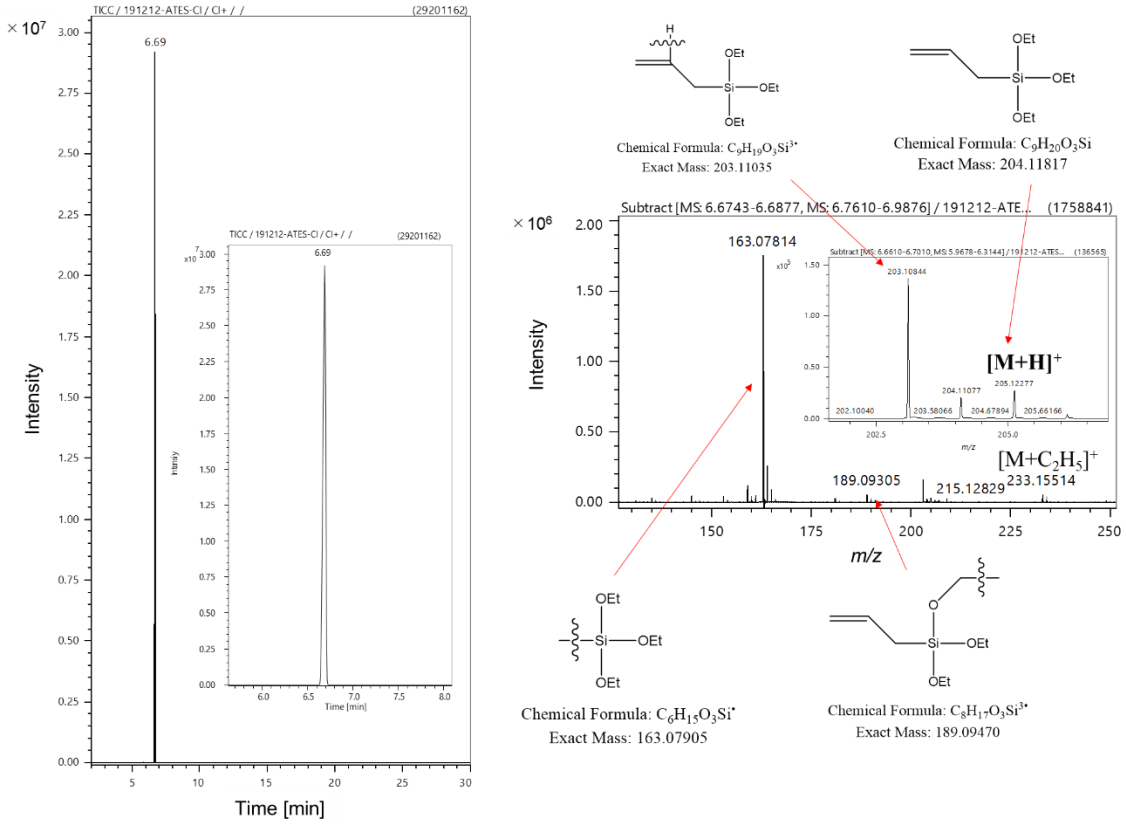

Fig. 5. GC chart of ATES and mass spectrum at retention time of 6.69 min. The expected structures were also shown. No impurities were detected.

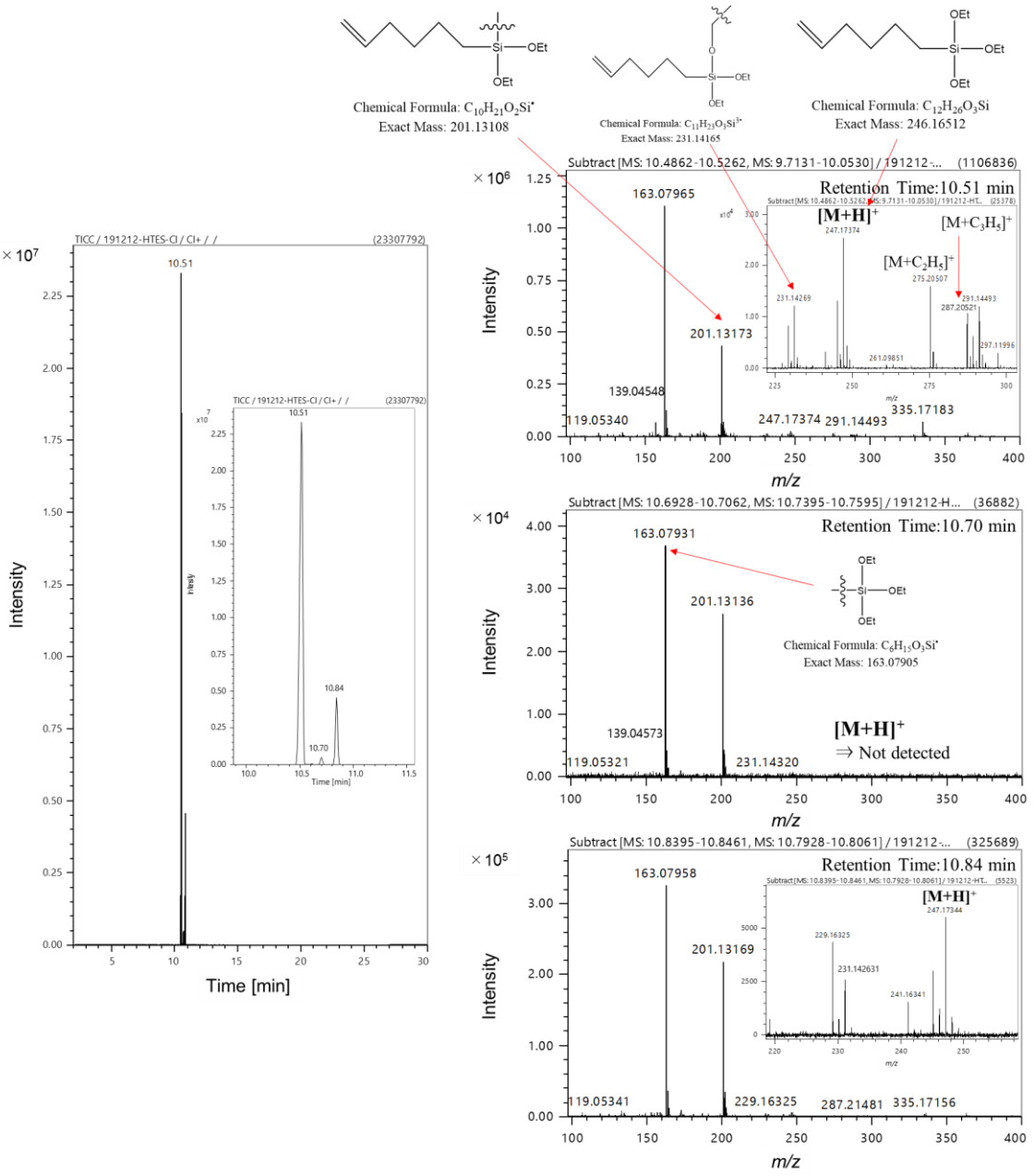

Fig. 6. GC chart of HTES and mass spectrum at each retention time. The expected structures were also shown. It is presumed that the protonated molecular ions $[M+H]^+$ of the impurity with a retention time of 10.70 min was not detected due to its low content. Similar to OTMS comonomer (*cf.* Fig. 3), the existence of isomers with different double bond positions was suggested.

The polymerization results of PP-X copolymers are summarized in Table 1. The activity of the catalyst was found to decrease by the addition of a comonomer. This can be attributed to the interactions between the alkoxy groups of a comonomer and the Lewis acid center(s) of the catalyst or the alkyl aluminum compound. These interactions were plausibly affected by the bulkiness of the alkoxy groups, as the catalytic activity was always higher in the copolymerization of alkoxysilanes with the OEt groups than that with the OMe groups, provided the spacer length was similar. In the case of comonomers with the same kind of alkoxy group, the activity of the catalyst was found to be strongly influenced by the spacer length; longer the spacer length, higher was the catalytic activity. This is because a long spacer would prevent the deactivation of the catalyst by keeping away the alkoxy groups from the metal center of the active site during olefin coordination.

Table 1. Synthesis of PP-X copolymers using various kinds of alkoxysilane [a]

Run	Sample	TEA [mmol]	Comonomer [mmol]	Activity [kg-polymer /mol-Ti·h·atm]	Comonomer content [b] [x 10^{-3} mol%]
1	HomoPP	5	n.a.	1260	n.a.
2	PP-VMDMS	15	10	19	Trace [c]
3	PP-OTMS	15	10	651	1.6
4	PP-VTES	15	10	434	Trace [c]
5	PP-ATES	15	10	743	Trace [c]
6	PP-HTES	15	10	1004	< 0.1 [c]

[a] Polymerization conditions: Propylene pressure = 0.5 MPa, heptane = 500 mL, t = 60 min, temperature 50 °C, H_2 = 16 mmol.

[b] Analyzed by ^{1}H NMR.

[c] Measured before reprecipitation.

The ^{1}H NMR spectra of PP-X samples are shown in Figs. 7–11 together with the spectrum of corresponding comonomers. In the case of comonomers, the peaks due to the OMe and the OEt groups are observed in the range of 3.5–4.0 ppm. However, except for PP-OTMS, in the NMR spectra of all other copolymers, these alkoxy peaks are hardly observed, even when the magnification was enlarged by 3000 times. The peak at δ = 3.7 ppm that is observed in PP-OTMS corresponds to the OMe groups, which was not affected by reprecipitation of the polymer in xylene/acetone. Also, the peaks due to the vinyl group (h, i, and j in Fig. 8) of the original comonomer were not observed in the NMR spectrum of PP-OTMS. These facts suggest that the OMe peak was likely due to the successful incorporation of the polar OTMS comonomer into PP chains. The OTMS content was calculated based on the ^{1}H NMR spectrum using the following equation,

$$\text{OTMS content} = \frac{H^{g}/9}{H^{m}} \times 100 \quad \text{Eq. (2),}$$

where H^{g} and H^{m} represent the peak areas of the OMe protons of incorporated OTMS and methine protons of polymer backbone. The OTMS content was determined as 1.6 × 10^{-3} mol%. As expected, this OTMS content is much smaller than that obtained in the ZN copolymerization of propylene with nonpolar monomers (*e.g.*, 1-hexene) [17], it was the first evidence for the successful insertion of the polar OTMS using a ZN catalyst. The successful insertion was plausibly due to the prevention of poisoning during the olefin coordination by the long spacer. This fact was also supported by the low catalytic activity and unsuccessful insertion of the VMDMS monomer in the copolymerization. On the other hand, in the case of comonomers with the OEt groups, though the catalytic activity was higher due to their less poisoning effect, the comonomer incorporation was found to be negligible due to the steric reasons. From the

above, it was found that even in a copolymerization using a ZN catalyst, a comonomer having both a long spacer and a non-bulky functional group can be incorporated into PP chains without significant deactivation.

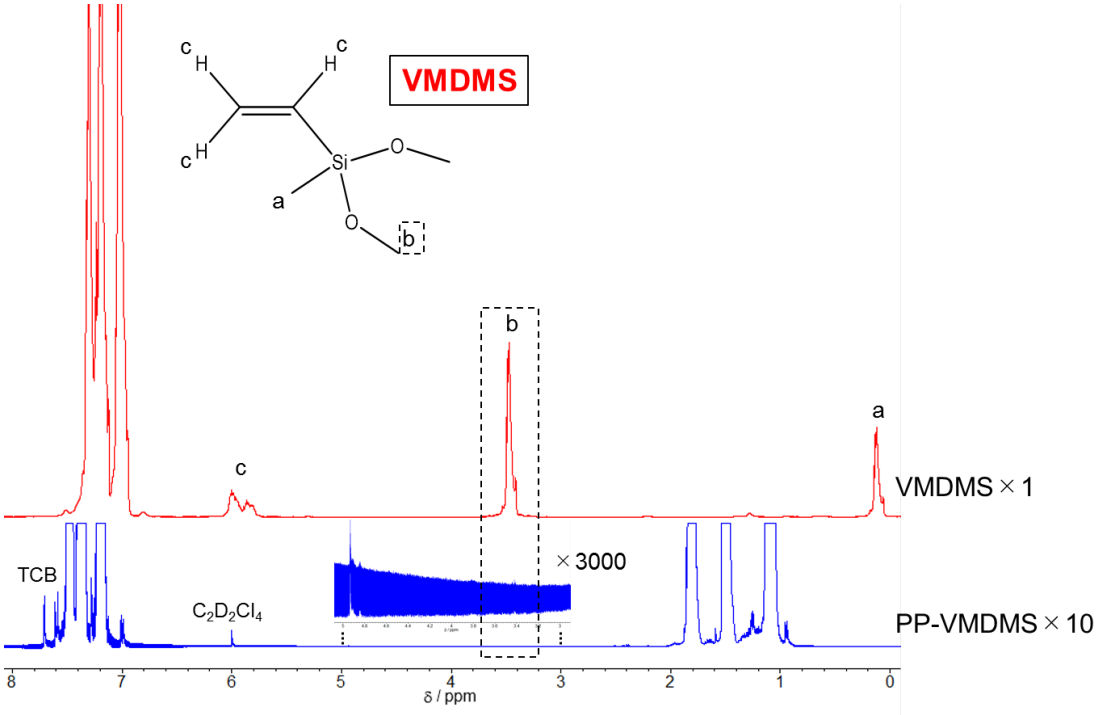

Fig. 7. ^{1}H NMR spectra of VMDMS and PP-VMDMS. The spectrum of PP-VMDMS was partially expanded for clarity.

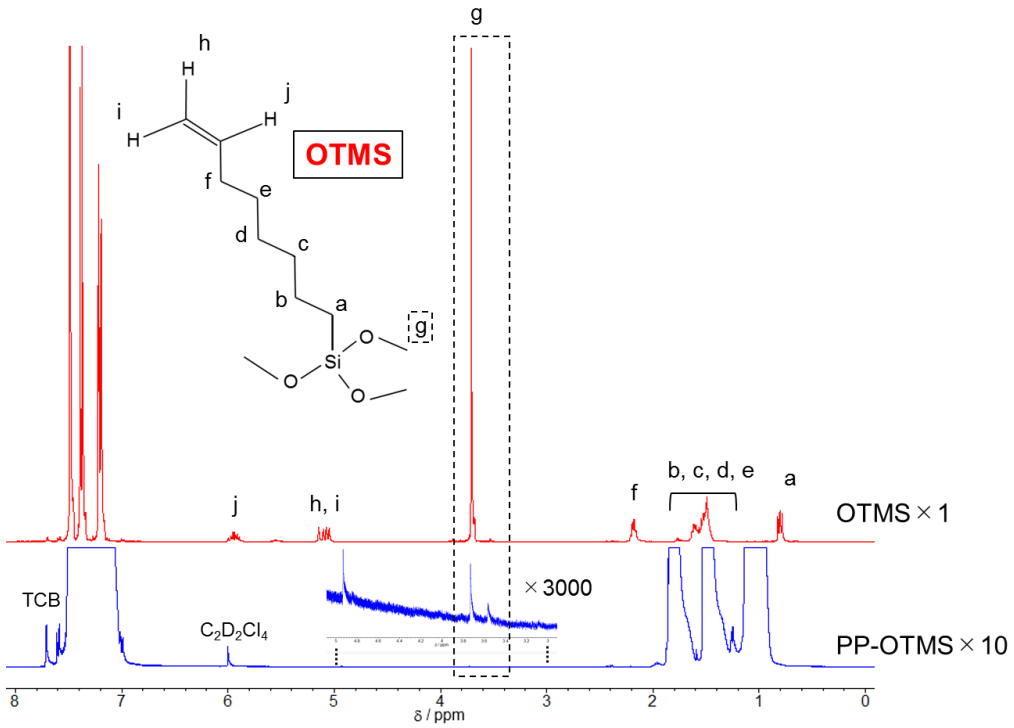

Fig. 8. ^{1}H NMR spectra of OTMS and PP-OTMS. The spectrum of PP-OTMS was partially expanded for clarity.

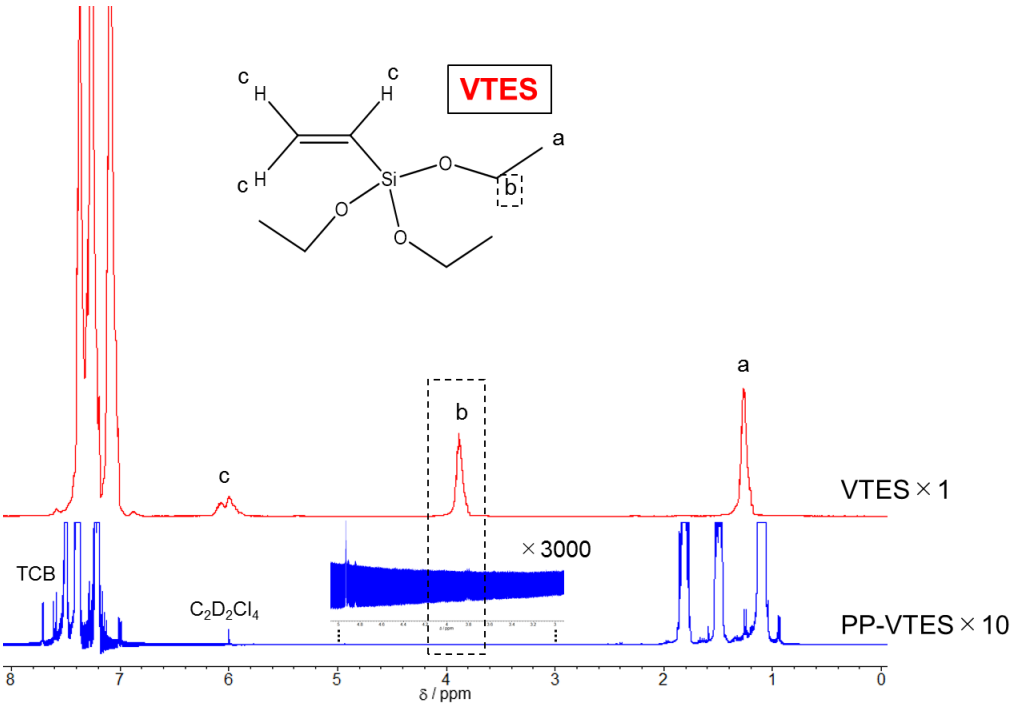

Fig. 9. ^{1}H NMR spectra of VTES and PP-VTES. The spectrum of PP-VTES was partially expanded for clarity.

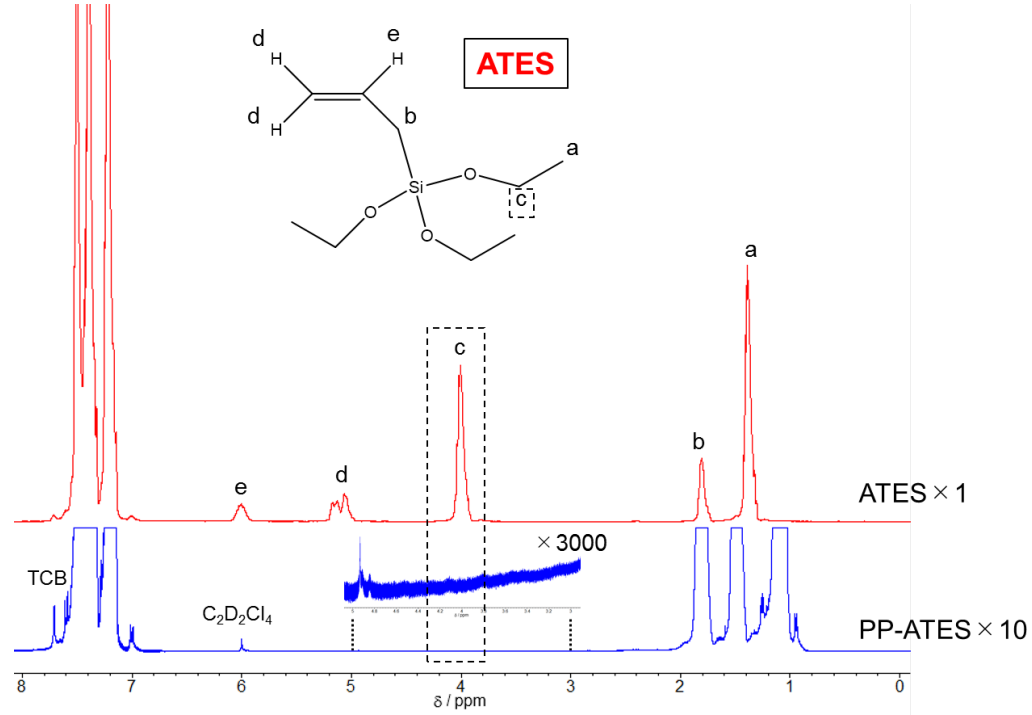

Fig. 10. ^{1}H NMR spectra of ATES and PP-ATES. The spectrum of PP-ATES was partially expanded for clarity.

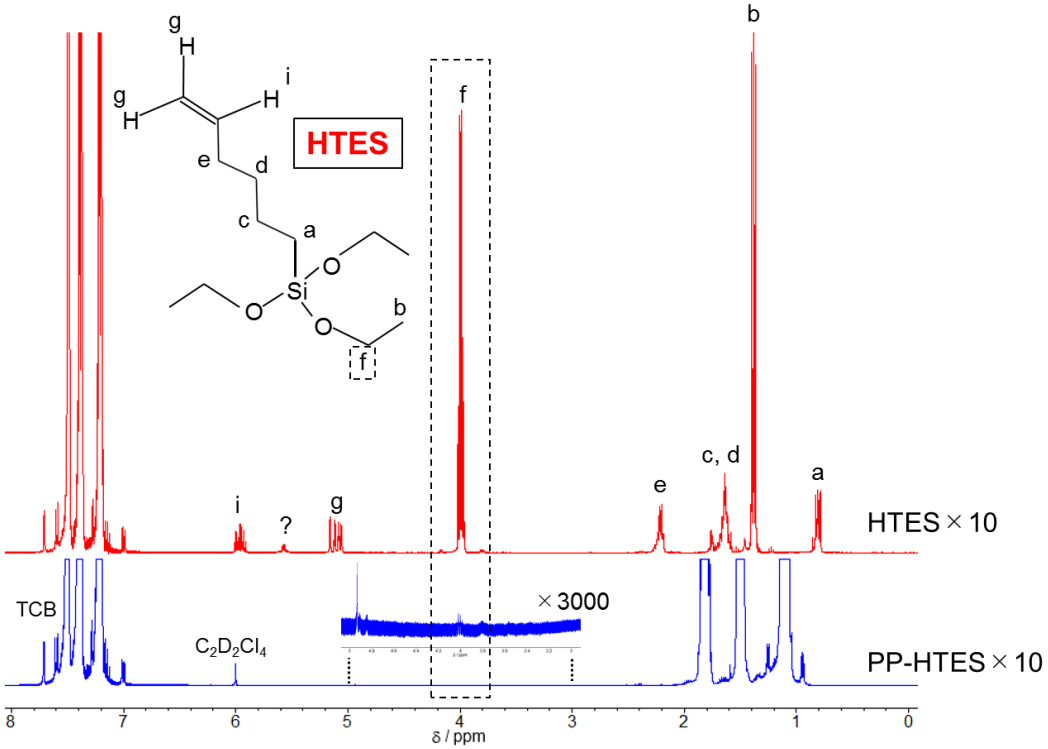

Fig. 11. ^{1}H NMR spectra of HTES and PP-HTES. The spectrum of PP-HTES was partially expanded for clarity.

In order to achieve the comonomer incorporation at a reasonable yield, it is important to understand the response of the catalyst at different polymerization conditions. Therefore, the dependence of the catalytic activity and the comonomer incorporation amount on temperature, co-catalyst (TEA), and H_2 addition amount were investigated. Table 2 is a summary of the polymerization results and Fig. 12 is the plot of the catalytic activity and OTMS content against the temperature. The polymerization temperature was changed in the range of 30 °C to 80 °C, and other polymerization conditions were fixed (Runs 7–12 in Table 2). The catalytic activity was found to be strongly dependent on the polymerization temperature and improved with the temperature up to 50 °C, plausibly due to temperature dependence of the rate constant. Thereafter, the activity quickly decreased with further increase of the temperature, plausibly due to catalyst deactivation by over reduction of Ti species and/or the enhanced poisoning effect of OTMS at a higher temperature. On the other hand, the OTMS content increased exponentially with the temperature and the exponential growth was not affected by the deactivation of the catalyst. This fact suggest that the insertion of OTMS during the polymerization would be less-selective and hardly affected by the state of activate sites.

Table 2. Synthesis of PP-OTMS under various polymerization conditions [a]

Run	Sample	Conditions			Activity	Comonomer
		Temp. [°C]	TEA [mmol]	H_2 [mmol]	[kg-polymer /mol-Ti·h·atm]	content [b] [x 10^{-3} mol%]
7	PP-OTMS	**30**	15	16	341	0.7
8		**40**	15	16	542	0.7
9		**50**	15	16	617	1.6
10		**60**	15	16	400	1.9
11		**70**	15	16	201	3.7 [c]
12		**80**	15	16	13	18.1 ± 1.9 [c]
13		50	**5**	16	49	8.3 ± 0.3
14		50	**15**	16	529	1.6 [d]
15		50	**25**	16	653	0.8
16		50	**35**	16	651	0.8
17		50	**45**	16	649	0.8
18		50	15	**0**	223	4.7
19		50	15	**4**	420	3.1
20		50	15	**8**	542	2.2
21		50	15	**16**	556	1.6 [d]
22		50	15	**33**	492	2.0

[a] Polymerization conditions: Propylene pressure = 0.5 MPa, heptane = 500 mL, t = 60 min, OTMS = 10 mmol.

[b] Analyzed by ^{1}H NMR.

[c] Some parts are not completely soluble in the solvent.

[d] Comonomer content expected similar to condition 10.

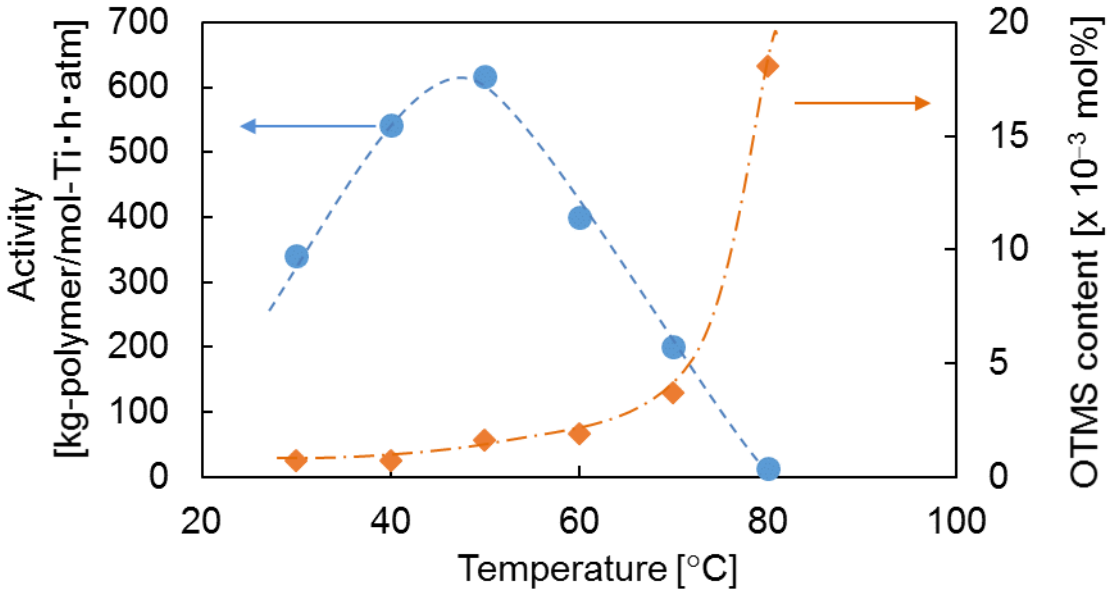

Fig. 12. The dependence of catalytic activity and OTMS content on the temperature.

Table 2 (Runs 13–17) and Fig. 13 show the TEA dependence of the catalytic activity and OTMS insertion in PP-OTMS synthesis. Both of them were highly dependent on the amount of TEA, especially at the initial stage. When PP-OTMS was produced with 5 mmol of TEA, an extremely less amount of polymer was obtained. Note that under the identical conditions, the activity in homopolymerization was 26 times higher. On increasing the amount of TEA up to 15 mmol, the activity dramatically improved. The activity improved further up to 25 mmol of TEA and reached a plateau. The lowest activity at the least TEA addition amount should be due to the insufficient activation of the catalyst, as most of the TEA would interact with OTMS as the masking agent [10,18]. Conversely, the OTMS content decreased with the increase of TEA amount *i.e.* with the increase of activity up to 25 mmol and remained at a minimum value above that. As explained earlier, the OTMS insertion would not be affected by the state of

active sites, the OTMS content was initially high at the low TEA amount due to a low polymer yield. It decreased with the increase of yield and reached a plateau with the minimum value when the yield level became constant.

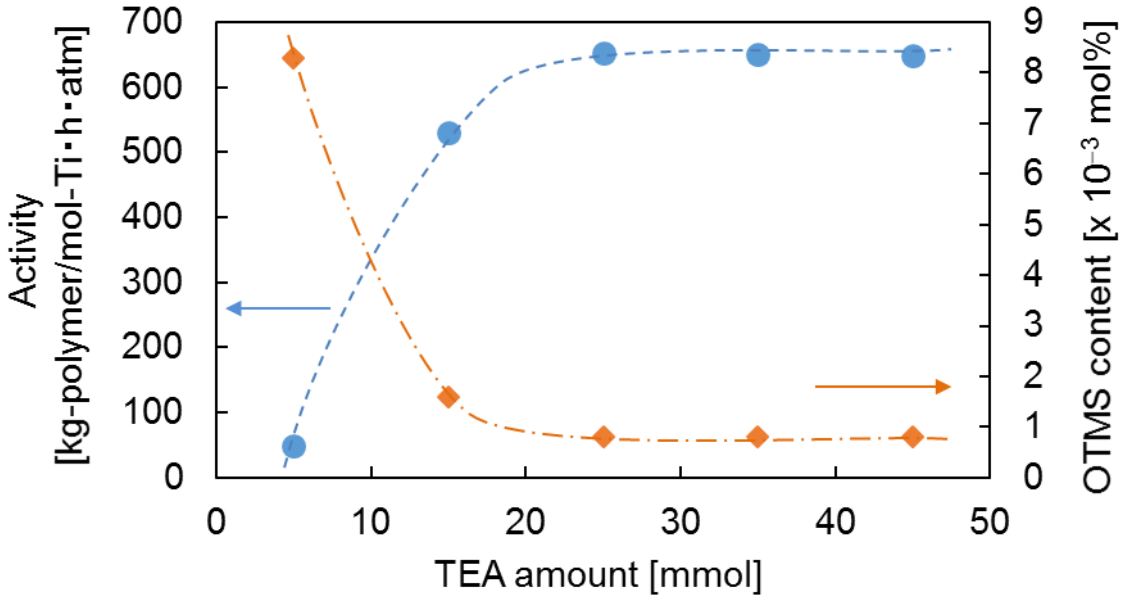

Fig. 13. The dependence of catalytic activity and OTMS content on the TEA addition amount.

H_2 functions as a chain transfer agent and is used in the industry to adjust the molecular weight of PP. Table 2 (Runs 18–22) and Fig. 14 show the H_2 dependence of the catalytic activity and OTMS insertion for PP-OTMS synthesis. The introduction of H_2 significantly improved the catalytic activity, and the introduction of 16 mmol of H_2 increased the activity up to 2.5 times than without H_2. The improvement in activity by the introduction of H_2 was regarded as the reactivation of dormant sites by the chain transfer reaction with H_2 as often seen in propylene polymerization. The slight decrease

in the activity at 33 mmol of H_2 is considered to be due to the decrease in propylene partial pressure by the high amount of H_2. Unfortunately, the improvement in activity by the addition of H_2 also sacrificed the OTMS insertion. This fact can be explained from the hypothesis of less-selective nature in OTMS insertion described above. Although the addition of H_2 accelerates the insertion of propylene, it is assumed that it does not affect the insertion of OTMS. In other words, the rate of propylene insertion would become faster in the presence of H_2. Thus, the OTMS content could decrease along with the H_2 amount. The slight increase in OTMS content at 33 mmol of H_2 seems plausible due to the increase in relative OTMS concentration by the decrease in the propylene concentration.

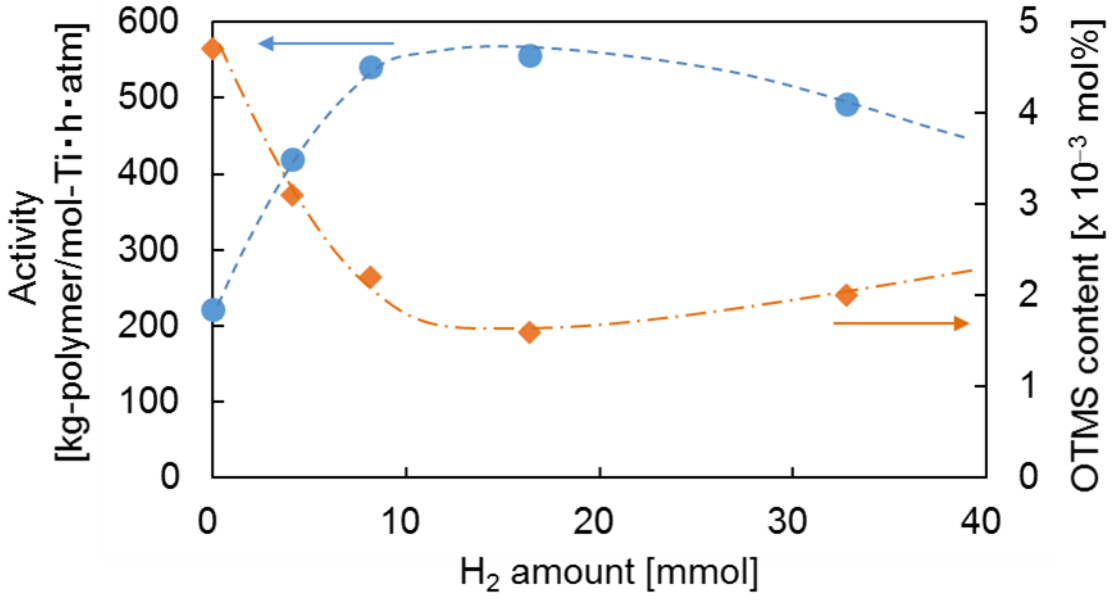

Fig. 14. The dependence of catalytic activity and OTMS content on the H_2 addition amount.

Finally, the effect of OTMS addition amount was investigated (Table 3). Note that PP-OTMSXX corresponds to the addition amount of XX mmol of OTMS. Since TEA is supposed to act both as a co-catalyst and a masking agent, when the molar amount of OTMS was increased, an equimolar amount of TEA was also added to ensure its masking effect. The plot of activity and OTMS content against the OTMS addition amount is shown Fig. 15. It was found that on increasing the OTMS amount, the activity decreased non-linearly. For instance, the increase in the OTMS amount by 4 times, sacrificed the activity of the catalyst by 90%. In contrast to the activity, the OTMS content increased non-linearly with the OTMS amount. For instance, the OTMS content of PP-OTMS40 was 12.0×10^{-3} mol%, 7.5 times higher than that of PP-OTMS10. These results can be explained as: On increasing the OTMS amount, both the coordination to metal centers through olefinic bond and through alkoxy groups should increase. The former would increase the OTMS incorporation, and the latter would decrease the activity.

Table 3. Synthesis of PP-OTMS at various OTMS amounts [a]

Run	Sample	TEA [mmol]	OTMS [mmol]	Activity [kg-polymer /mol-Ti·h·atm]	Comonomer content [b] [x 10^{-3} mol%]
1	HomoPP	5	n.a.	1260	n.a.
23	PP-OTMS5	10	5	279 [c]	0.9
3	PP-OTMS10	15	10	651	1.6
24	PP-OTMS30	35	30	169 ± 14	6.0
25	PP-OTMS40	45	40	64 ± 3	12.0

[a] Polymerization conditions: Propylene pressure = 0.5 MPa, heptane = 500 mL, t = 60 min, temperature = 50 °C, H_2 = 16 mmol.

[b] Analyzed by ^{1}H NMR.

[c] The low activity is due to aging of the catalyst (only for tensile test).

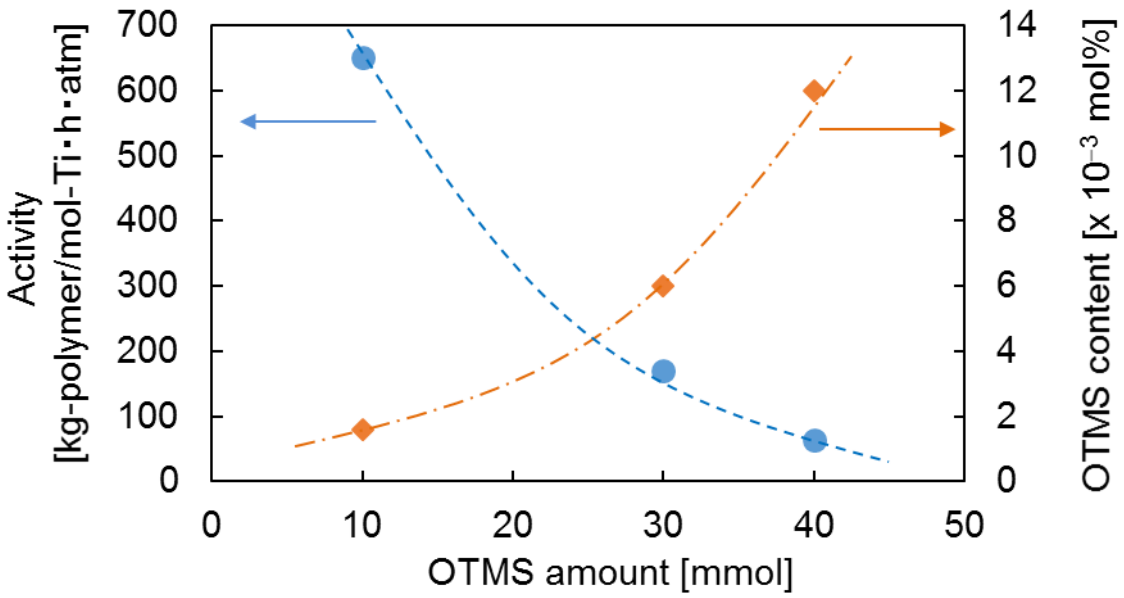

Fig. 15. The dependence of catalytic activity and OTMS content on the OTMS addition amount.

From the above, the behavior of a ZN catalyst in propylene copolymerization with a polar comonomer was studied under different polymerization conditions. It was found that both the catalytic activity and comonomer content were greatly affected by polymerization conditions. The catalytic activity and comonomer content are in a trade-off relationship, and hence it was difficult to simultaneously improve both. However, it was possible to obtain a sufficient amount of functionalized PP without serious deactivation by choosing appropriate the conditions.

In order to understand the effect of the incorporation OTMS groups into the PP chain, the thermal and mechanical properties were evaluated using a series of PP-OTMS (PP-OTMS10, 30 and 40) synthesized under the suitable polymerization conditions. The effect of OTMS on the melting and crystallization behaviors was evaluated by DSC. Fig. 16 shows the DSC thermograms of PP-OTMS, and the results are shown in Table 4 together with other melting and crystallization behavior data. The trace amount of OTMS did not deteriorate the melting point (T_m) and the crystallinity (X_c) of homoPP. It is noteworthy that a small peak was observed around 148 °C in the thermogram of the heating scan in all PP-OTMS samples. This peak could be ascribed to the formation of a small amount of β-form of PP. It is widely known that PP can take multiple crystal forms depending on processing conditions. Among them, only α- and β-forms can be observed under normal processing conditions. The T_m of isotactic PP in the α-form that is most common and stable is about 165 °C, and that in the β-form is about 150 °C [19]. The crystallization temperature (T_c) increased dramatically with the introduction of a trace amount of OTMS (PP-OTMS10). Further increase of the OTMS content slightly increase the T_c (PP-OTMS40). The increase in T_c seems to be due to the acceleration in the crystallization by the presence of OTMS groups itself or by the formation of long-chain branched (LCB) structure that is formed by the sol-gel reaction between two OTMS groups in the presence of residual water [20,21].

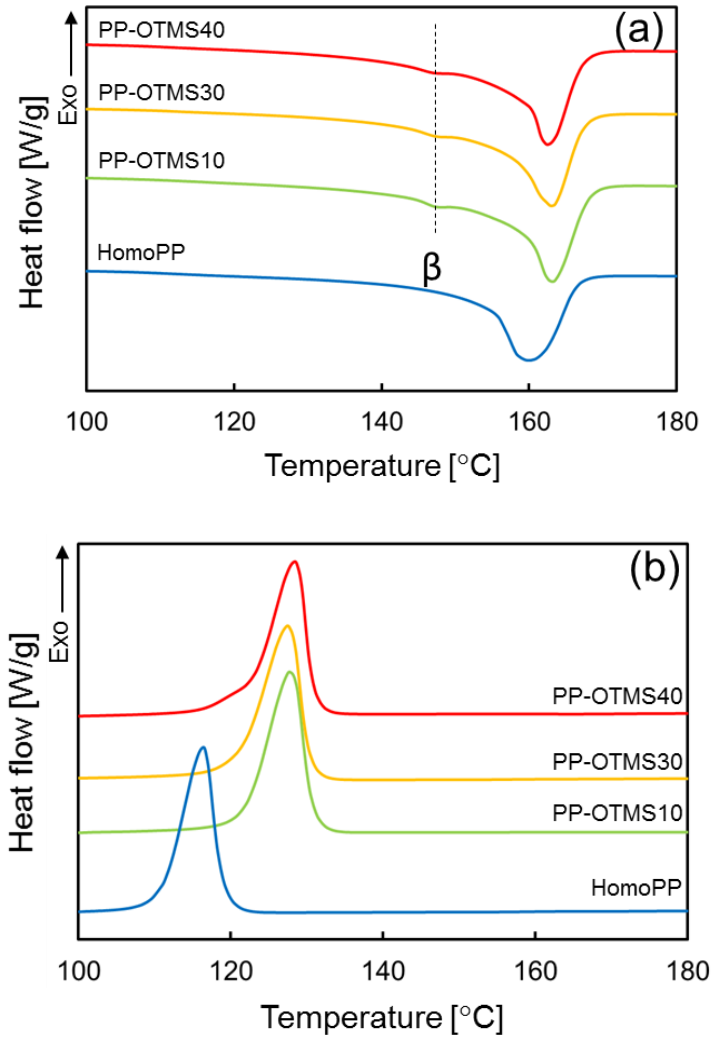

Fig. 16. DSC thermograms of PP-OTMS: a) heating scan and b) cooling scan.

Table 4. Melting and crystallization behaviors of PP-OTMS

Sample	OTMS [mmol]	H_2 [mmol]	Force [a] [N]	T_m [b] [°C]	X_c [b] [%]	T_c [b] [°C]	k [c] [%]
HomoPP	0	16	928	162	50	115	Only α
PP-OTMS10	10	16	868	164	53	126	5.9
PP-OTMS30	30	16	959	164	50	126	10.0
PP-OTMS40	40	16	1033	164	52	127	14.7
PP-OTMS	10	0	(3260) [d]	163	44	124	12.5
PP-OTMS	10	33	593	163	53	125	4.2

[a] Force value was recorded during melt mixing. The representative data was obtained just before taking out the extrudate.

[b] Determined by DSC.

[c] The β-form fraction among crystalline parts obtained from WAXD.

[d] Melt mixing was performed with half amount of the sample because the force value was too high for proper functioning of the extruder.

Additional studies for understanding the crystal structure of PP-OTMS were conducted by WAXD. Fig. 17 shows the WAXD patterns of PP-OTMS film samples. As shown in Fig. 17, in all the samples, the multiple peaks assigned to the α-form were observed. On the other hand, the PP-OTMS samples showed an additional peak at $2\theta = 15.8°$, which was attributed to the (3 0 0) diffraction of the β-form. The intensity at (3 0 0) peak appeared to increase along with the OTMS amount. Therefore, the β-form fraction (*k* value) was calculated using Eq. (1), and the results are shown in Table 4. The *k* value increased with the amount of OTMS, reaching up to 14.7% for PP-OTMS40. It is known that the β-form are generated when a specific nucleating agent is used such as amide compounds [22] or a specific environment is applied such as a temperature gradient [23] and a controlled shear [24]. The possibility of β-form generation by the *in-situ* formed LCB structure was confirmed by adding a small amount of commercial

LCBPP to homoPP. The WAXD pattern of homoPP/LCBPP blend is shown in Fig. 18. The small amount of LCBPP helped to generate the β-form. Therefore, PP-OTMS is likely to contain LCBPP partially. The increase in the force value along with the OTMS amount could be attributed to the formation of a relatively large amount of LCB structures. Furthermore, the effect of the force value to the *k* value was investigated using PP-OTMS prepared with different H_2 contents. The results of DSC and WAXD measurement of them are also summarized in Table 4. The amount of H_2 greatly affected the force value (which is associated with polymer melt viscosity), and the large force value gave the small X_c and large *k* value. It is presumed that the low mobility of the large molecular weight hinders crystallization in the cooling process during hot pressing, resulting in more unstable crystallization. From the above, it can be inferred that the increase in *k* value along with the OTMS contents is caused by the local increase in viscosity due to the *in-situ* formed LCBPP.

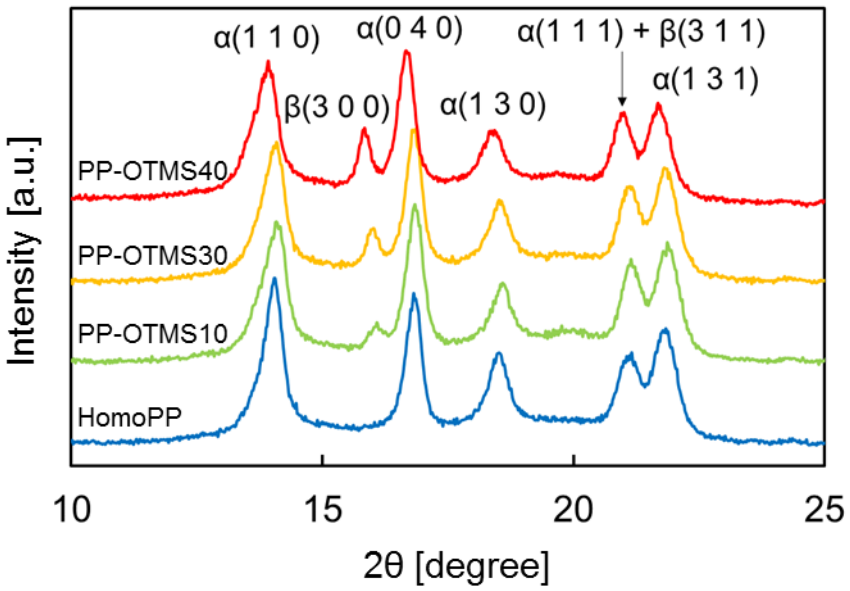

Fig. 17. WAXD patterns of PP-OTMS.

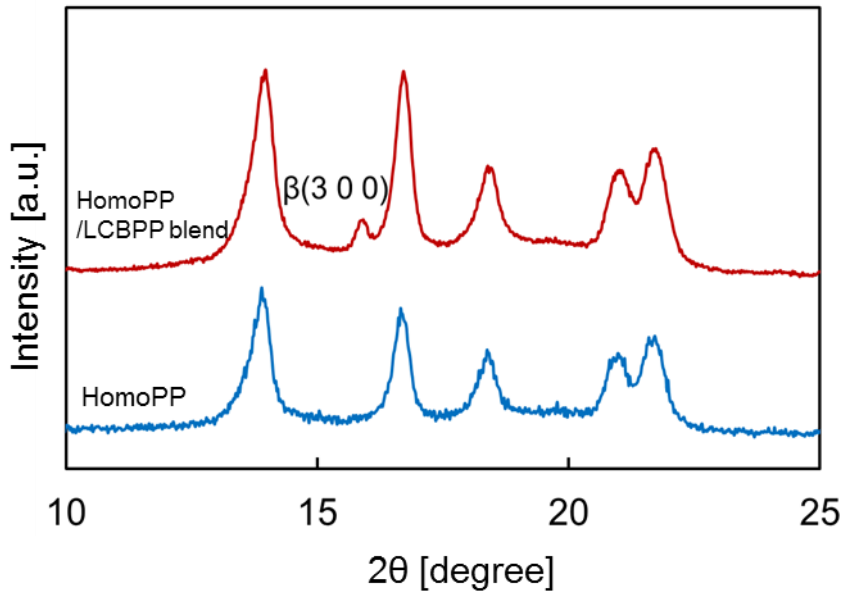

Fig. 18. WAXD patterns of homoPP and homoPP/LCBPP blend. The content of LCBPP is 1.0 wt%.

Uniaxial tensile tests were performed to investigate the mechanical properties of PP-OTMS. Table 5 summarize the results of the tensile tests of PP-OTMS with different OTMS contents. The introduction of a trace amount of OTMS into PP (up to PP-OTMS10) enhanced the yield strength and Young's modulus by 8% and 19%, respectively. Considering that β-form PP usually exhibit lower strength and modulus than α-form PP and that the X_c values were similar among PP-OTMS samples with different OTMS contents, these improvements should be attributed to the formation of the LCB structure. However, the further introduction of OTMS (PP-OTMS30 and PP-OTMS40) deteriorated the strength and modulus. In particular, the deterioration in PP-OTMS40 was severe enough to lose the almost all the benefits of the initial OTMS incorporation. As shown in Table 5, a dramatic increase in molecular weight decreases the strength and the modulus by inhibiting crystallization (*cf.* Table 4). Fortunately, the

increment in the force value in PP-OTMS30 and PP-OTMS40 did not change the X_c values, so the main cause of these deteriorations is presumed to be an increase in β-form fraction [25]. The reason for the temporary decrease and subsequent improvement in the elongation at break with increasing OTMS content was elucidated by *in-situ* SAXS measurements during stretching (there is no data in this chapter. Refer to the minor-research at the end of this dissertation). The formation of the initial trace amount of cross-linking point could worked as a stress concentrator, and the growth of the cross-linked structure suppressed the generation of voids by forming a physical cross-linked structure via multiple lamellae. From the above, it was found that an increase in the OTMS amount promoted the generation of β-form and decreases the benefits of mechanical properties provided by the LCB structures.

For the purpose of promoting the intermolecular reaction, PP-OTMS40 was melt-mixed at 215 °C instead of 185 °C, and ^{1}H NMR measurement and tensile test were performed. The OTMS contents calculated from the residual amount of OMe protons in PP-OTMS40 after melt mixing at 185 °C and 215 °C were 7.7 x 10^{-3} mol% and 6.1 x 10^{-3} mol%, respectively. The expansion of OMe consumption by increasing the mixing temperature suggests that the intermolecular reaction was promoted. The yield strength and Young's modulus of the PP-OTMS40 melt-mixed at 215 °C were 33.3 MPa and 682 MPa, respectively, which were higher than those melt-mixed at 185 °C (Table 5). These results indicate that the mechanical properties can be further enhanced by controlling the intermolecular reaction such as melt mixing conditions and molding conditions.

Table 5. Results of tensile tests of PP-OTMS [a]

Sample	OTMS [mmol]	H_2 [mmol]	Yield strength [MPa]	Young's modulus [MPa]	Elongation at break [%]
HomoPP	0	16	31.7 ± 0.5	611 ± 36	Non-breaking [b]
PP-OTMS5	5	16	32.1 ± 0.5	692 ± 30	35.7 ± 17.3
PP-OTMS10	10	16	34.1 ± 0.4	729 ± 40	61.0 ± 25.0
PP-OTMS30	30	16	33.6 ± 0.5	713 ± 40	Non-breaking [b]
PP-OTMS40	40	16	31.3 ± 0.3	641 ± 49	Non-breaking [b]
PP-OTMS40 (melt-mixed at 215 °C)	40	16	33.3 ± 0.5	682 ± 31	Non-breaking [b]
PP-OTMS	10	0	29.5 ± 0.6	520 ± 42	Non-breaking [b]
PP-OTMS	10	33	34.2 ± 0.5	753 ± 32	17.1 ± 2.8

[a] Tensile properties were determined as averages at least over 5 specimens.

[b] Includes multiple unbroken samples at the instrument limit of 470% strain.

2.4. Conclusions

In this chapter, copolymerization of propylene (PP) with five alkoxysilanes using a Ziegler-Natta (ZN) catalyst was carried out. Using OTMS with long spacers and non-bulky functional groups, it was possible to incorporate a polar comonomer into PP. The polymerization temperature, TEA, H_2, and OTMS addition amount all significantly influenced both the catalytic activity and comonomer content. By choosing the polymerization conditions appropriately, meaningful amount of OTMS could be incorporated without significant deactivation. The PP-OTMS seemed to react with each other to produce partially long-chain branched structures. The introduction of OTMS did not affect the melting point (T_m) or crystallinity (X_c), but it helped the generation of β-forms, and the additional OTMS increased the fraction of it. The introduction of a trace amount of OTMS (PP-OTMS10 and PP-OTMS30) greatly improved the yield strength and Young's modulus in the tensile test, but the increase in the introduction of OTMS groups suppressed these improvements (PP-OTMS40). In conclusion, it was possible to synthesize functionalized PP with a trace amount of polar functional groups using a ZN catalyst by selecting the comonomer and controlling polymerization conditions by means of copolymerization. This study will help to understand the functionalization of PP and contribute to the development of PP.

References

[1] J.-Y. Dong, Y. Hu, Coord. Chem. Rev. 250 (2006) 47–65.

[2] D. Shi, J. Yang, Z. Yao, Y. Wang, H. Huang, W. Jing, J. Yin, G. Costa, Polymer 42 (2001) 5549–5557.

[3] P. Chammingkwan, M. Toyonaga, T. Wada, M. Terano, T. Taniike, Comp. Sci. Techol. 165 (2018) 183–189.

[4] Z. M. Wang, H. Hong, T. C. Chung, Macromolecules 38 (2005) 8966–8970.

[5] T. C. Chung, D. Rhubright, Macromolecules 24 (1991) 970–972.

[6] T. C. M. Chung, Functionalization of Polyolefins, Academic Press, London (2002).

[7] T. Taniike, M. Toyonaga, M. Terano, Polymer 55 (2014) 1012–1019.

[8] H. Hagihara, T. Ishihara, H. T. Ban, T. Shiono, J. Polym. Sci. Part A: Polym. Chem. 46 (2008) 1738–1748.

[9] K. Hakala, B. Löfgren, T. Helaja, Eur. Polym. J. 34 (1998) 1093–1097.

[10] S. Paavola, B. Löfgren, J. V. Seppälä, Eur. Polym. J. 41 (2005) 2861–2866.

[11] S. Gupta, X. Yuan, T. C. M. Chung, M. Cakmak, R. A. Weiss, Polymer 55 (2014) 924–935.

[12] Y. Iizuka, J. Sugiyama, H. Hagihara, Macromolecules 42 (2009) 2321–2323.

[13] T. Nagai, P. Chammingkwan, M. Terano, T. Taniike, Curr. Trends Polym. Sci. 17 (2016) 59–69.

[14] L. K. Johnson, S. Mecking, M. Brookhart, J. Am. Chem. Soc. 118 (1996) 267–268.

[15] Y. Hiraoka, S. Y. Kim, A. Dashti, T. Taniike, M. Terano, Macromol. React. Eng. 4 (2010) 510–515.

[16] W. Wang, J. Wu, J. Appl. Polym. Sci. 135 (2018) 45887.

[17] T. Taniike, T. Funako, M. Terano, J. Catal. 311 (2014) 33–40.

[18] J. Chen, A. Motta, B. Wang, Y. Gao, T. J. Marks, Angew. Chem. 131 (2019) 7104–7108.

[19] Q.-F. Yi, X.-J. Wen, J.-Y. Dong, C. C. Han, Polymer 49 (2008) 5053–5063.

[20] J. Tian, W. Yu, C. Zhou, J. Appl. Polym. Sci. 104 (2007) 3592–3600.

[21] S. H. Tabatabaei, P. J. Carreau, A. Ajji, Chem. Eng. Sci. 64 (2009) 4719–4731.

[22] M. Kersch, H.-W. Schmidt, V. Altstädt, Polymer 98 (2016) 320–326.

[23] A. J. Lovinger, J. O. Chua, C. C. Gryte, J. Polym. Sci. Polym. Phys. Ed. 15 (1977) 641–656.

[24] V. Chivatanasoontorn, K. Yamada, M. Kotaki, Polymer 72 (2015) 104–112.

[25] T. Labour, C. Gauthier, R. Séguéla, G. Vigier, Y. Bomal, G. Orange, Polymer 42 (2001) 7127–7135.

Chapter 3

Synthesis of Polypropylene Functionalized with a Trace Amount of Silicon Trimethoxy Groups and its Utilization in Graft-Type Nanocomposites

Abstract

In the preparation of polypropylene (PP)-based nanocomposites, grafting end-functionalized PP to nano-sized fillers is a promising strategy to alleviate the compatibility and interfacial problems at once, while poor synthetic efficiency for the end-functionalized PP and its grafting has been a major issue to be addressed. In this chapter, I synthesized functionalized PP with one or less silicon methoxy groups per chain by means of copolymerization using a Ziegler-Natta catalyst, and utilized it as a reactive matrix in melt-mixing with spherical SiO_2 nanoparticles. In addition to its synthetic advantage, the introduction of a trace amount of reactive functional groups delivered several profitable consequences to the nanocomposites that are typical for end-functionalized PP, such as improved dispersion, dramatically accelerated crystallization, and mechanical reinforcements.

3.1. Introduction

In a script of sustainable society, lightweight materials for building blocks are indispensable to reduce energy consumption of transportation and logistics, which occupies *ca.* 30% of the whole energy consumption [1,2]. Polypropylene (PP), as the lightest material among commodity plastics, finds its application over numerous fields, including daily consumables, electronic goods, automobile parts, and medical products, owing to its balanced properties despite of its low production cost. Undoubtedly, further expansion of the application of PP will lower the above-mentioned loading. For such a purpose, compounding PP with inorganic fillers has been an issue of industrial significance for enhancing mechanical properties and imparting novel functionalities [3,4]. On the other hand, concomitant drawbacks caused by the addition of fillers need to be addressed, especially in terms of the density and moldability [5].

Polymer nanocomposites are promising materials in a sense that a desired level of mechanical reinforcement or functionalization can be achieved at a filler loading significantly lower than that required for conventional microcomposites [6-10]. However, tremendous efforts on PP-based nanocomposites have stressed an extreme difficulty to import the concept of the nanocomposites to PP by simply replacing the matrix. To be rational, PP does not have any functional groups that are active to interact with most of inorganic fillers, thus leading to poor dispersion of fillers and weak interfacial bonding between the matrix and fillers [11,12]. The group of Taniike and Terano have studied graft-type PP nanocomposites, in which inorganic nanoparticles grafted to PP chains are melt-compounded with pristine PP as the matrix [13,14]. Specifically, PP-grafted SiO_2 nanoparticles (PP-*g*-SiO_2) were tailored by synthesizing terminally hydroxylated PP through controlled chain transfer reaction in metallocene

catalyzed propylene polymerization and subsequently reacting it with the hydroxyl groups of SiO_2 nanoparticles. Besides the excellent dispersion of the SiO_2 nanoparticles, the PP/PP-*g*-SiO_2 nanocomposites exhibited peculiar advantages which are not attainable by other methods. Most importantly, the reinforcement in the yield strength reached +27% at the 5.0 wt% loading. The extent of the improvement was much greater than +4–18% when other polymers are grafted instead of PP [13], and exceptional for spherical nanoparticles [15]. End-functionalized PP chains whose one end is pinned to SiO_2 become crystallization nuclei for the matrix chains, and co-crystallization between the matrix and grafted chains affords a sort of physical cross-linkage, where SiO_2 nanoparticles connect neighboring lamellae by the grafted chains. This co-crystallization mechanism is of course not available for polymers other than PP even if their one end is properly grafted. Moreover, one end-grafted PP chains offer completely different consequences on the properties of the resultant nanocomposites when compared to side-functionalized PP as a compatibilizer (*i.e.* maleic anhydride-grafted PP (PP-*g*-MA)) [14-17]. This is because a side-functionalized PP chain interacts with a single nanoparticle through its multiple functional groups, and this forms a compatibilizing soft interface between the matrix and the inorganic nanoparticle. In the case of end-functionalized PP, the grafted chain is kept away from the inorganic surface (due to the poor affinity) and thus available for the interdiffusion/entanglement/co-crystallization.

Contrast to excellent properties of graft-type PP nanocomposites, laborious preparation of end-functionalized PP chains remains a major obstacle [13]. First, polymerization at a low temperature is essential to control the chain transfer reaction, but it severely restricts the yield at the same time. Second, as metallocene-catalyzed PP generally has lower stereoregularity (*i.e.* lower crystallinity), it is necessary to

repetitively remove out an ungrafted portion of end-functionalized PP before melt compounding. In order to access end-functionalized PP more easily, post-treatment that combines vis-breaking and subsequent hydrosilylation was proposed [18]. However, in this process, the extent of the functionalization was compensated with the deterioration of PP through a radical mechanism [19]. Copolymerization is a facile way to access functionalized PP [20,21], but the introduction of multiple functional groups per chain is disadvantageous for the nanocomposites. Moreover, the susceptibility of early transition metal catalysts to polar or electron donating functional groups severely limits the direct usage of olefins having useful functional groups in copolymerization.

The aim of this chapter is to establish a new synthetic protocol for graft-type PP nanocomposites that combines the advantages of end-functionalized PP for the properties and those of side-functionalized PP for the synthesis. Utilizing a trace amount of comonomer bearing silicon methoxy groups in Ziegler-Natta catalyzed copolymerization, one functional group per PP chain was introduced at a reasonable yield without disrupting the stereoregular sequence of the PP chain. This functionalized PP was melt-mixed as a reactive matrix with SiO_2 nanoparticles. The *in-situ* reaction during the melt mixing, crystallization behavior, and rheological and mechanical characteristics of the resultant nanocomposites were investigated and discussed. The utilization of the functionalized PP led to the following consequences: i) suppression of the viscosity increment caused by the addition of nanoparticles, ii) dramatic promotion of the crystallization, iii) improved dispersion of nanoparticles, and iv) enhancements of the yield strength and Young's modulus. It was concluded that PP bearing a trace amount of functional groups did not act as an ordinary compatibilizer like PP-*g*-MA, rather behaved like end-functionalized PP grafted to the nanoparticles through its one end.

3.2. Experimental

3.2.1. Materials

Propylene of a polymerization grade was donated by Japan Polypropylene Corporation and used as delivered. (7-octen-1-yl)trimethoxysilane (OTMS) was used as a comonomer without further purification. A $TiCl_4/MgCl_2$ Ziegler-Natta (ZN) catalyst containing diether as an internal donor was prepared based on our previous publication [22]. Triethylaluminum (TEA, donated by Tosoh Finechem Corporation) was used as an activator. *n*-Heptane as a polymerization solvent was dried over molecular sieve 4A. Nano-sized SiO_2 (average diameter = 26 nm, surface area = 110 m^2/g) was purchased from Kanto Chemical. Octadecyl-3-(3,5-di-tert-butyl-4-hydroxyphenyl)propionate (AO-50, donated by ADEKA Corporation) was used as a stabilizer. Long-chain branched PP (LCBPP, MFI = 2.4 g/10 min at 230 °C/2.16 kg) and PP-*g*-MA (Chemtura Corporation, MFI = 120 g/10 min at 190 °C/2.16 kg, MA content = 1 wt%) were used after removing additives by reprecipitation (xylene to acetone).

3.2.2. Synthesis of PP-OTMS

PP copolymer with OTMS (PP-OTMS) was synthesized by catalyzed propylene polymerization using OTMS as a comonomer. The polymerization was conducted in a 1 L stainless steel reactor using the ZN catalyst in a semi-batch mode. To the reactor that was sufficiently blanked by nitrogen, 500 mL of heptane, 5–20 mmol of TEA, and 0–15 mmol of OTMS were introduced in this order. Subsequently, the solution was saturated with 0.5 MPa of propylene at 50 °C for 30 min. Followed by the introduction of 16 mmol of hydrogen, 50 mg of the catalyst was injected to initiate the polymerization. The polymerization was continued for 60 min at 50 °C under the constant pressure of

propylene, and terminated by depressurization. The supernatant of the reaction slurry was removed by decantation under nitrogen, and the remaining polymer powder was repetitively washed with ethanol and acetone. Thus obtained powder was finally purified by reprecipitation (xylene to acetone), followed by drying in *vacuo* at room temperature. Four samples were synthesized: HomoPP, PP-OTMS5, PP-OTMS10, and PP-OTMS15, corresponding to the addition amount of OTMS of 0, 5, 10, and 15 mmol, respectively.

3.2.3. Preparation of Nanocomposites

PP-OTMS that was pre-impregnated with 1.0 wt% of AO-50 was melt-mixed with 5.0 wt% of SiO_2 nanoparticles using Micro Compounder MC5 (Xplore) at 185 °C and 100 rpm for 15 min under nitrogen atmosphere. After melt mixing, the extrudate was hot-pressed into films with a thickness of 200 μm at 230 °C under 20 MPa for 5 min, followed by quenching at 100 °C and subsequently at 0 °C. As reference samples, i) homoPP was melt-mixed instead of PP-OTMS, ii) PP-OTMS or homoPP was melt-mixed without the addition of SiO_2, iii) homoPP was melt-mixed in the presence of 1.0 wt% of LCBPP or 5.0 wt% of PP-*g*-MA. These samples were prepared according to the same procedure.

3.2.4. Characterizations

The primary structure of polymer samples was analyzed by NMR (Bruker 400 MHz) operated at 120 °C. About 60 mg of a polymer sample was dissolved in 0.2 mL of 1,1,2,2-tetrachloroethane-d_2 (internal lock and reference) and 0.5 mL of 1,2,4-trichlorobenzene (TCB) containing 0.006 wt% of

2,6-di-*tert*-butyl-4-methylphenol (BHT). The content of OTMS incorporated into PP was determined based on ^{1}H NMR (the number of scan = 1,000) and the stereoregularity of PP was determined by ^{13}C NMR (the number of scan = 5,000).

The molecular weight distribution of polymer samples was determined by high-temperature gel permeation chromatography (GPC, Waters 150C) equipped with polystyrene gel columns (Showa Denko AD806M/S) and an IR detector (MIRAN 1A) at 140 °C using *o*-dichlorobenzene as an eluent. The molecular weight was calibrated by polystyrene standards.

Differential scanning calorimetry (DSC) measurements were performed on Mettler Toledo DSC 822 under nitrogen. About 8 mg of a sample was placed in an aluminum pan, and heated to 230 °C at the heating rate of 20 °C/min. The melting temperature (T_m) and the crystallinity (X_c) were determined from the endotherm of the melting. After erasing the thermal history at 230 °C for 10 min, the sample was cooled down to 25 °C at the cooling rate of 20 °C/min for acquiring the crystallization temperature (T_c), or to a specified temperature at 50 °C/min for isothermal crystallization experiments. The crystallization rate was derived as the inverse of the half time of the crystallization (denoted as $t_{1/2}^{-1}$) at each specified temperature.

Melt viscoelasticity was evaluated using a cone-and-plate rheometer (TA AR2000ex) with a diameter of 25 mm and a cone angle of 4°. A strain sweep test was first performed from the strain value of 0.1% to 600% at the angular frequency of 1 rad/s in order to determine the linear viscoelastic region (Fig. 1). Then, a frequency sweep test was performed from the angular frequency of 500 rad/s to 0.01 rad/s at the strain value of γ = 1%. These measurements were carried out at 200 °C under nitrogen.

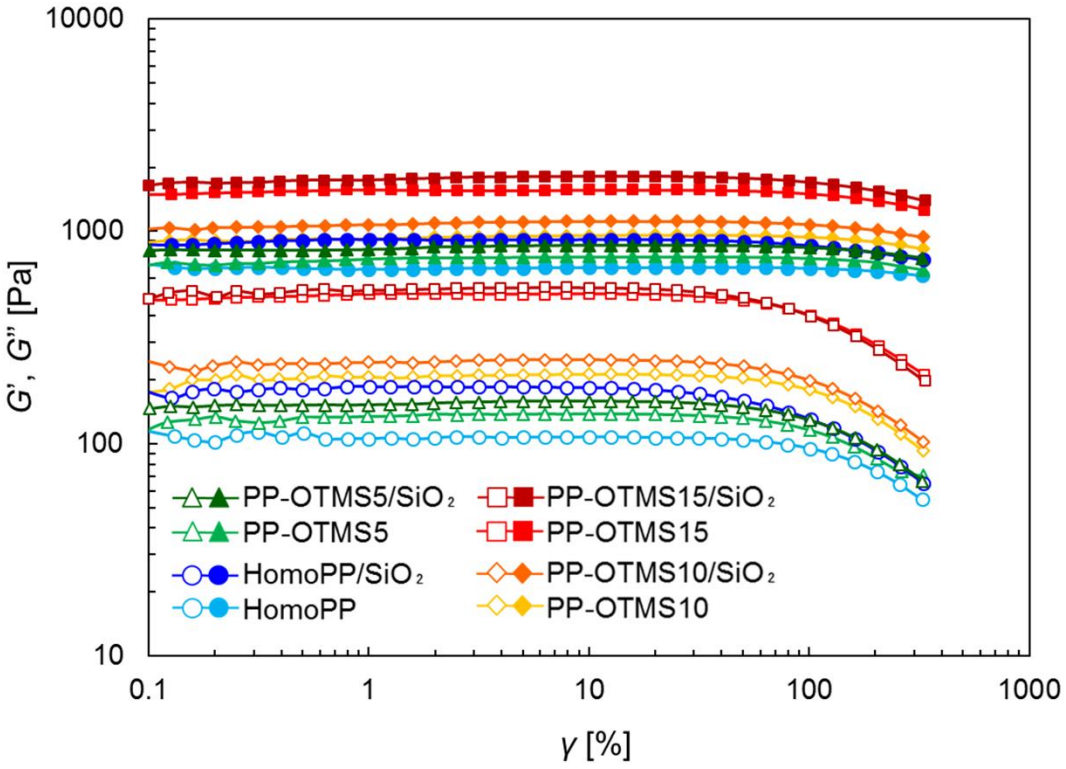

Fig. 1. Strain sweep test results for PP-OTMS and PP-OTMS/SiO_2 nanocomposites: *G*' (open symbols) and *G*'' (filled symbols).

The dispersion of SiO_2 nanoparticles in the nanocomposites was observed by a transmission electron microscope (TEM, Hitachi H-7100) operated at 100 kV. Sample specimens with a thickness of *ca.* 100 nm were prepared by an ultramicrotome (Leica ULTRACUTS FCS) equipped with a diamond knife. The dispersion of SiO_2 nanoparticles was quantified based on a dispersion parameter (*D*) as

$$D = \frac{0.2}{\sqrt{2\pi}} \times \frac{\mu}{\sigma} \quad \text{Eq. (1),}$$

where μ and σ are the average value and the standard deviation of the distance between neighboring SiO_2 nanoparticles (or its aggregates), respectively [23]. The analysis of the TEM images was performed by image J software, where the interparticle distance was

obtained from Delaunay triangulation with the aid of a Delaunay Voronoi plugin. The analysis covered at least 200 nanoparticles per sample.

The spherulites in the films were observed using a polarized optical microscope (POM, OLYMPUS DP12). Films with a thickness of *ca.* 60 μm were prepared based on the aforementioned method.

Tensile properties were measured using a tensile tester (Abecks Inc., Dat-100) at a crosshead speed of 1 mm/min at room temperature. Dumbbell-shaped specimens were cut out from a 200 μm-thick film. The yield strength and Young's modulus reported in this study correspond to the average over five or more specimens per sample.

3.3. Results and Discussion

PP-OTMS samples with different OTMS contents were synthesized by changing the introduction amount of OTMS in catalyzed propylene polymerization. The ^{1}H NMR spectra of PP-OTMS samples are shown in Fig. 2 together with the spectrum of the OTMS comonomer and that of homoPP. The NMR spectra of PP-OTMS were almost the same with that of homoPP except the minor presence of the OMe peak at 3.7 ppm. The intensity of the OMe peak increased by the addition amount of OTMS, while it was not reduced or eliminated by additional reprecipitation. Besides, the peaks related to the unreacted vinyl groups (broad peaks at 5.1 and 6.0 ppm) were not observed. These facts let us conclude that the OMe peak was purely attributed to OTMS copolymerized with propylene. Table 1 summarizes the results of the polymerization. The addition of OTMS decreased the catalytic activity, as the OMe groups of OTMS poisoned active sites. However, a reasonable yield was retained at the minimum addition of OTMS. The activity would be completely eliminated when a usual amount for copolymerization was added, *i.e.* a clear advantage of the trace functionalization was found at the usability of poisonous comonomers without the necessity of protection [24]. The stereoregularity (*mmmm*) and the molecular weight of the polymer were slightly enlarged by the addition of OTMS that acted as an alkoxysilane external donor [25,26]. The OTMS content was calculated by the following equation,

$$\text{OTMS content} = \frac{\mathrm{H^g}/9}{\mathrm{H^m}} \times 100 \qquad \text{Eq. (2),}$$

where $\mathrm{H^g}$ and $\mathrm{H^m}$ are the peak areas for the OMe protons of OTMS and methine protons of PP, respectively. The OTMS content of PP-OTMS was determined as 1.5–7.1 × 10^{-3} mol% to propylene units, and this corresponds to the introduction of 0.02–0.12 side

chains per main chain. A $MgCl_2$-supported ZN catalyst is known as a multi-site catalyst [27] and the insertion rate of a comonomer may vary among different active sites, especially between isospecific and aspecific sites [28,29]. In order to examine the potential heterogeneity of the OTMS incorporation, xylene-soluble components were extracted and their OTMS contents were determined (Table 2). Consistent with the *mmmm* values of the whole polymers, the addition of OTMS decreased the xylene-soluble fraction. It was found that the OTMS contents of xylene-soluble components were identical to those in the corresponding whole polymers despite the extremely lower stereoregularity (less than 30% in *mmmm*). This fact allowed us to assume that OTMS was rather evenly incorporated among PP chains. On the basis of the even distribution and the measured content per main chain, it was believed that PP-OTMS was composed of homoPP as a majority while copolymer having only one side chain as a minority.

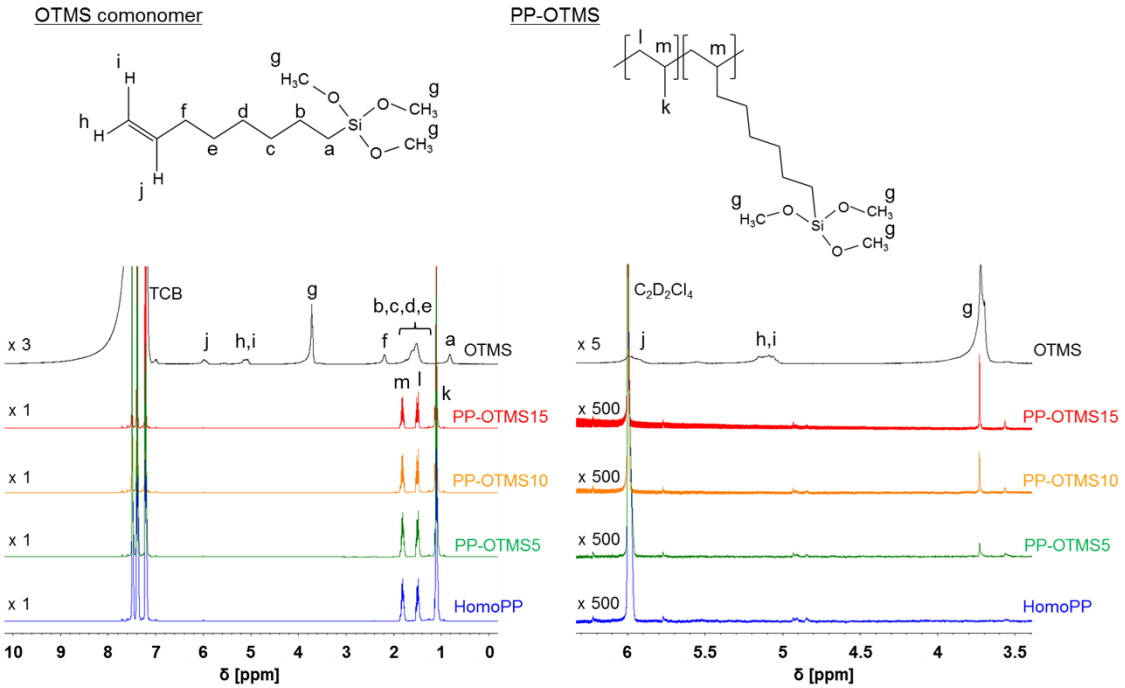

Fig. 2. ^{1}H NMR spectra of homoPP and PP-OTMS. The right figure shows expanded spectra.

Table 1. Synthesis of PP-OTMS

Sample	OTMS [mmol]	Activity [kg-polymer /mol-Ti·h·atm]	*mmmm* [a] [mol%]	M_n [b]	M_w [b]	M_w/M_n [b]	OTMS content [$\times 10^{-3}$ mol%] [c]	OTMS content [Number per main chain] [d]
HomoPP	0	1030 ± 8	95	6.3×10^4	2.4×10^5	3.9	n.a.	0
PP-OTMS5	5	470 ± 5	97	6.3×10^4	2.4×10^5	3.8	1.5 ± 0.2	0.02
PP-OTMS10	10	230 ± 8	98	7.3×10^4	2.7×10^5	3.7	3.2 ± 0.2	0.06
PP-OTMS15	15	93	98	7.3×10^4	2.9×10^5	3.9	7.1	0.12

[a] Determined by ^{13}C NMR.

[b] Determined by GPC.

[c] Determined by ^{1}H NMR.

[d] Calculated using the OTMS content and M_n.

Table 2. Characterization of xylene-soluble components

Sample	Xylene-soluble fraction [a] [wt%]	OTMS content [$\times 10^{-3}$ mol%]	*mmmm* [mol%]
HomoPP	2.58 ± 0.01	n.a.	24
PP-OTMS5	1.36 ± 0.07	1.3	27
PP-OTMS10	1.16 ± 0.14	3.4	25

[a] 1.0 g of a polymer sample was dissolved in 50 mL of hot xylene (containing 0.03 wt% of BHT) and then the solution was cooled to 20 °C. After removing the insoluble components, the xylene-soluble components were recovered from the solution.

PP-OTMS samples with different OTMS contents were compounded with 5.0 wt% of SiO_2 nanoparticles and subjected to characterizations. During the melt mixing process, the OMe groups of PP-OTMS were expected to react with silanol groups of SiO_2 surfaces to form Si-O-Si bonds, by which PP-OTMS would be grafted to the SiO_2 nanoparticles. In order to confirm the occurrence of the reaction, the consumption of the OMe groups before and after melt mixing was examined based on ^{1}H NMR (Fig. 3). Melt mixing of PP-OTMS and SiO_2 nanoparticles clearly decreased the OMe content. However, even in the absence of SiO_2 nanoparticles, the melt mixing reduced the OMe content. This fact suggested that the OMe groups belonging to different chains reacted with each other in the presence of residual water. The proportion of this self-consumption tended to increase along the OTMS content, which was consistent with the hypothesis of the interchain reaction. In Fig. 3, the presence of SiO_2 nanoparticles obviously enlarged the OMe consumption as compared with the self-consumption, which suggested that (a part of) PP-OTMS was grafted to the SiO_2 nanoparticles in the course of the melt mixing.

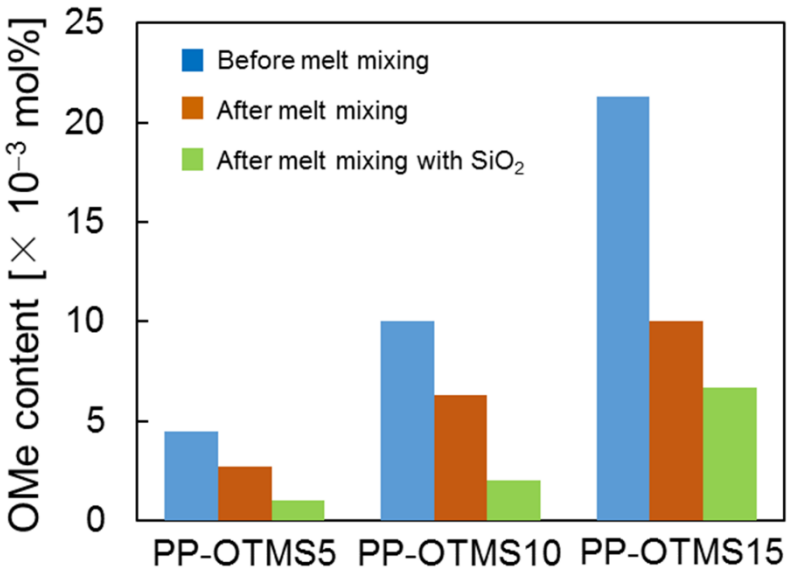

Fig. 3. Consumption of the OMe groups before and after melt mixing.

The effects of the OTMS incorporation and the addition of SiO_2 nanoparticles on the melt viscoelasticity were evaluated by dynamic frequency sweep tests (Fig. 4). In the absence of SiO_2, homoPP exhibited the steepest slope of the storage modulus (*G*') in the low frequency region. The slope of log *G*' was 1.6, slightly lower than 2 for the terminal flow (a fraction of polymer chains with large molecular weights was not fully relaxed). The OTMS incorporation tended to increase the *G*' value especially at lower frequencies, making the terminal feature less evident. This tendency was attributed to the fact that the interchain reaction through the OMe groups formed less relaxable components. Judging from the results and discussion on only one reactive functional group per PP chain, it was believed that the less flexible components predominantly corresponded to *in-situ* generated LCB rather than crosslinked PP [30]. The addition of the SiO_2 nanoparticles greatly raised the *G*' value of homoPP as a result of the cohesive attraction among the nanoparticles [13]. Contrary, the addition of the SiO_2 nanoparticles to PP-OTMS hardly

increased the *G*' value. The *G*' value of PP-OTMS5/SiO_2 and PP-OTMS10/SiO_2 was even lower than that of homoPP/SiO_2 in the terminal region. This result clearly indicated that (a part of) the cohesive attraction among the nanoparticles was suppressed in the presence of the functional groups. In our previous study, it was reported that the grafted PP chains formed a polymer overlayer on SiO_2 surfaces to inhibit the cohesive attraction between nanoparticles in melt, as a result of which the increment of *G*' by the addition of SiO_2 was suppressed [13]. The trend of the loss modulus (*G*'') by the incorpolation of OTMS and the addition of SiO_2 nanoparticles was similar to that of *G*' except for the slope value.

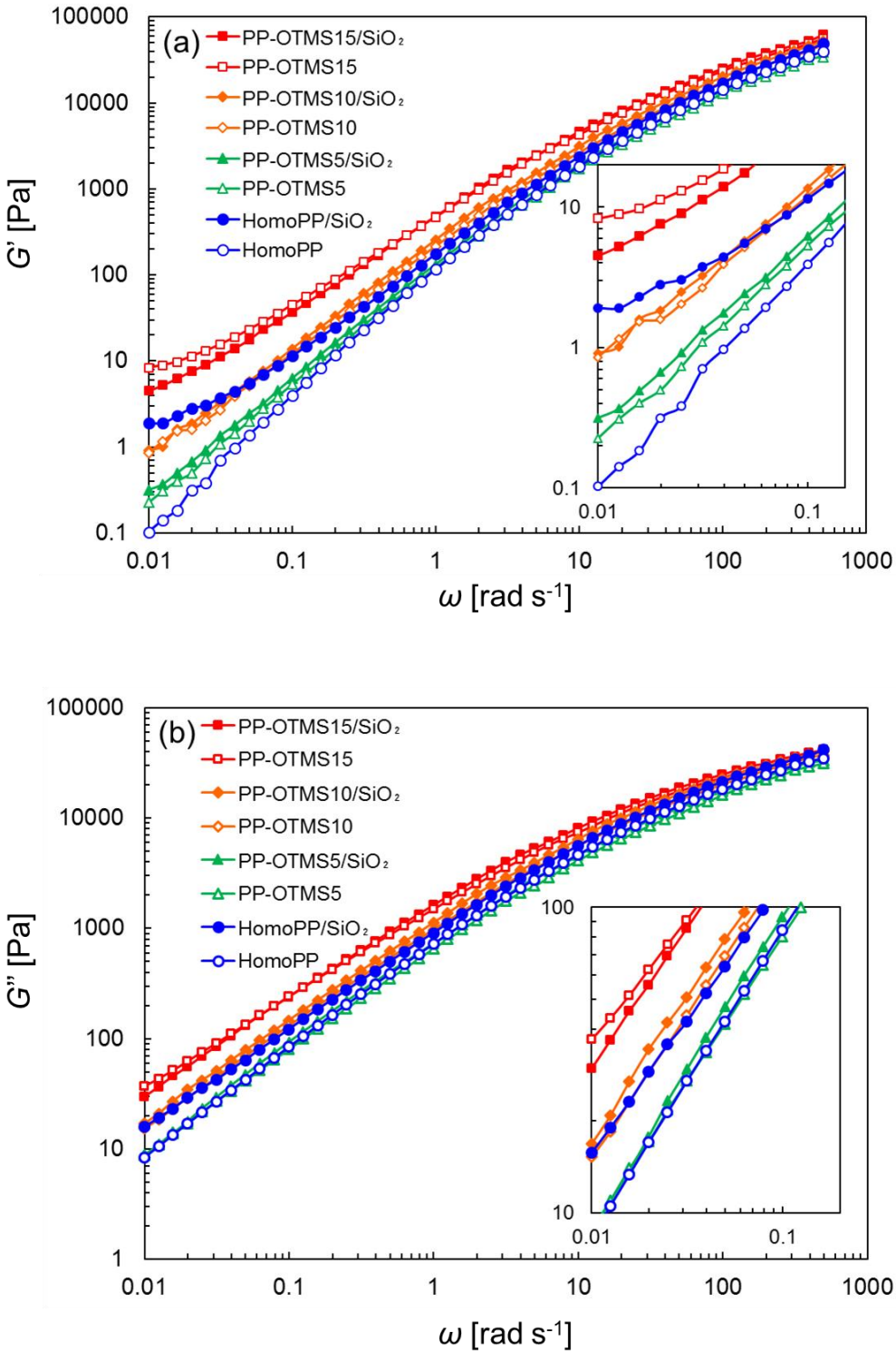

Fig. 4. Melt viscoelastic behavior of PP-OTMS and PP-OTMS/SiO_2 nanocomposites: (a) storage modulus (*G*') and (b) loss modulus (*G*'').

Fig. 5 shows TEM images of the nanocomposites together with the dispersion parameter (*D*) calculated based on Eq. (1). In the case of homoPP/SiO_2 (Fig. 5a,e), huge aggregates of several hundred nm were observed with the lowest *D* value of 0.104. The OTMS incorporation greatly improved the dispersion, where the size of aggregates became smaller than that of homoPP/SiO_2 and the *D* value became larger. There were two potential explanations for the improved dispersion: i) The interchain reaction enhanced the shear force during the melt mixing at a fixed screw speed, and ii) the *in-situ* grafting of PP-OTMS to the SiO_2 nanoparticles improved the compatibility. Considering the observed insensitivity of the dispersion to the OTMS content, the latter explanation was believed more plausible and consistent with our previous finding that the dispersion was not sensitive to the density of the grafted chains (as long as grafted) [13,14]. Moreover, it must be noted that the addition of 1.0 wt% of LCBPP to homoPP hardly improved the dispersion (Fig. 6).

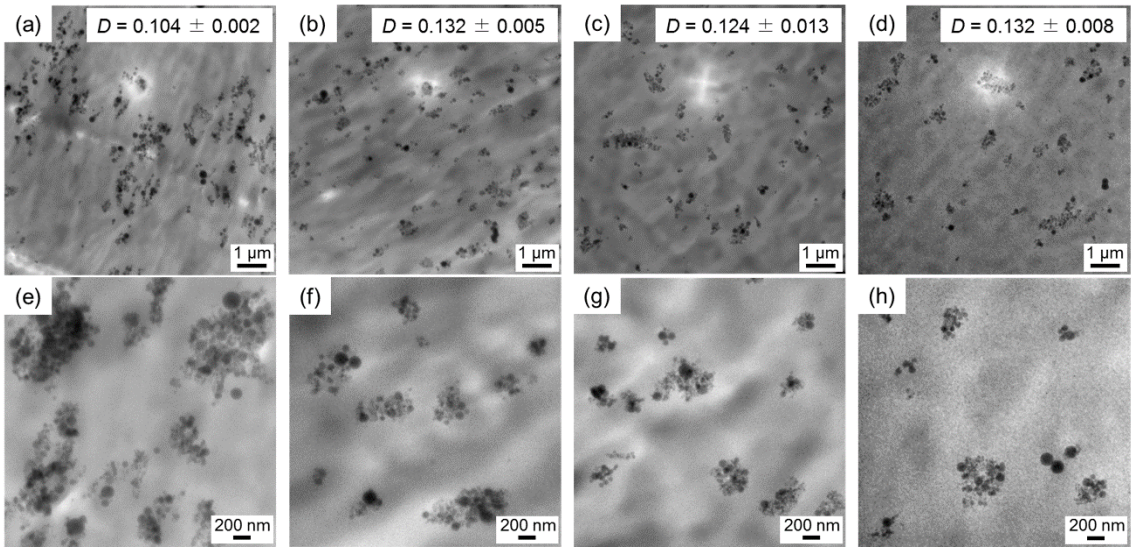

Fig. 5. TEM images of nanocomposites at two magnifications: (a,e) homoPP/SiO_2, (b,f) PP-OTMS5/SiO_2, (c,g) PP-OTMS10/SiO_2, and (d,h) PP-OTMS15/SiO_2. The content of SiO_2 was 5.0 wt%.

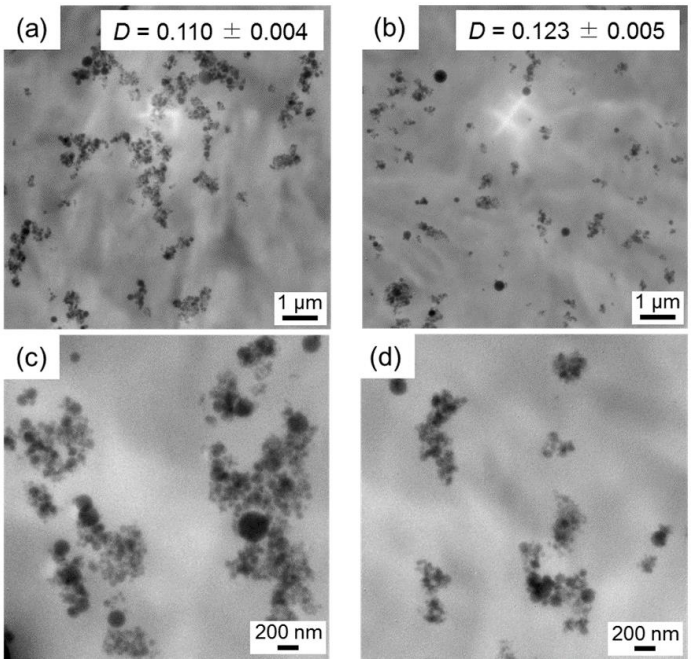

Fig. 6. TEM images of reference nanocomposite samples at two magnifications: (a,c) homoPP/LCBPP/SiO_2 and (b,d) homoPP/PP-g-MA/SiO_2. The content of SiO_2 was 5.0 wt%.

Table 3 summarizes DSC results. As mentioned earlier, the OTMS contents were set sufficiently small not to alter the basic properties of PP, so that the melting point (T_m) and the crystallinity (X_c) of PP-OTMS were almost identical to those of homoPP. On the other hand, the crystallization temperature (T_c) and the crystallization rate at an isothermal condition ($t_{1/2}^{-1}$) were quite sensitive to the OTMS incorporation at such small contents. Along the OTMS content, the crystallization temperature rose up to 128 °C with respect to 115 °C for homoPP, and the crystallization rate at 144 °C was dramatically increased from 0.13×10^{-3} s^{-1} to 4.36×10^{-3} s^{-1}. The observed crystallization promotion was ascribed to a nucleating ability of *in-situ* formed LCBPP [31-33]. In order to confirm this idea, a reference sample, homoPP/LCBPP, was prepared and its crystallization behavior was examined. It was found that the presence of 1.0 wt% of LCBPP raised the crystallization temperature to 124 °C and the crystallization rate to 1.12×10^{-3} s^{-1}. Upon the addition of SiO_2 nanoparticles, crystallization promotion was hardly observed for homoPP as unmodified SiO_2 agglomerates do not act as a nucleating agent [13,14,34]. On the other hand, the addition of SiO_2 further reinforced the crystallization promotion induced by the OTMS incorporation, irrespective of the temperature for the isothermal crystallization (Fig. 7). In our previous study, it was demonstrated that a PP chain with its one end grafted to a nanoparticle acts as a nucleating agent [13,14]. Considering all of these results, the additional crystallization promotion for PP-OTMS/SiO_2 nanocomposites safely indicated that the PP-OTMS chains were *in-situ* grafted to the SiO_2 nanoparticles, leading to the consumption of the OMe groups (*cf*. Fig. 3), the suppression of cohesive attraction among the nanoparticles in melt (*cf*. Fig. 4), improved dispersion of the nanoparticles (*cf*. Fig. 5) and finally the crystallization promotion (*cf*. Table 3).

Table 3. Melting and crystallization behaviors

Sample	T_m [°C]	X_c [%]	T_c [°C]	$t_{1/2}^{-1}$ [a] [$\times 10^{-3}$ s^{-1}]
HomoPP	161	51	115	0.13
PP-OTMS5	163	53	122	0.89
PP-OTMS10	163	53	127	2.40
PP-OTMS15	162	51	128	4.36
HomoPP/SiO_2	163	49	117	0.19
PP-OTMS5/SiO_2	163	53	127	3.16
PP-OTMS10/SiO_2	163	53	130	5.36
PP-OTMS15/SiO_2	163	53	130	6.20
HomoPP/LCBPP [b]	159	52	124	1.12

[a] Inverse of the half time of isothermal crystallization at 144 °C.

[b] HomoPP was melt-mixed with 1.0 wt% of commercially available LCBPP.

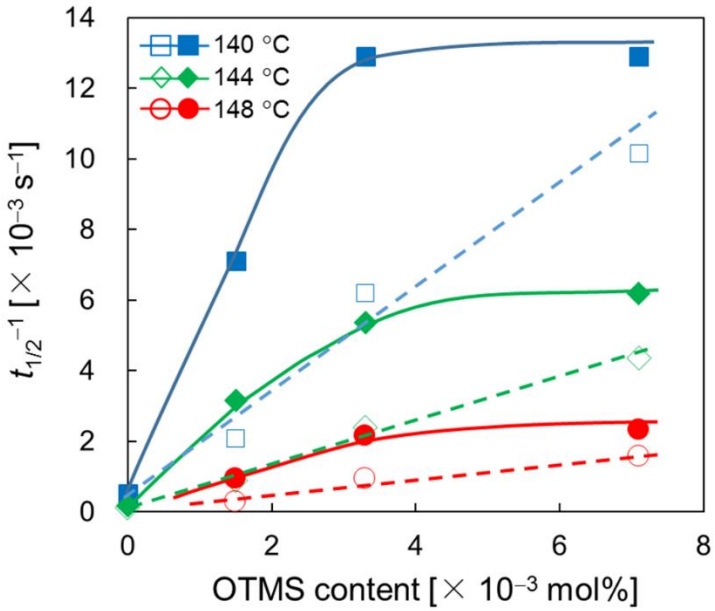

Fig. 7. Isothermal crystallization rate (defined as $t_{1/2}^{-1}$) at various temperatures. The open and filled symbols correspond to the samples without and with 5.0 wt% of SiO_2 nanoparticles, respectively.

Fig. 8 shows the spherulite structures observed by POM. In good agreement with the DSC results, both the incorporation of OTMS and the addition of SiO_2 nanoparticles promoted the nucleation so as to reduce the spherulite size (Fig. 9).

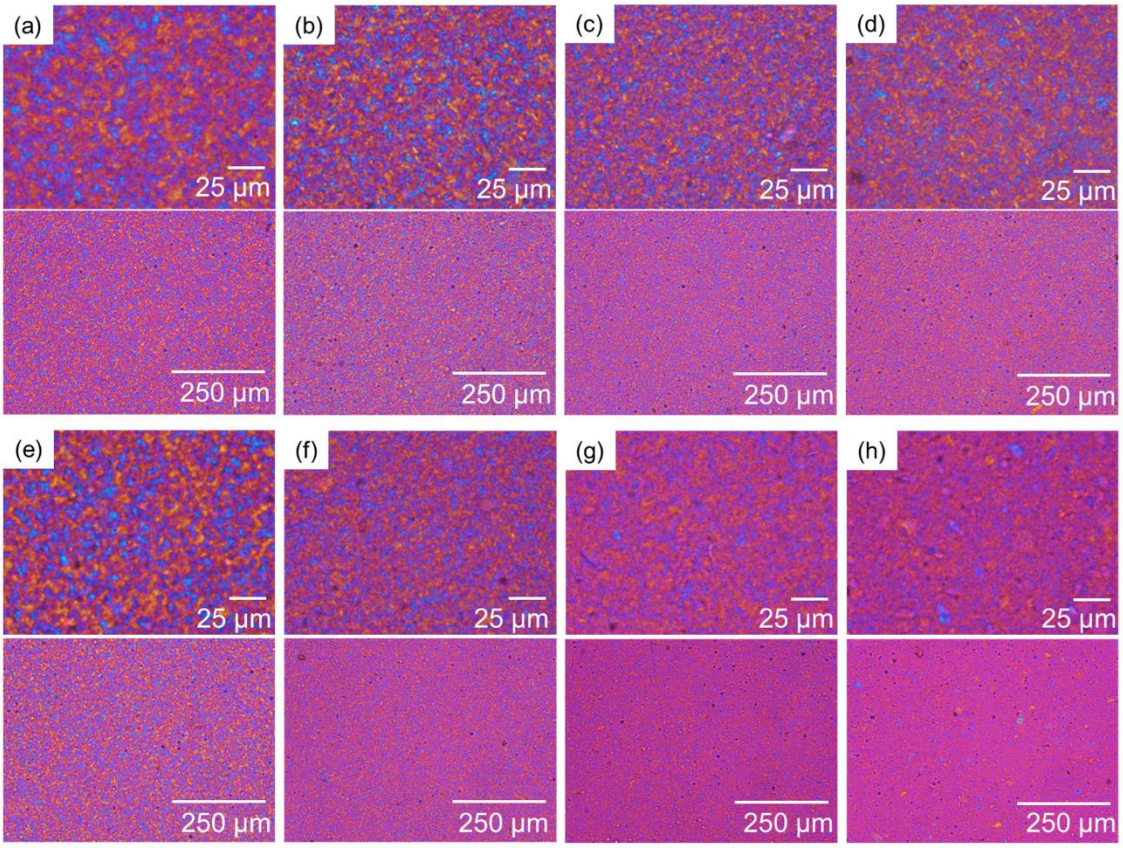

Fig. 8. POM images of a) homoPP, b) PP-OTMS5, c) PP-OTMS10, d) PP-OTMS15, e) homoPP/SiO_2, f) PP-OTMS5/SiO_2, g) PP-OTMS10/SiO_2, and h) PP-OTMS15/SiO_2.

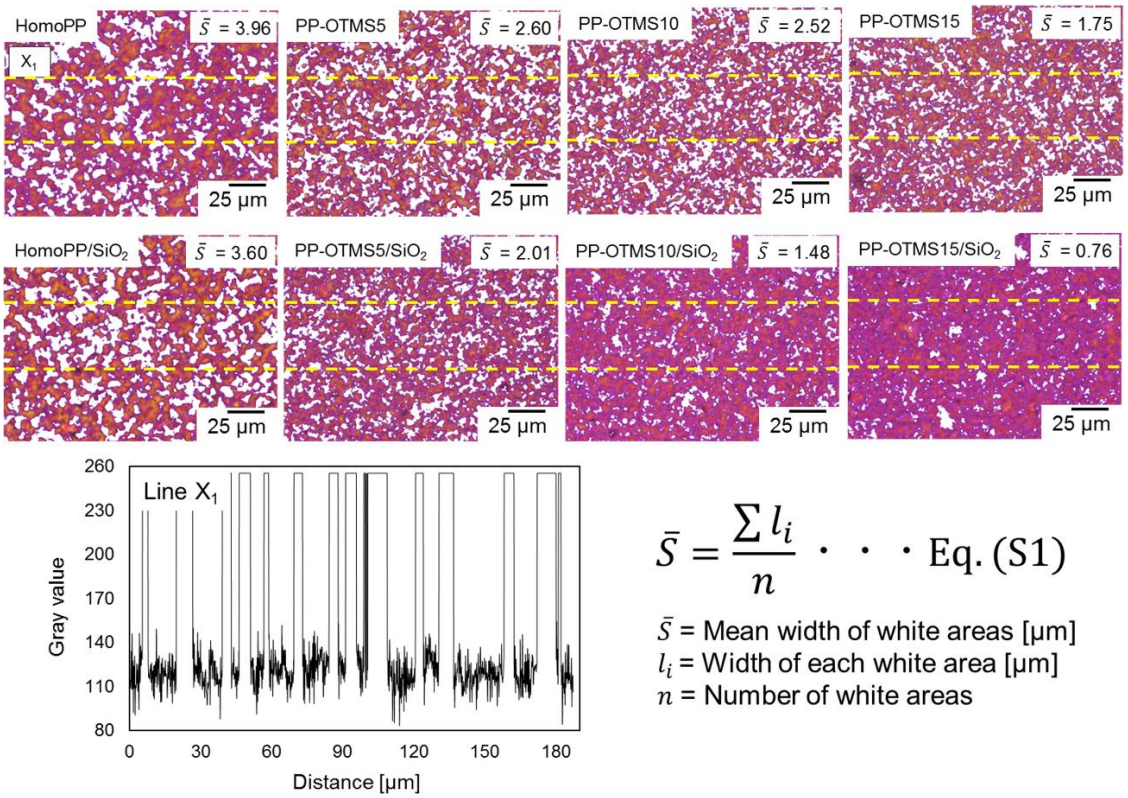

Fig. 9. Estimation of spherulite sizes. The spherulite size was estimated based on Eq. (S1), where the blue areas of a POM image were colored in white, and the mean width of the white areas were determined from line profiles.

Uniaxial tensile tests were performed to investigate the mechanical properties of the nanocomposites. Typical S-S curves are shown in Fig. 10. Table 4 and Fig. 11 summarize representative properties in the tensile tests. It should be noted that the X_c values of the samples were similar among each other, so that any difference in the mechanical properties could be ascribed to the OTMS incorporation and/or to the addition of SiO_2 nanoparticles. In the absence of SiO_2, the introduction of OTMS into PP monotonously enhanced the yield strength by 13% as a consequence of the LCB formation [33]. When SiO_2 was added to homoPP, there was no improvement in the

tensile properties. Rather, the elongation at break was damaged, as poorly connected interfaces at agglomerates worked as a stress concentrator [13,14]. The presence of the reactive functional groups altered the consequence of the addition of SiO_2 nanoparticles even though its content was as small as 10^{-3} mol%. The yield strength and modulus of PP-OTMS15/SiO_2 were 16% and 10% higher than those of PP/SiO_2, and 14% and 13% higher than those of homoPP, respectively. The improvement of the yield strength was attributed to the LCB formation in one part and the grafting in the other part, where grafted chains were assumed to interdiffuse, entangle, and co-crystallize with matrix chains [13,14]. On the combination of PP and spherical SiO_2 nanoparticles, inspection over literatures identifies a critical role of interfacial bonding for the yield strength. It is hardly improved when a compatibilizer or organic modification using short aliphatic chains is applied (*cf.* homoPP/PP-*g*-MA/SiO_2 in Table 4 and Fig. 6). The best improvement is attained when polymeric chains are grafted to the SiO_2 surfaces: Typical improvements are +4–18% when the grafted chains are not co-crystallizable with the matrix, and +27% when PP chains are grafted [13,14]. The improvement of the modulus was explained by the improved dispersion of the nanoparticles. Such improvements were hardly obtained when LCBPP was melt-mixed together (*cf.* homoPP/LCBPP/SiO_2 in Table 4 and Fig. 6), and validated the occurrence of the *in-situ* grafting when PP-OTMS was melt-mixed with SiO_2. The deterioration in the elongation at break in spite of the improved dispersion was considered as a sign of rigidly embedded nanoparticles in the matrix.

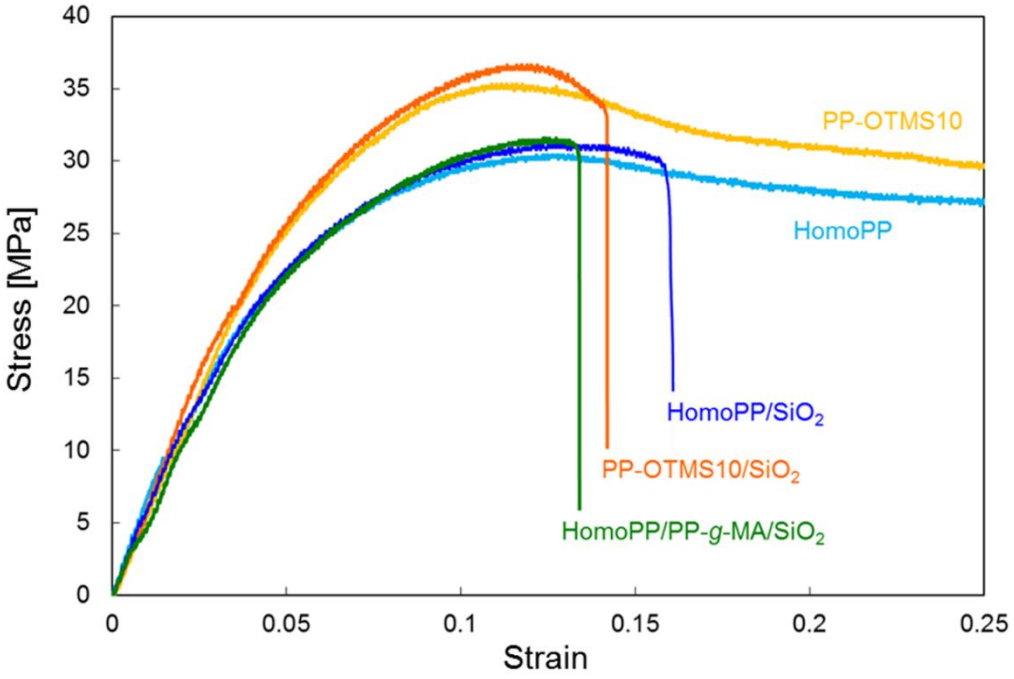

Fig. 10. Typical stress-strain curves for PP-OTMS and its nanocomposites.

Table 4. Results of tensile tests [a]

Sample	Yield strength [MPa]	Young's modulus [MPa]	Elongation at break [%]
HomoPP	31.1 ± 0.9	603 ± 24	26.9 ± 10.3
PP-OTMS5	33.3 ± 1.0	616 ± 43	21.6 ± 6.4
PP-OTMS10	34.2 ± 0.7	622 ± 40	32.5 ± 9.8
PP-OTMS15	35.0 ± 0.9	637 ± 20	48.0 ± 11.0
HomoPP/SiO_2	30.6 ± 0.9	620 ± 46	15.9 ± 2.3
PP-OTMS5/SiO_2	34.7 ± 0.7	657 ± 52	11.9 ± 1.2
PP-OTMS10/SiO_2	36.5 ± 0.7	656 ± 49	13.0 ± 1.0
PP-OTMS15/SiO_2	35.6 ± 0.6	682 ± 56	12.8 ± 1.7
HomoPP/LCBPP/SiO_2 [b]	30.3 ± 0.8	564 ± 55	29.6 ± 7.0
HomoPP/PP-*g*-MA/SiO_2 [b]	31.9 ± 0.4	580 ± 62	12.8 ± 1.3

[a] Tensile properties were determined as averages at least over 5 specimens.

[b] HomoPP was melt-mixed with 5.0 wt% of SiO_2 in the presence of 1.0 wt% of LCBPP or 5.0 wt% of PP-*g*-MA.

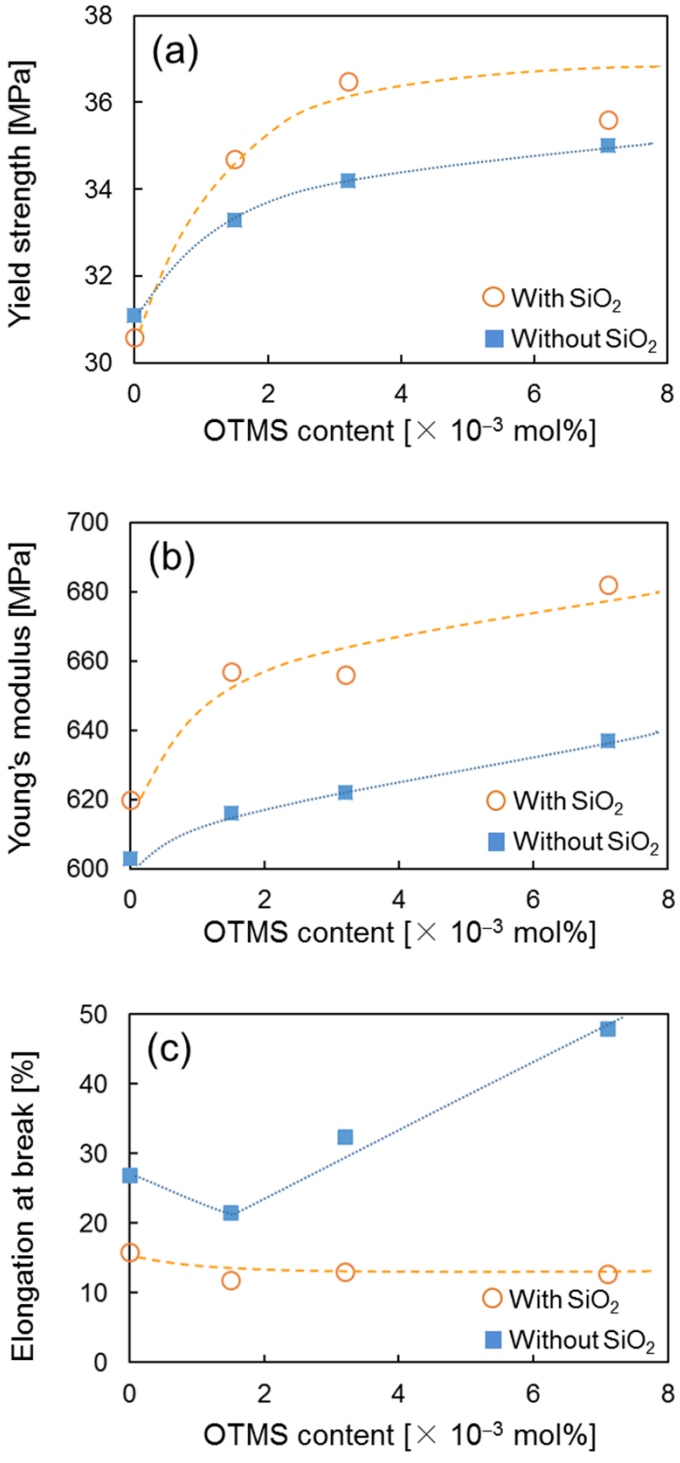

Fig. 11. Tensile properties: a) yield strength, b) Young's modulus and c) elongation at break.

Finally, the physical properties of PP-OTMS/SiO_2 nanocomposites with different SiO_2 contents were evaluated. The SiO_2 content was varied between 0–10.0 wt%, where the change in SiO_2 amount was expected to play a role in changing the ratio of the interchain reaction and grafting reaction to SiO_2 nanoparticles. When the SiO_2 loading is small, the reduction in grafting expected only improves the elongation at break at the expense of stiffness reinforcement, while the promotion of the interchain reaction has the potential to improve all tensile properties (*i.e.*, strength, modulus, and elongation at break). It must be noted that the data in the current set of experiments can not be completely comparable with the earlier results, due to the fact that another batch of PP-OTMS (defined as PP-OTMS1.6, OTMS content = 1.6×10^{-3} mol%) and nano-sized SiO_2 (average diameter = 30 nm, surface area = 91 m^2) were uesd. However, it is important to note, that the results showed a trend similar to that shown in previous series of experiments. The consumptions of the OMe groups during the melt mixing and hot pressing are summarized in Table 5 and Fig. 12. The consumption of OMe groups during both melt mixing and hot pressing suggested the progress of the reactions in the two steps. An increase in the addition amount of SiO_2 nanoparticles promoted the consumption of the OMe groups at the melt mixing, where in the case of the sample having 10.0 wt% of SiO_2 nanoparticles, all the OMe groups were consumed during the melt mixing. It was suggested that the hydrolysis of the OMe groups was promoted by the increase of released physisorbed water and surface hydroxyl groups along with the SiO_2 loading. Therefore, it was speculated that the intermolecular reaction between PP-OTMS and/or the grafting reaction of PP-OTMS to SiO_2 nanoparticles also promoted with the increase of SiO_2 loading. Interestingly, it was observed that, even when 3.0 wt% or more SiO_2 was added, all the OMe groups (4.8×10^{-3} mol%) in

PP-OTMS1.6 were consumed after the compression molding.

Table 5. Consumption of OMe groups during melt mixing and hot pressing

Sample	SiO_2 content [wt%]	OMe content [a] [x 10^{-3} mol%]		
		Before melt mixing	After melt mixing (Extrudate)	After hot pressing (Film)
PP-OTMS1.6/SiO_2	0	4.8 ± 0.3	3.3	1.7
	1		2.7	0.3
	3		0.7	trace
	5		< 0.3	trace
	10		trace	trace

[a] Analyzed by ^{1}H NMR.

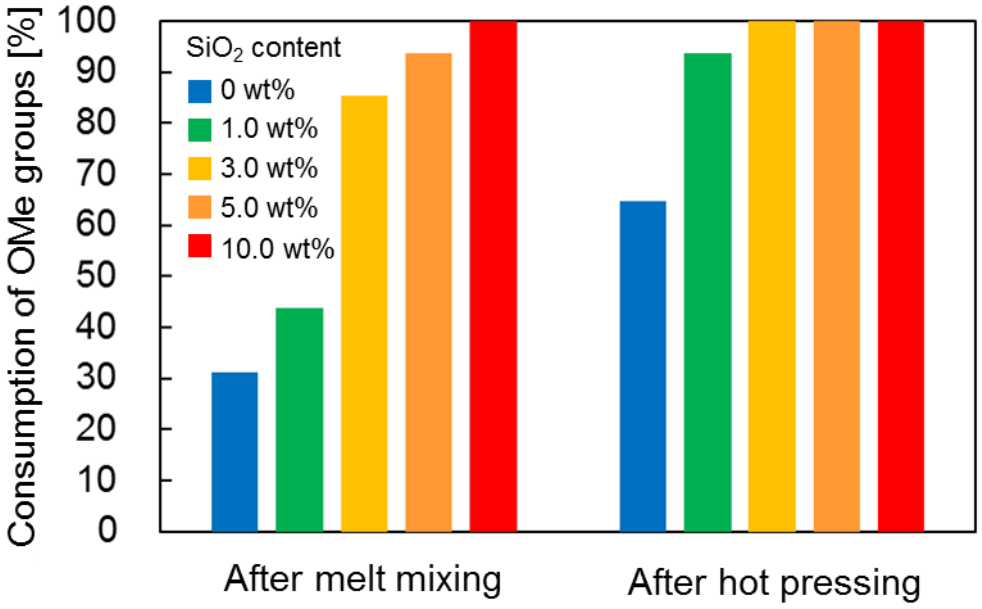

Fig. 12. Consumption of OMe groups during melt mixing (185 °C, 15 min) and hot pressing (230 °C, 11 min) for PP-OTMS1.6/SiO_2 nanocomposite with various SiO_2 contents.

The crystallization behavior of PP-OTMS1.6/SiO_2 nanocomposites with different SiO_2 contents was evaluated by DSC in order to confirm the progress of the two reactions (*i.e.,* interchain reaction and grafting). As mentioned earlier, both reactions were quite sensitive to the T_c and $t_{1/2}^{-1}$ (*cf.* Table 3), therefore DSC measurements were performed investigating the progress of the reactions. The results are summarized in Table 6 and Fig. 13. Note that the isothermal crystallization for homoPP at 144 °C requires a very long time of about 5 h, so that the comparison was made at 136 °C to minimize undesired degradation. The content of SiO_2 nanoparticles did not affect the T_m and X_c regardless of the matrix. On the other hand, the T_c and $t_{1/2}^{-1}$ were enhanced with the increase of the SiO_2 content. The degree of acceleration of the crystallization for PP-OTMS/SiO_2 was far greater than that in the homoPP/SiO_2. It increased linearly below 3.0 wt%, while the increment saturated over 3.0 wt% (*cf.* Fig. 2). These improvements in PP-OTMS were caused due to the nucleating ability of long branched chains and grafted chains. Together with the NMR results (*cf.* Fig 1), these results indicated that all OMe group were consumed at SiO_2 loading of 3.0 wt% or more, because of which the LCB structure or grafting for nucleation did not increase. The slight improvement in homoPP system could be attributed to the nucleation ability of nano-sized SiO_2.

Table 6. Melting and crystallization behaviors of homoPP/SiO_2 and PP-OTMS1.6/SiO_2 nanocomposites with various SiO_2 contents.

Sample	SiO_2 content [wt%]	T_m [°C]	X_c [%]	T_c [°C]	$t_{1/2}^{-1}$ [a] [× 10^{-3} s^{-1}]	
					136 °C	144 °C
HomoPP	0	163	51	114	0.69	—
	1	162	50	116	1.11	—
	3	164	51	116	1.04	—
	5	162	51	118	1.10	—
	10	163	51	118	1.39	—
PP-OTMS1.6	0	164	54	125	10.22	1.81
	1	165	53	127	—	3.92
	3	164	54	128	—	4.90
	5	165	53	128	—	4.59
	10	164	54	128	—	4.77

[a] Inverse of the half time of isothermal crystallization.

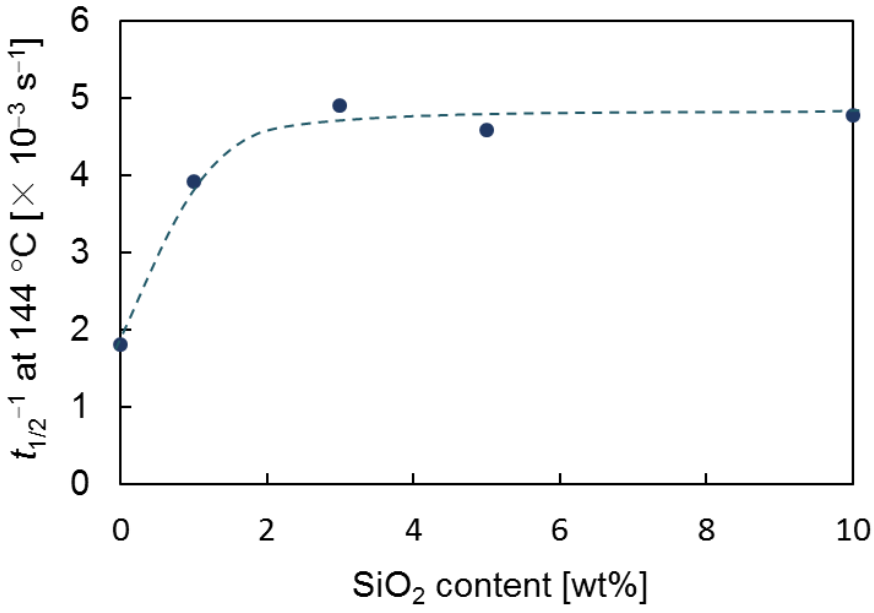

Fig. 13. Isothermal crystallization rate (defined as $t_{1/2}^{-1}$) at 144 °C for PP-OTMS1.6/SiO_2 nanocomposite with various SiO_2 contents.

Fig. 14 shows TEM images of the homoPP/SiO_2 and PP-OTMS1.6/SiO_2 nanocomposites with 3.0 wt% and 10.0 wt% of SiO_2 nanoparticles. As can be seen, even at high loading like 10.0 wt% of SiO_2 nanoparticles, the dispersion of SiO_2 nanoparticles was dramatically improved when only 1.6 x 10^{-3} mol% of OTMS was incorporated into PP to be used as a matrix.

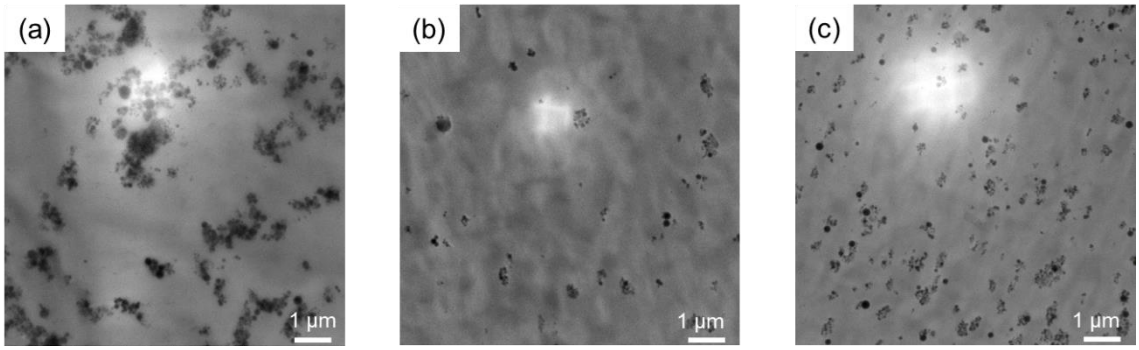

Fig. 14. TEM images of (a) homoPP/SiO_2 (10.0 wt%), (b) PP-OTMS1.6/SiO_2 (3.0 wt%), and (b) PP-OTMS1.6/SiO_2 (10.0 wt%).

The effect of 1.6 x 10^{-3} mol% of OTMS on the melt viscoelasticity was also evaluated using a rheometer. The *G*' of homoPP/SiO_2 and PP-OTMS1.6/SiO_2 nanocomposites with SiO_2 contents of 0, 3.0 and 10.0 wt% are shown in Fig. 15. The addition of 10.0 wt% of SiO_2 nanoparticles in homoPP led to the aggregation of SiO_2 nanoparticles due to the cohesive attraction among the nanoparticles, which was continuously present throughout the PP matrix. Due to such kind of continuous aggregation, it showed solid-like behavior, with significant raise in the *G*' value particularly in the low frequency region. However, in the presence of 1.6 x 10^{-3} mol% of OTMS, the results were dramatically altered. The grafting of PP-OTMS to SiO_2 nanoparticles significantly

suppressed the increment of *G*' value even when the SiO_2 content was 10.0 wt% because the cohesive attraction was greatly weakened by grafted chains in melt. On the basis of these results, it can be inferred that the addition of SiO_2 nanoparticles should preferentially promote the graft reaction rather than the interchain reaction, and the PP-OTMS chains grafted to a SiO_2 nanoparticles at a single point effectively reduced the interaction between PP-OTMS and SiO_2 nanoparticles by widely covering the SiO_2 surface in the molten state.

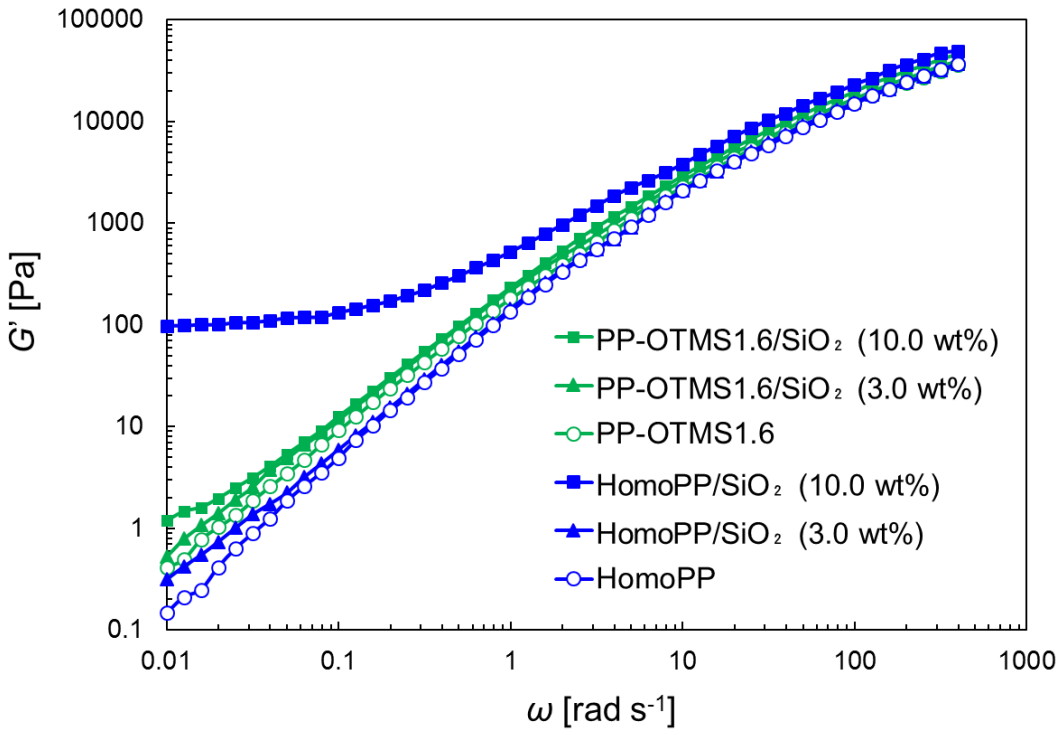

Fig. 15. Storage modulus of homoPP/SiO_2 and PP-OTMS1.6/SiO_2 nanocomposites with various SiO_2 contents.

The mechanical properties of PP-OTMS1.6/SiO_2 nanocomposites with different SiO_2 contents were evaluated by uniaxial tensile test. The results are summarized in Table 7 and Fig. 16. In the case of homoPP, the yield strength did not improve with the increase of the SiO_2 content, while the Young's modulus enhanced marginally. On the other hand, in the case of PP-OTMS, both the yield strength and Young's modulus increased up to 5.0 wt% of SiO_2 nanoparticles and thereafter remained nearly constant. The reason of the saturation in the enhancements, when the SiO_2 content was higer than 5.0 wt%, would be presumed that there was no significant difference in the total amount of cross-linking and grafting (*cf*. Fig. 12 and Fig. 13). The elongation at break decreased with the increase of the SiO_2 content regardless of the matrix. Compared with homoPP, the severe deterioration of the elongation by the addition of only 1.0 wt% of SiO_2 nanoparticles in PP-OTMS was enough to cancel the benefit of the matrix. This is because the physical cross-linkage formed via SiO_2 nanoparticles between lamellae cannot follow the elongation. As a result, the reduction in the SiO_2 content improved the elongation slightly, while suppressed the degree of improvement in the strength and modulus of nanocomposites. Therefore, 5.0 wt% of SiO_2 nanoparticles was required for maximum reinforcement in PP-OTMS1.6. This result suggested that maximum reinforcements could be achieved under the condition where all reactions were uniformly completed during melt mixing (*cf.* Table 5).

In order to further improve the mechanical properties, the particle size of SiO_2 was reduced from 30 nm to 7 nm (surface area = 300 m^2/g). The results of tensile test are shown in Table 7. It was also found that a small amount of SiO_2 can achieve the same or higher reinforcement by reducing the particle size.

Table 7. Results of tensile tests [a]

Matrix	SiO_2 content [wt%]	Yield strength [MPa]	Young's modulus [MPa]	Elongation at break [%]
HomoPP	0	31.3 ± 1.0	567 ± 76	24.8 ± 7.3
	1	31.7 ± 0.3	595 ± 38	18.6 ± 0.8
	3	31.5 ± 0.5	598 ± 42	15.1 ± 2.0
	5	32.0 ± 0.4	608 ± 57	14.2 ± 1.8
	10	31.6 ± 0.4	621 ± 61	10.9 ± 0.6
PP-OTMS1.6	0	32.5 ± 0.5	644 ± 96	28.9 ± 6.7
	1	33.7 ± 0.6	638 ± 71	17.1 ± 4.4
	3	34.4 ± 0.4	658 ± 74	12.7 ± 1.7
	5	35.1 ± 0.8	703 ± 66	12.2 ± 1.7
	10	35.0 ± 0.4	710 ± 47	12.5 ± 0.9
PP-OTMS1.6	0.2 [b]	34.9 ± 0.3	743 ± 56	18.2 ± 2.7
	1 [b]	35.5 ± 0.3	755 ± 56	15.5 ± 1.9
	5 [b]	35.5 ± 0.2	753 ± 27	13.8 ± 1.1

[a] Tensile properties were determined as averages at least over 5 specimens.

[b] 7 nm SiO_2 nanoparticle was used instead of 30 nm.

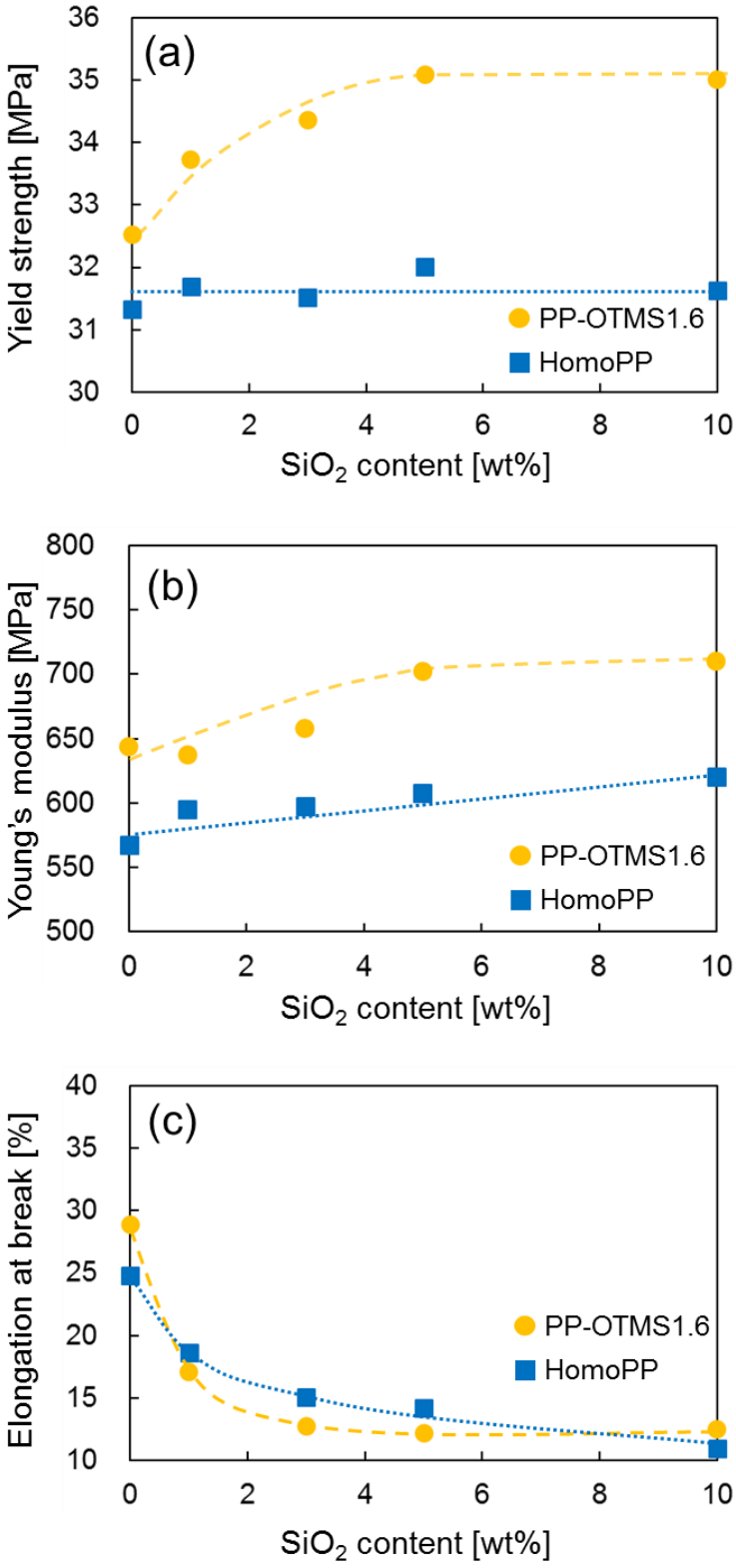

Fig. 16. Tensile properties of homoPP/SiO_2 and PP-OTMS1.6/SiO_2 nanocomposites with various SiO_2 contents: a) yield strength, b) Young's modulus and c) elongation at break.

3.4. Conclusions

In this chapter, a facile strategy to prepare graft-type PP nanocomposites was proposed, where PP containing a trace amount of reactive functional groups (PP-OTMS) was melt-mixed with SiO_2 nanoparticles. PP-OTMS was readily prepared by common Ziegler-Natta polymerization using OTMS as a comonomer. The incorporation of OTMS at the content of 10^{-3} mol% did not affect the basic properties of PP, but endowed the nucleation ability and the reactivity to PP chains. The melt mixing of PP-OTMS led to the interchain reaction among OMe groups to introduce the LCB structure, as well as *in-situ* grafting to SiO_2 nanoparticles by reacting with surface silanol groups. The combination of the LCB structure and the grafted chains dramatically promoted the crystallization as compared to pristine PP and its nanocomposites. The grafted chains also improved the dispersion of the SiO_2 nanoparticles, and strengthened the interfacial bonding with the matrix for the tensile reinforcement. Such reinforcement was never obtained by adding "heavily" functionalized PP like PP-*g*-MA. In conclusion, the proposed strategy using a trace amount of the reactive functional groups is promising for realizing the advantages of polymer grafting in a synthetically facile manner.

References

[1] L. Perez-Lombard, J. Ortiz, C. Pout, Energy Build. 40 (2008) 394–398.

[2] C. Fiori, K. Ahn, H. A. Rakha, Appl. Energy 168 (2016) 257–268.

[3] Q. T. H. Shubhra, A. K. M. M. Alam, M. A. Quaiyyum, J. Termoplast. Compos. Mater. 26 (2013) 362–391.

[4] H. T. Oyama, M. Sekikawa, Y. Ikezawa, J. Macromol. Sci. B Phys. 50 (2011) 463–483.

[5] J. Z. Liang, C. Y. Chen, S. Y. Zou, C. P. Tsui, C. Y. Tang, S. D. Zhang, Polym. Test. 45 (2015) 41–46.

[6] Y. Kojima, A. Usuki, M. Kawasumi, A. Okada, Y. Fukushima, T. Kurauchi, O. Kamigaito, J. Mater. Res. 8 (1993) 1185–1189.

[7] J. Jordan, K. I. Jacob, R. Tannenbaum, M. A. Sharaf, I. Jasiuk, Mater. Sci. Eng. A 393 (2005) 1–11.

[8] K. Kaneko, N. Yadav, K. Takeuchi, B. Maira, M. Terano, T. Taniike, Compos. Sci. Technol. 102 (2014) 120–125.

[9] B. Maira, P. Chammingkwan, M. Terano, T. Taniike, Macromol. Mater. Eng. 300 (2015) 679–683.

[10] B. Maira, P. Chammingkwan, M. Terano, T. Taniike, Compos. Sci. Technol. 144 (2017) 151–159.

[11] D. N. Bikiaris, A. Vassiliou, E. Pavlidou, G. P. Karayannidis, Eur. Polym. J. 41 (2005) 1965–1978.

[12] W. Yuan, F. Wang, Z. Chen, C. Gao, P. Liu, Y. Ding, S. Zhang, M. Yang, Polymer 151 (2018) 242–249.

[13] T. Taniike, M. Toyonaga, M. Terano, Polymer 55 (2014) 1012–1019.

[14] M. Toyonaga, P. Chammingkwan, M. Terano, T. Taniike, Polymers 8 (2016) 300–313.

[15] N. Hasegawa, H. Okamoto, M. Kato, A. Usuki, J. Appl. Polym. Sci. 78 (2000) 1918–1922.

[16] M. Z. Rong, M. Q. Zhang, S. L. Pan, K. Friedrich, J. Appl. Polym. Sci. 92 (2004) 1771–1781.

[17] Z. M. Wang, H. Hong, T. C. Chung, Macromolecules 38 (2005) 8966–8970.

[18] P. Chammingkwan, M. Toyonaga, T. Wada, M. Terano, T. Taniike, Compos. Sci. Technol. 165 (2018) 183–189.

[19] S. M. B. Nachtigall, F. C. Stedile, A. H. O. Felix, R. S. Mauler, J. Appl. Polym. Sci. 72 (1999) 1313–1319.

[20] S. Gupta, X. Yuan, T. C. M. Chung, M. Cakmak, R. A. Weiss, Polymer 55 (2014) 924–935.

[21] R. Watanabe, M. Kunioka, H. Sato, J. Mizukado, H. Hagihara, Polym. Adv. Technol. 29 (2018) 417–423.

[22] Y. Hiraoka, S. Y. Kim, A. Dashti, T. Taniike, M. Terano, Macromol. React. Eng. 4 (2010) 510–515.

[23] T. Glaskova, M. Zarrelli, A. Borisova, K. Timchenko, A. Aniskevich, M. Giordano, Compos. Sci. Technol. 71 (2011) 1543–1549.

[24] J.-Y. Dong, Y. Hu, Coord. Chem. Rev. 250 (2006) 47–65.

[25] T. Wada, T. Taniike, I. Kouzai, S. Takahashi, M. Terano, Macromol. Rapid Commun. 30 (2009) 887–891.

[26] S. Poonpong, S. Dwivedi, T. Taniike, M. Terano, Macromol. Chem. Phys. 215 (2014) 1721–1727.

[27] N. Kashiwa, J. Imuta, Catal. Surveys Jpn. 1 (1997) 125–142.

[28] J. Xu, L. Feng, S. Yang, Macromolecules 30 (1997) 7655–7660.

[29] A. Khan, Y. Guo, Z. Zhang, A. Ali, Z. Fu, Z. Fan, J. Appl. Polym. Sci. 135 (2018) 46030.

[30] J. A. Langston, R. H. Colby, T. C. M. Chung, F. Shimizu, T. Suzuki, M. Aoki, Macromolecules 40 (2007) 2712–2720.

[31] S. H. Tabatabaei, P. J. Carreau, A. Ajji, Chem. Eng. Sci. 64 (2009) 4719–4731.

[32] J. Tian, W. Yu, C. Zhou, J. Appl. Polym. Sci. 104 (2007) 3592–3600.

[33] W. Zhao, Y. Huang, X. Liao, Q. Yang, Polymer 54 (2013) 1455–1462.

[34] Y. Fukuyama, T. Kawai, S. Kuroda, M. Toyonaga, T. Taniike, M. Terano, Therm. Anal. Calorim. 113 (2013) 1511–1519.

Chapter 4

Design of Graft-Type PP/Elastomer/SiO_2 Ternary Nanocomposites for Balanced Toughness and Stiffness

Abstract

Polypropylene (PP) is often compounded with fillers and elastomers to enhance the stiffness and impact strength of PP. In PP/elastomer/nanofiller ternary nanocomposites, the localization and uniform dispersion of fillers in matrix PP are few of the most important goals. In order to achieve this, grafting strategy was adopted in the current chapter. Two types of ethylene-octene copolymer (EOC) having different melt index were melt-mixed with functionalized PP having a trace amount of reactive silicon trimethoxy groups (defined as PP-OTMS) and SiO_2 nanoparticles. It was found that, although the introduction of OTMS did not affect the dispersion and phase size of the EOCs, the EOC with higher viscosity could suppress the phase coarsening of the EOC during compression molding. During melt mixing, PP-OTMS was *in-situ* grafted to SiO_2 nanoparticles, leading to the improvement of dispersion of SiO_2 nanoparticles in PP matrix resulting into strength and modulus enhancement. On the other hand, the grafted chain to SiO_2 nanoparticles could not follow the flexible deformation of the elastomers and sacrificed the toughness.

4.1. Introduction

Polypropylene (PP) has a glass transition temperature around 0 °C, which makes the impact strength low especially at low temperatures, limiting its usage in cold regions. Therefore, homo PP is often substituted by impact PP, which is obtained by synthesizing an ethylene-propylene rubber (EPR) in a PP granule as a second step after homopolymerization. Unfortunately, since EPR is synthesized using a heterogeneous catalyst with homo PP granule as a matrix, it often results into a wide distribution of ethylene composition and sometimes is not sufficient to be used as an impact modifier [1]. On the other hand, a polyolefin elastomer, which is polymerized using a homogeneous catalyst, is often added together with additives such as stabilizers in a granulation process. However, an addition of elastomer greatly deteriorates the stiffness of PP [2].

The addition of various inorganic fillers such as talc, glass fiber, calcium carbonate, silica, etc. has been studied and used for a long time to compensate for the deterioration in stiffness in PP/elastomer blends [3-5]. The nanocomposite with an addition of a small amount of filler were reported in the polyamide/clay system in the 1990s [6], with significant improvement in physical properties. Besides, there after many studies on ternary nanocomposites have also been reported [7-14]. In PP/elastomer/nanofiller ternary nanocomposites, the key factor is to control the morphology of nanocomposites, in order to realize noticeable properties from each component. Specifically, the desirable optimum conditions are: i) Uniform dispersion of nanofiller, ii) localization of a nanofiller in the PP matrix, and (iii) well dispersion and refinement of the elastomer. In addition to these factors, the physical properties of each component and interfacial bonding between each component are also crucial [15]. An addition of nanofillers limits

the mobility of an elastomer dispersed by melt mixing and suppresses the phase coarsening to refine the phase size of the elastomer [9,10,13]. Thus, much of considerations is necessary for the material design with special attention regarding the dispersion and localization of nanofillers.

In order to effectively improve the stiffness without compromising the impact strength, nanofillers should be localized in the continuous phase of the matrix PP [7,12]. Many factors affect the filler localization in immiscible polymer blends. Among them, two factors are particularly important. The first is the viscosity ratio between each polymer, and it is possible to change the distribution of the filler by controlling the viscosity ratio [16]. The second is the interfacial tension between each polymer and the fillers, and it is generally considered that the fillers localized in a polymer phase with a closer interfacial tension, thereby chemical modification of the filler surface is effective [17,18]. The migration is likely to occur when the filler is pre-dispersed in a thermodynamically disadvantageous polymer phase [7]. It should be noted that some blend systems have also been identified where these theories do not apply [16]. Furthermore, it is recognized that it will vary depending on the preparation and mixing protocol [7,19]. Liu *et al*. reported that organoclay and nanosilica (nanoSiO_2) were localized in the maleic anhydride-grafted phase using a maleic anhydride-grafted PP (PP-*g*-MA) or a maleic anhydride-grafted elastomer in PP/elastomer/nanofiller ternary blends [13,14]. However, the addition of PP-*g*-MA to localize the nanofillers in the PP phase reduces the stiffness of the matrix PP due to its own softening. Therefore, a method for achieving localization of the fillers while maintaining the stiffness of the matrix is required.

In Chapter 3, the functionalized PP with 1.0×10^{-3} mol% of reactive silicon

trimethoxy groups (defined as PP-OTMS) was developed by copolymerization of PP with (7-octen-1-yl)trimethoxysilane (OTMS), which was used in the current chapter as a matrix for the formation of graft-type nanocomposites [20]. It is important to notice that less than one functional groups per molecular chain of PP enabled to maintain the melting point and crystallinity of PP and acted as an end-functionalized PP. In nanocomposite with SiO_2 nanoparticles, PP-OTMS could graft to SiO_2 nanoparticles during melt mixing and the dispersion of SiO_2 nanoparticles was greatly improved. In addition, PP-OTMS reacted with each other to form a small amount of cross-linking points, resulting in the presence of partially long-chain branched (LCB) structures. Both these effects improved the yield strength and Young's modulus. By utilizing this grafting strategy, it was considered that both well dispersion and localization of the nanofillers could be achieved and the stiffness of the nanocomposites could be enhanced efficiently. The fact that the PP chain is grafted to the nanofiller can be expected to have an effect on migration of the grafted SiO_2 nanoparticles into the PP phase when the grafted SiO_2 nanoparticles can exist in the elastomer phase during melt mixing. In addition, it is also expected that the impact strength can be improved by reducing the spherulite size accompanying the promotion of nucleation by the grafted chains.

The purpose of this chapter is to understand the effects of grafting on the stiffness and toughness of PP/elastomer/SiO_2 ternary nanocomposites, where ethylene-octene copolymer (EOC) is used as an elastomer, which has excellent impact properties at low temperatures. Two types of EOC with different melt index (MI) were used for the present research. PP-OTMS/EOC/SiO_2 ternary nanocomposites were prepared using a twin-screw extruder, and the effects of the presence of a trace amount of reactive functional groups and grafting were investigated focusing on the morphology and

physical properties of the formed nanocomposites. Although many ternary nanocomposite systems have been studied, but to the best of our knowledge, there are no reports of PP-based ternary nanocomposites using fillers with PP as grafted chains. This study will be helpful to develop deep understanding on the graft-type nanocomposites and can be useful to provide a bridge towards high performance nanocomposite materials.

4.2. Experimental

4.2.1. Materials

Propylene of a polymerization grade was donated by Japan Polypropylene Corporation and used as delivered. (7-octen-1-yl)trimethoxysilane (OTMS, purchased from Tokyo Chemical Industry) was used as a comonomer without further purification. A $TiCl_4/MgCl_2$ Ziegler-Natta (ZN) catalyst containing diether as an internal donor was prepared based on our previous publication [21]. Triethylaluminum (TEA, donated by Tosoh Finechem Corporation) was used as an activator. *n*-Heptane as a polymerization solvent was dried over molecular sieve 4A. Nano-sized SiO_2 (average diameter = 30 nm, surface area = 91 m^2/g) was purchased from Kanto Chemical. Octadecyl-3-(3,5-di-tert-butyl-4-hydroxyphenyl)propionate (AO-50, donated by ADEKA Corporation) was used as a stabilizer. Two types of ethylene-octene copolymer (EOC, Dow Chemical Company, melt index (MI) = 1 and 30 g/10 min at 190 °C/2.16 kg, and the octene content = 38 wt% and 40 wt%) were used as an impact modifier after removing additives by reprecipitation (xylene to acetone). The density of two samples was identically 0.870 g/cm^3. EOC-1 and EOC-30 correspond to EOC having MI = 1 and 30, respectively.

4.2.2. Synthesis of PP-OTMS

PP-OTMS was synthesized by catalyzed propylene copolymerization with OTMS, referring to the previous chapter [20]. The polymerization was conducted in a 1 L stainless steel reactor using the ZN catalyst in a semi-batch mode. To the reactor that was sufficiently blanked by nitrogen, 500 mL of heptane, 15 mmol of TEA, and 10 mmol of OTMS were introduced in this order. Subsequently, the solution was saturated

with 0.5 MPa of propylene at 50 °C for 30 min. Followed by the introduction of 16 mmol of hydrogen, 50 mg of the catalyst was injected to initiate the polymerization. The polymerization was continued for 60 min at 50 °C under the constant pressure of propylene, and terminated by depressurization. The supernatant of the reaction slurry was removed by decantation under nitrogen, and the remaining polymer powder was repetitively washed with ethanol and acetone. Thus obtained powder was finally purified by reprecipitation (xylene to acetone), followed by drying in *vacuo* at room temperature. Unfunctionalized PP (termed as homoPP) was synthesized in the same procedure using 5 mmol of TEA in the absence of OTMS.

Table 1 summarizes the results of the polymerization. The OTMS content of PP-OTMS was calculated based on Eq. (1) shown in the following NMR characterization part, and was determined as 1.6×10^{-3} mol% to propylene units. Therefore, the same effects with those reported in the previous chapter are expected, that is, the formation of a long-chain branched (LCB) structure and grafting to fillers through the sol-gel reaction.

Table 1. Synthesis of PP-OTMS

Sample	OTMS [mmol]	Activity [kg-polymer /mol-Ti·h·atm]	*mmmm* [a] [mol%]	OTMS content [$\times 10^{-3}$ mol%] [b]
HomoPP	0	737 ± 41	97	n.a.
PP-OTMS	10	321 ± 9	98	1.6

[a] Determined by ^{13}C NMR.

[b] Determined by ^{1}H NMR.

4.2.3. Preparation of Nanocomposites with EOC

PP-OTMS that was pre-impregnated with 1.0 wt% of AO-50 was melt-mixed with 20.0 wt% of EOC and 5.0 wt% of SiO_2 nanoparticles using Micro Compounder MC5 (Xplore) at 185 °C and 100 rpm for 15 min under nitrogen atmosphere. PP-OTMS, EOC, and SiO_2 nanoparticles were added simultaneously. After melt mixing, the extrudate was hot-pressed into films with a thickness of 200 μm at 230 °C under 20 MPa for 5 min, followed by quenching at 100 °C and subsequently at 0 °C. As reference samples, i) homoPP was melt-mixed instead of PP-OTMS, ii) PP-OTMS or homoPP was melt-mixed without the addition of EOC and/or SiO_2 nanoparticles. These samples were prepared according to the same procedure.

4.2.4. Characterizations

The primary structure of polymer samples was analyzed by NMR (Bruker 400 MHz) operated at 120 °C. About 60 mg of a polymer sample was dissolved in 0.2 mL of 1,1,2,2-tetrachloroethane-d_2 (internal lock and reference) and 0.5 mL of 1,2,4-trichlorobenzene (TCB) containing 0.006 wt% of 2,6-di-*tert*-butyl-4-methylphenol (BHT). The OTMS content was determined by the following equation based on ^{1}H NMR measurement (the number of scan = 1,000),

$$\text{OTMS content} = \frac{\mathrm{H}^{\mathrm{OMe}}/9}{\mathrm{H}^{\mathrm{methine}}} \times 100 \quad \text{Eq. (1),}$$

where H^{OMe} and $H^{methine}$ are the peak areas for the methoxy protons of OTMS and methine protons of PP, respectively.The stereoregularity (*mmmm*) of PP was determined by ^{13}C NMR, and the content of octene in EOC was also calculated by ^{13}C NMR according to the ASTM standard [22].

Differential scanning calorimetry (DSC) measurements were performed on Mettler Toledo DSC 822 under nitrogen. About 8 mg of a sample was placed in an aluminum pan, and heated to 230 °C at the heating rate of 20 °C/min. The melting temperature (T_m) and the crystallinity (X_c) were determined from the endotherm of the melting. After erasing the thermal history at 230 °C for 10 min, the sample was cooled down to 25 °C at the cooling rate of 20 °C/min for acquiring the crystallization temperature (T_c), or to a specified temperature at 50 °C/min for isothermal crystallization experiments. The crystallization rate was derived as the inverse of the half time of the crystallization (denoted as $t_{1/2}^{-1}$) at each specified temperature.

Melt viscoelasticity was evaluated using a cone-and-plate rheometer (TA AR2000ex) with a diameter of 25 mm and a cone angle of 4°. A frequency sweep test was performed from the angular frequency of 500 rad/s to 0.01 rad/s at the strain value of γ = 1%. The measurements were carried out at 200 °C under nitrogen.

The dispersion of SiO_2 nanoparticles in the nanocomposites was observed by a transmission electron microscope (TEM, Hitachi H-7100) operated at 100 kV. Sample specimens with a thickness of *ca.* 100 nm were prepared by an ultramicrotome (Leica ULTRACUTS FCS) equipped with a diamond knife.

Tensile properties were measured using a tensile tester (Abecks Inc., Dat-100) at a crosshead speed of 1 mm/min at room temperature. Dumbbell-shaped specimens were cut out from a 200 μm-thick film. The yield strength and Young's modulus reported in this study correspond to the average over five or more specimens per sample.

The presence of talc in EOC was confirmed by Fourier-transformed infrared spectroscopy with a resolution of 4 cm^{-1} in ATR (PerkinElmer Spectrum 100) as well as in transmission (JASCO FT/IR 6100) modes. The cumulation number was 4 and 32

times, respectively. In the ATR mode, the sample was measured as it was, on the other hand, for the transmission mode, a film with thickness of about 30 μm was prepared by hot pressing at 100 °C.

The dispersion of EOC in the nanocomposites was observed by a scanning electron microscope (SEM, JEOL JCM-6000) operated at 15 kV. A film was cooled in liquid nitrogen for 10 min and ruptured. Subsequently, the film was immersed in *n*-heptane at 60 °C for 2 h in order to extract EOC. After repetitive washing, the etched film was dried in *vacuo* at 60 °C for 6 h. Gold sputtering was applied before SEM observation.

Impact strength of film sample was evaluated using a DuPont impact tester (Yasuda, No. 517-L DUPONT TYPE FALLING IMPACT TESTER) at 20°C. The film was kept at the measurement temperature for more than 3 hours before measurement. The setup of the tester is illustrated in Table 2 and Fig. 1. When the punch makes a crack in the film, the result was judged as “broken”.

Table 2. Specification of DuPont impact tester.

Height [mm]	50, 100, 150 mm
Weight [g]	300
Punch [inch]	φ 0.625
Stand [inch]	φ 0.64

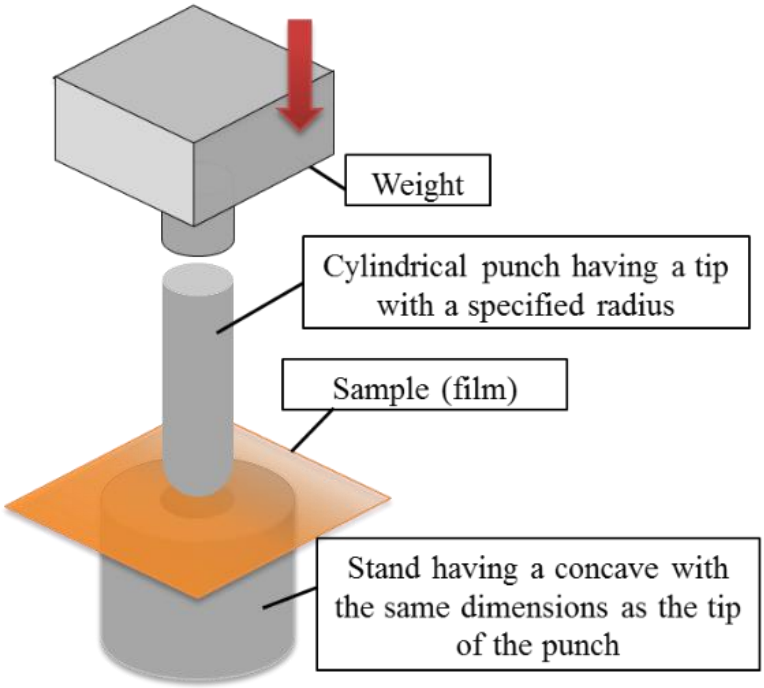

Fig. 1. Schematic diagram of DuPont impact tester.

4.3. Results and Discussion

As shown in chapter 3, in PP-OTMS/SiO_2 binary nanocomposite, it was shown that 5.0 wt% of SiO_2 nanoparticles is required to sufficiently improve the strength and modulus for PP-OTMS with 1.6×10^{-3} mol% of OTMS. However, the elongation at break deteriorated greatly by the addition of SiO_2 nanoparticles due to grafting. Therefore, in the current chapter, an attempt was made to balance the stiffness and toughness by adding EOC.

Two types of EOC (EOC-1 and EOC-30) with different MI were used for the ternary nanocomposites. Commercial EOC pellets may contain several additives, which can cause unexpected results. Therefore, the EOC pellets were reprecipitated with xylene/acetone for purification in advance. In order to confirm the effect of the reprecipitation on an octene content, the octene contents of the EOCs before and after the reprecipitation was calculated from ^{13}C NMR, because the octene-rich components can be dissolved in acetone (Table 3). No change in the octene content before and after the reprecipitation indicated that there was no significant loss by the reprecipitation. EOC-30 was coated with a small amount of talc on the surface to prevent sticking between pellets, so the presence of the talc in the reprecipitated EOC-30 was observed by FT-IR. Fig. 2 shows the IR spectra of EOC samples before and after the reprecipitation. It was confirmed by both ATR and transmission modes that the talc which was observed on the surface of the EOC-30 pellet was negligible in the sample after the reprecipitation.

Table 3. Octene content in EOC before and after reprecipitation [a]

Sample	EOC-1	EOC-30
Pellet [mol%]	9.3	9.4
After reprecipitation [mol%]	9.4	9.6

[a] Analyzed by ^{13}C NMR.

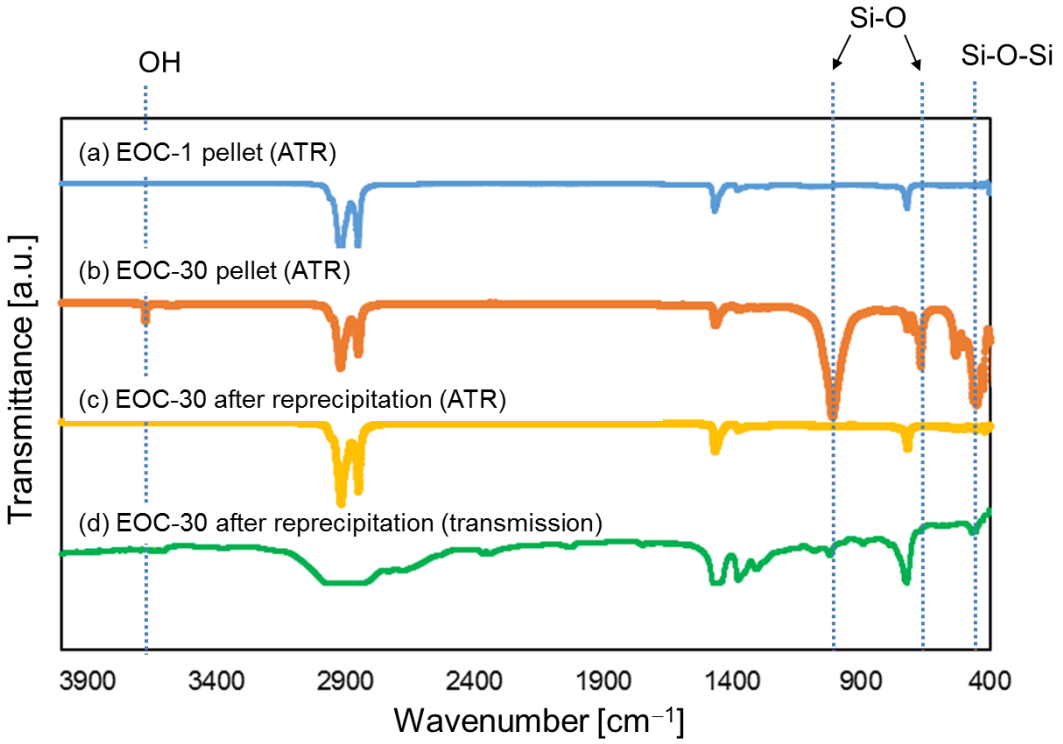

Fig. 2. IR spectra of EOC samples before and after the reprecipitation.

PP-OTMS or homoPP was compounded with 20.0 wt% of EOC and 5.0 wt% of SiO_2 nanoparticles and subjected to characterizations. PP-OTMS, EOC, and SiO_2 nanoparticles were added simultaneously in the melt mixing. In order to observe the dispersion of the EOC phase, EOC was selectively extracted with *n*-heptane. Fig. 3 shows SEM images of the nanocomposites after etching. The hollow structure observed in the images is attributed to the EOC phase, which was extracted by heptane. For all

the samples, relatively large EOC droplets were present near the film surfaces, and the droplets became smaller in the core area. It was considered that phase coarsening of EOC happened preferentially near the film surfaces during hot pressing. The EOC droplet size when using the same EOC was almost constant regardless of the matrix. On the other hand, the EOC phase of nanocomposites with EOC-1 clearly formed a smaller droplet phase than that of nanocomposites with EOC-30. This is either because EOC-1 having higher viscosity led to improved dispersion by generating high shear forces or because it surpressed the phase coarsening during hot pressing.

To understand the cause of the morphology, the phase morphology of PP-OTMS/EOC-30/SiO_2 was tracked along hot pressing time. Fig. 4 shows the SEM images of the nanocomposites after etching of EOC. In the extrudate, a very fine EOC phase of ~ 3 μm was uniformly dispersed. In the film obtained by a pressing time of 1 min, it was observed that ~ 5 μm of EOC phase was relatively dispersed homogeneously. When the pressing time was elongated to 5 min, some EOC phase of about ~ 10 μm was observed in the surface layer, and the difference in EOC size between the skin and core areas became also noticeable. When the pressing time reached 10 min, the droplets of 15 μm or more were observed. In addition, the EOC size increased as a whole including the core phase, while the number of EOC phases decreased accordingly. From the above, it can be judged that the remarkable coarsening of the EOC phase particularly in the surface layer is re-aggregation of EOC caused by heat during hot pressing. Thus, the smaller droplets for EOC-1 phase are attributed to the suppression of phase coarsening due to higher viscosity of EOC-1.

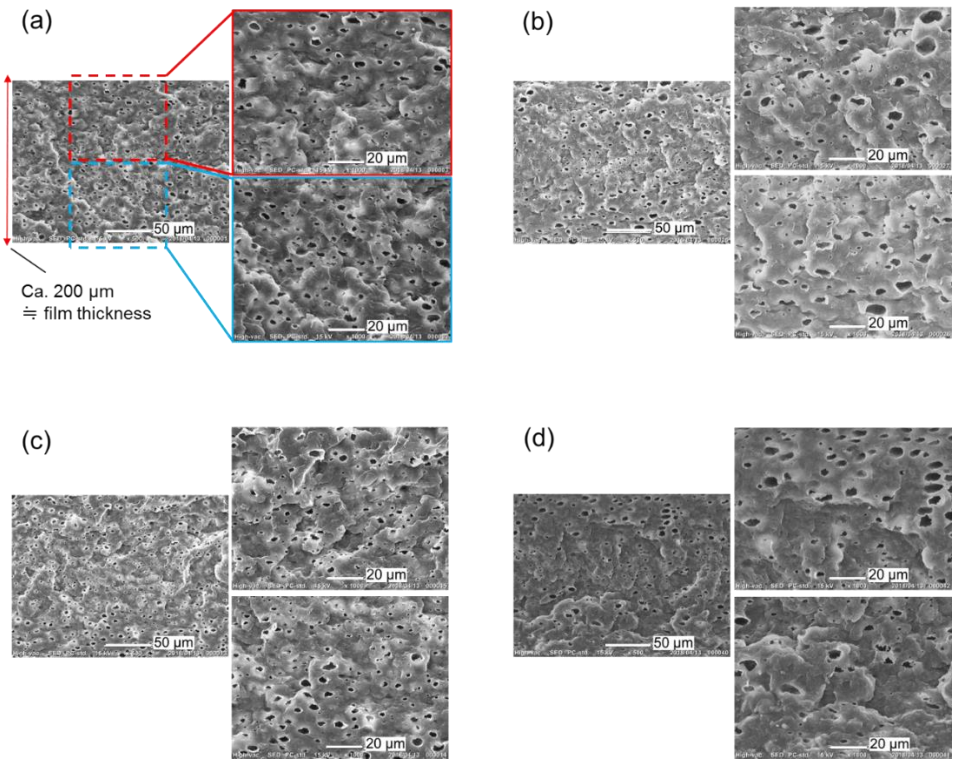

Fig. 3. SEM images of PP/EOC/SiO_2 nanocomposites at two magnifications: (a) homoPP/EOC-1/SiO_2, (b) homoPP/EOC-30/SiO_2, (c) PP-OTMS/EOC-1/SiO_2, and (d) PP-OTMS/EOC-30/SiO_2. For the left figure of each sample, the vertical length is about 200 μm, which roughly corresponds to the film thickness. Thus, the upper and lower limits are approximately the film surfaces.

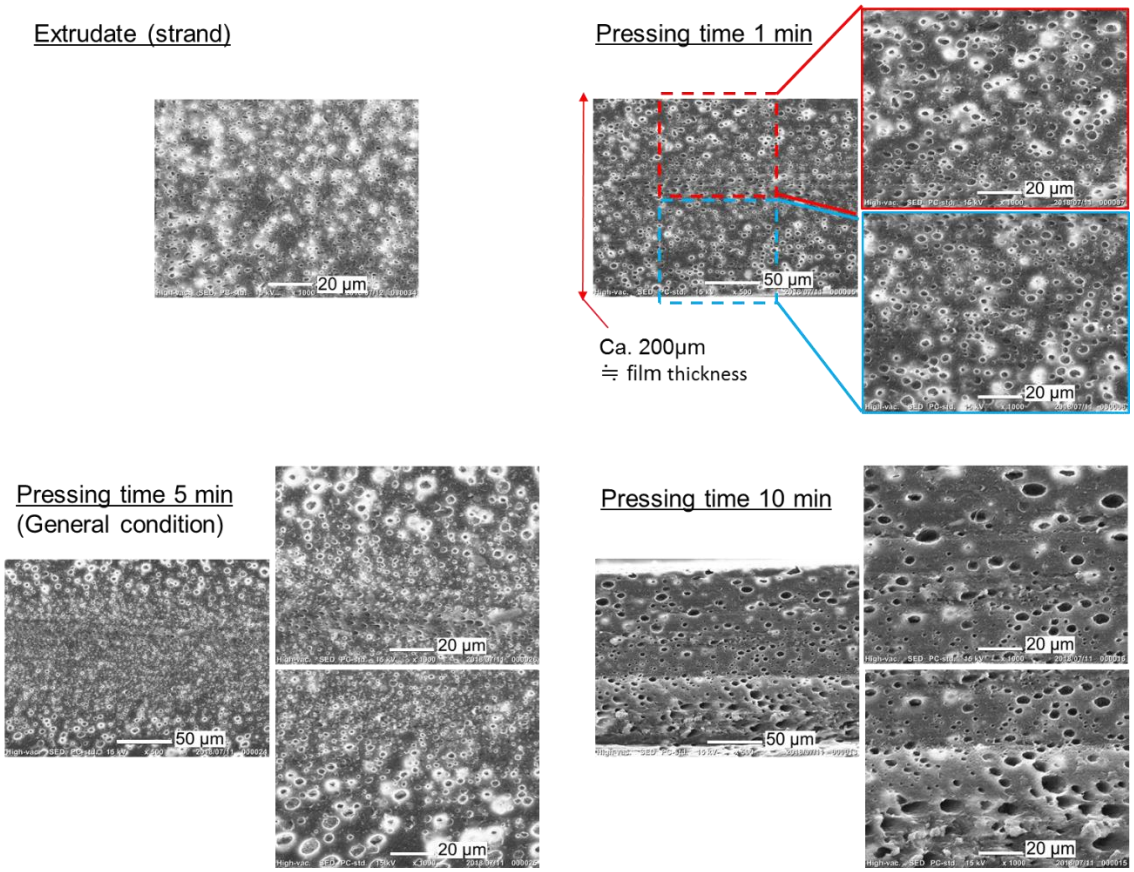

Fig. 4. SEM images of PP-OTMS/EOC-30/SiO_2 nanocomposite strand and films prepared at various hot pressing times at 230 °C. The surface was smoothed with a glass knife.

Fig. 5 shows TEM images of the PP/EOC/SiO_2 nanocomposites. The droplet phase seen in the image corresponds to the EOC phase dispersed by melt mixing. In the case of homoPP/EOC/SiO_2 (Fig. 5a–e), huge aggregates of SiO_2 nanoparticles of several hundred nm could be observed. As in the case of without EOC (previous chapter), the introduction of OTMS significantly improved the dispersion of SiO_2 nanoparticles in the PP phase (Fig. 5g–l). It should be noted that there is almost no SiO_2 nanoparticles in the EOC phase regardless of the matrix. Therefore, the SiO_2 nanoparticles present in the continuous phase efficiently contributes to the stiffness of the material. In addition, the

dispersion of SiO_2 nanoparticles seems to be slightly improved when EOC-1 was used. This is because EOC-1 having a high viscosity suppressed re-aggregation of SiO_2 nanoparticles that occurs during hot pressing, like the coarsening of EOC. This tendency was remarkably observed as a result of additional experiment observing SiO_2 nanoparticles before and after hot pressing (Fig. 6). In Fig. 6, homoPP/EOC-30/SiO_2 was prepared in two stages; premixing of EOC and SiO_2 nanoparticles for 5 min and subsequent melt mixing with PP for 15 min. It seems that the SiO_2 nanoparticles thermodynamically favors the PP phase.

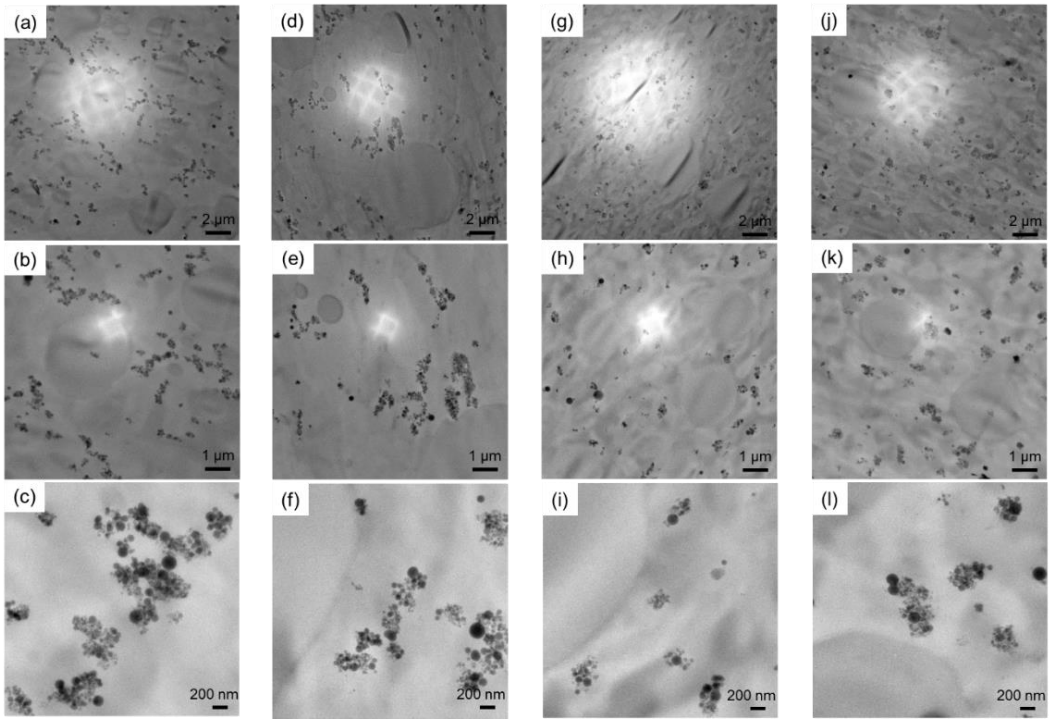

Fig. 5. TEM images of nanocomposite films at three magnifications: (a,b,c) homoPP/EOC-1/SiO_2, (d,e,f) homoPP/EOC-30/SiO_2, (g,h,i) PP-OTMS/EOC-1/SiO_2, and (j,k,l) PP-OTMS/EOC-30/SiO_2. The content of SiO_2 nanoparticles was 5.0 wt%.

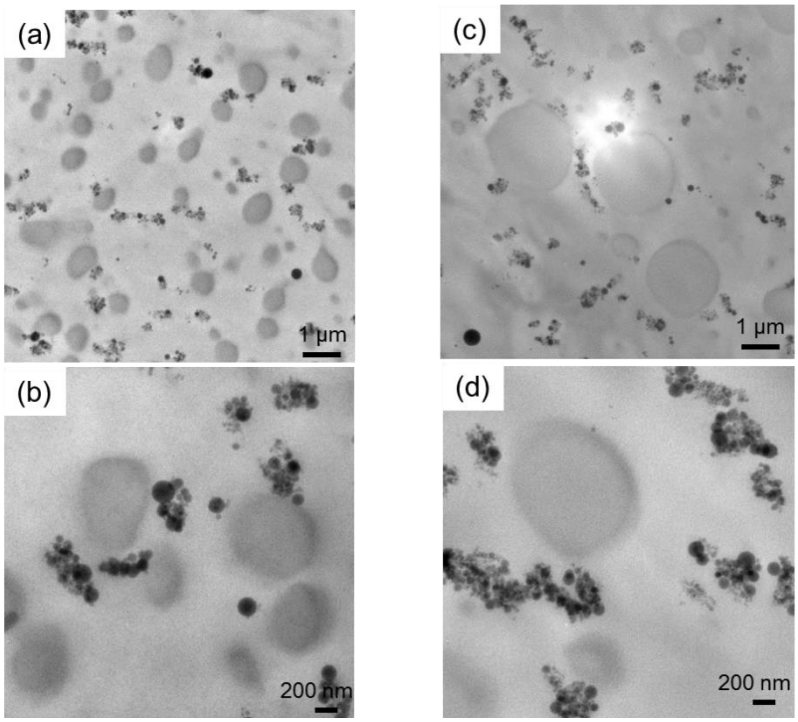

Fig. 6. TEM images of homoPP/EOC-30/SiO_2 nanocomposite at two magnifications: (a,b) before hot pressing (strand) and (c,d) after hot pressing (film). The nanocomposite was obtained by melt-mixing EOC and SiO_2 nanoparticles for 5 min in prior to the addition of PP for further melt mixing for 15 min.

Table 4 summarizes the results of DSC measurements. The presence of OTMS did not affect the melting and crystallization behavior of EOC. On the other hand, the effect on PP was the same as without EOC. The melting point (T_m) and the crystallinity (X_c) of PP-OTMS in the ternary nanocomposites were similar to those of homoPP. On the other hand, the crystallization temperature (T_c) of PP increased with the introduction of OTMS and the addition of SiO_2 nanoparticles. From the fact that the dispersion of SiO_2 nanoparticles was also improved (*cf.* Fig. 5), it seems that the grafting of PP-OTMS to

SiO_2 nanopaticles was successful in the ternary nanocomposites. There was no difference in the effect of EOC viscosity on the melting and the crystallization behavior.

Table 4. Melting and crystallization behaviors

Sample	$T_{m\ EOC}$ [°C]	$X_{c\ EOC}$ [a] [%]	$T_{m\ PP}$ [°C]	$X_{c\ PP}$ [%]	$T_{c\ PP}$ [°C]
HomoPP	n.a.	n.a.	161	52	115
HomoPP/EOC-1/SiO_2	62	5	161	52	120
HomoPP/EOC-30/SiO_2	65	5	160	53	120
PP-OTMS	n.a.	n.a.	162	56	125
PP-OTMS/EOC-1/SiO_2	63	5	163	54	129
PP-OTMS/EOC-30/SiO_2	65	6	163	57	129

[a] Calculated from the percentage of PE part using the heat of fusion of 100% polyethylene crystals.

The effect of EOC addition on mechanical properties was evaluated by uniaxial tensile test. In this chapter, as a value related to elongation at break, a toughness value was calculated from the area of the S-S curve and X axis. The samples containing EOC-1 with better dispersion of EOC and SiO_2 nanoparticles were used for testing. The results of the tensile tests are summarized in Table 5, and the stress-strain curves are shown in Fig. 7. For comparison, the results for samples without EOC are also shown. The addition of EOC drastically attenuated the tensile strength and Young's modulus of the matrices in cost of a significant improvement in toughness. The reinforcement of PP-OTMS/EOC by the addition of SiO_2 nanoparticles was higher than that of homoPP/EOC. Needless to say, this is the effect of strengthening the interfacial bonding between PP-OTMS and SiO_2 nanoparticles and improving the dispersion of SiO_2 nanoparticles in the PP-OTMS matrix by grafting. The degree of deterioration in the

elongation at break by the addition of SiO_2 nanoparticles was more remarkable in the PP-OTMS/EOC composite, resulting in the severe deterioration of toughness. It is presumed that the PP-OTMS matrix embrittled by grafting could not follow the deformation of the EOC. Fig. 8 is the plot of the Young's modulus against the toughness of the ternary nanocomposites. As clearly seen in Fig. 8, the current strategy for graft-type nanocomposites is very effective for stiffness, but at the expense of toughness. To overcome this problem, it is necessary to improve the resistance to cracking while taking advantage of the graft-type nanocomposites. For example, one of the potential way is to create a network around the grafted filler, which will improve the toughness by distributing the stress or delaying the crack growth. This is suggested by the improvement in elongation at break when PP-OTMS had a large amount of OTMS in chapter 3. In addition, the combination with short graft chains that can be relaxed along deformation, along with long graft PP chains for high strength will be effective.

Table 5. Results of tensile tests [a]

Sample	Yield strength [MPa]	Young's modulus [MPa]	Elongation at break [%]	Toughness [MJ/m^3]
HomoPP	30.9 ± 0.9	600 ± 48	29.5 ± 7.2	7.1 ± 2.1
HomoPP/SiO_2 [c]	31.9 ± 1.4	599 ± 35	12.6 ± 2.1	2.9 ± 0.6
HomoPP/EOC-1 [b]	19.4 ± 0.3	338 ± 43	127.7 ± 39.8	22.7 ± 7.1
HomoPP/EOC-1/SiO_2 [b,c]	19.8 ± 0.3	359 ± 46	66.1 ± 20.7	11.8 ± 3.8
PP-OTMS	32.5 ± 0.5	644 ± 96	28.9 ± 6.7	7.8 ± 1.9
PP-OTMS/SiO_2 [c]	33.4 ± 0.7	661 ± 76	11.2 ± 0.9	2.6 ± 0.3
PP-OTMS/EOC-1 [b]	20.2 ± 0.3	406 ± 58	114.7 ± 45.3	21.6 ± 8.8
PP-OTMS/EOC-1/SiO_2 [b,c]	21.3 ± 0.3	460 ± 62	46.5 ± 16.8	8.9 ± 3.4

[a] Tensile properties were determined as averages at least over 5 specimens.

[b] The content of EOC was 20.0 wt%.

[c] The content of SiO_2 was 5.0 wt%.

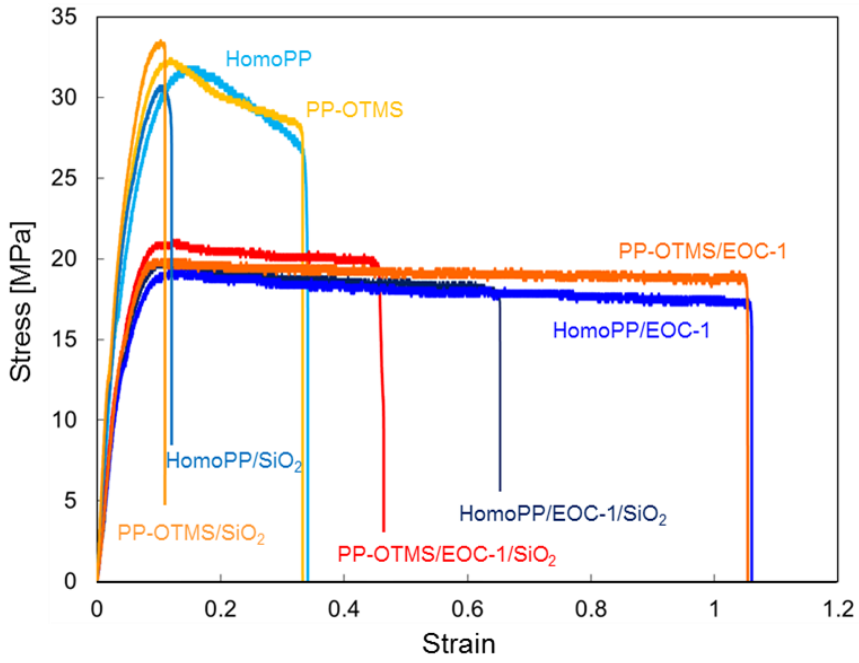

Fig. 7. Stress-strain curves for PP-OTMS and its composite materials.

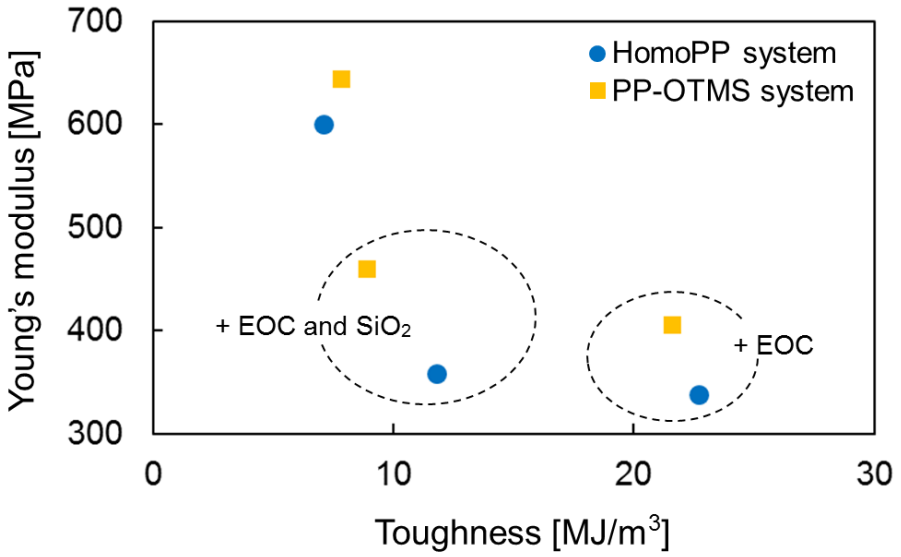

Fig. 8. Toughness and stiffness balance for matrices, matrix/EOC blends, and ternary nanocomposites.

For further understanding in the toughness of the ternary nanocomposites, the impact strength of the nanocomposite was evaluated by DuPont impact test. The results of the samples without SiO_2 nanoparticles (and EOC) are also shown. The results are summarized in Table 6, and the photographs of the sample films after the test are shown in Fig. 9. The impact was applied by dropping a weight of 300 g from the height of 50, 100 and 150 mm, three times for each height as shown in Fig. 9. In the absence of SiO_2 nanoparticles and EOC, homoPP film was easier to crack than PP-OTMS film. This is due to the reduction in spherulite size by the introduction of OTMS as compared to homoPP (*cf.* Table 4; raised crystallization temperature suggests a reduction in spherulite size). In the case of homo PP, cracking were dramatically suppressed by the addition of EOC, and further addition of SiO_2 nanparticles did not change the results. On the other hand, in the case of PP-OTMS, cracking were hardly suppressed by the adding of EOC,

and further addition of SiO_2 nanparticles worsened the results. Since the dispersion of EOC did not change between the matrix (*cf*. Fig. 3) and the spherulite size should be smaller, it was inferred that these deteriorations were caused by stress concentration at the moment of impact on the cross-linking point due to the interchain reaction or physical cross-linking point by the grafting, which became the starting point of crack. As described earlier in the tensile test, further efforts are required for the development of graft-type nanocomposites to solve these problems.

Table 6. Results of DuPont impact tests [a]

Sample	50 mm	100 mm	150 mm
HomoPP	○	△	××
HomoPP/EOC-1[b]	○	○	○
HomoPP/EOC-1/SiO_2 [b, c]	○	○	○
PP-OTMS	○	△	△
PP-OTMS/EOC-1 [b]	○	○	△
PP-OTMS/EOC-1/SiO_2 [b, c]	○	○	×

○: None of them cracked △: One cracked

×: Two cracked ××: All cracked

[a] Impact was applied by a 300 g weight from a specific height.

[b] The content of EOC was 20.0 wt%.

[c] The content of SiO_2 was 5.0 wt%. The nanocomposite was obtained by melt mixing PP-OTMS and SiO_2 nanoparticles for 15 min in prior to the addition of EOC for further melt mixing for 5 min.

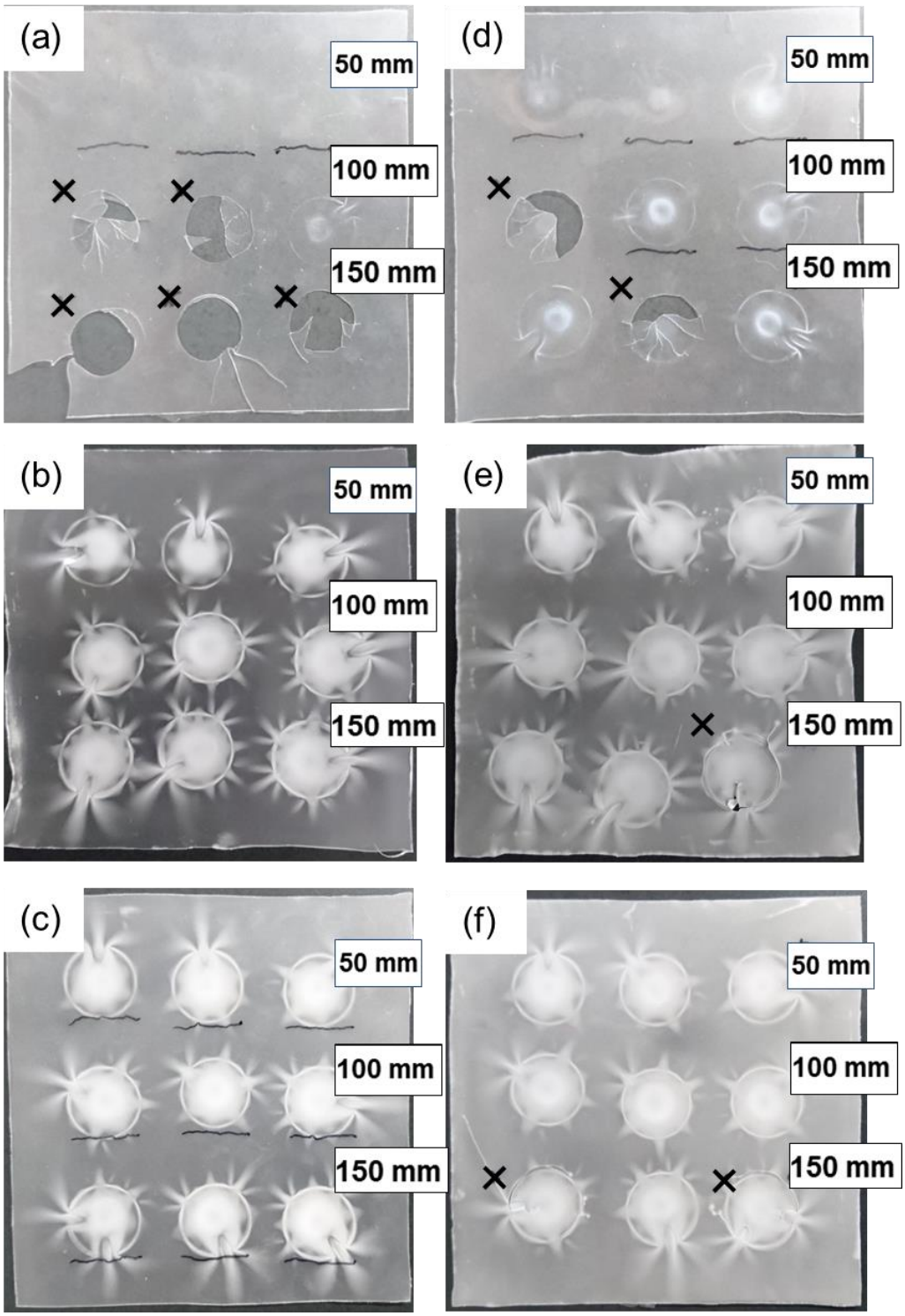

Fig. 9. The photographs of film sample after Dupont impact test: (a) homoPP, (b) homoPP/EOC-1, (c) homoPP/EOC-1/SiO_2, (d) PP-OTMS, (e) PP-OTMS/EOC-1, and (f) PP-OTMS/EOC-1/SiO_2.

4.4. Conclusions

In this chapter, PP-OTMS/EOC/SiO_2 nanocomposites were prepared using the two types of EOC having different melt index to understand the effects of grafting on the stiffness and toughness. EOC-1 with higher viscosity suppressed the phase coarsening of EOC and SiO_2 nanoparticles during compression molding and maintained better dispersion. The introduction of OTMS improved the dispersion of SiO_2 nanoparticles selectively present in the PP phase and contributed to the improvement of strength and modulus. However, the grafted chain to rigid SiO_2 nanoparticles could not follow the flexible EOC deformation and sacrificed the toughness. In the impact test, the addition of EOC dramatically suppressed the occurrence of crack in homoPP, but only a little improvement in PP-OTMS due to the local cross-linking point could become the stress concentrator for the impact. The addition of SiO_2 nanoparticles into PP-OTMS/EOC made the stress concentration more prominent by grafting. In conclusion, in order to improve stiffness and toughness simultaneously, it would be necessary to overcome these challenges by applying some additional modifications, for example, by combiting a network structure and/or short graft chains together with long graft PP chains for crack suppression.

References

[1] R. A. Bubeck, Mater. Sci. Eng. R 39 (2002) 1–28.

[2] T. McNally, P. McShane, G. M. Nally, W. R. Murphy, M. Cook, A. Miller, Polymer 43 (2002) 3785–3793.

[3] P. Toro, R. Quijada, M. Yazdani-Pedram, J. L. Arias, Mater. Lett., 61 (2007) 4347–4350.

[4] Y. W. Leong, M. B. A. Bakar, Z. A. M. Ishak, A. Ariffin, B. Pukanszky, J. Appl. Polym. Sci. 91 (2004) 3315–3326.

[5] P. Mareri, S. Bastide, N. Binda, A. Crespy, Compos. Sci. Technol. 58 (1998) 747–752.

[6] A. Usuki, M. Kawasumi, Y. Kojima, A. Okada, J. Mater. Res. 8 (1993) 1174–1178.

[7] R. Wiwattananukul, B. Fan, M. Yamaguchi, Compos. Sci. Technol. 141 (2017) 106–112.

[8] R. R. Tiwari, D. R. Paul, Polymer 52 (2011) 4955–4969.

[9] R. R. Tiwari, D. R. Paul, Polymer 52 (2011) 5595–5605.

[10] S. H. Lee, M. Kontopoulou, C. B. Park, Polymer 51 (2010) 1147–1155.

[11] M. Bailly, M. Kontopoulou, Polymer 50 (2009) 2472–2480.

[12] Y. Liu, M. Kontopoulou, J. Vinyl. Add. Tech. 13 (2007) 147–150.

[13] Y. Liu, M. Kontopoulou, Polymer 47 (2006) 7731–7739.

[14] J. R. Austin, M. Kontopoulou, Polym. Eng. Sci. 46 (2006) 1491–1501.

[15] T. Taniike, M. Toyonaga, M. Terano, Polymer 55 (2014) 1012–1019.

[16] J. Plattier, L. Benyahia, M. Dorget, F. Niepceron, J. Tassin, Polymer 59 (2015) 260–269.

[17] X. Q. Liu, Z. Y. Sun, R. Y. Bao, W. Yang, B. H. Xie, M. B. Yang, RSC Adv. 4

(2014) 41059–41068.

[18] D. Wu, D. Lin, J. Zhang, W. Zhou, M. Zhang, Y. Zhang, D. Wang, B. Lin, Macromol. Chem. Phys. 212 (2011) 613–626.

[19] L. Elias, F. Fenouillot, J. C. Majesté, P. Alcouffe, P. Cassagnau, Polymer 49 (2008) 4378–4385.

[20] E. Kurahashi, T. Wada, T. Nagai, P. Chammingkwan, M. Terano, T. Taniike, Polymer 158 (2018) 46–52.

[21] Y. Hiraoka, S. Y. Kim, A. Dashti, T. Taniike, M. Terano, Macromol. React. Eng. 4 (2010) 510–515.

[22] ASTM D 5017−96, Determination of Linear Low Density Polyethylene (LLDPE) Composition by Carbon-13 Nuclear magnetic Resonance (Reapproved 2003).

Chapter 5

General Conclusions

This dissertation covered a wide range of studies from the synthesis of functionalized PP with a trace amount of reactive functional groups to the application to composites including nanocomposites.

Chapter 1 described the structure, polymerization catalyst, functionalization, and composite for polypropylene. A brief summary of history, methods, mechanisms, etc. was provided for each unit based on the objective of this dissertation.

Chapter 2 described the synthesis of functionalized PP in copolymerization with vinyl alkoxysilane comonomers using a Ziegler-Natta (ZN) catalyst. (7-octen-1-yl) trimethoxysilane (OTMS), a comonomer with a good balance both the bulkiness of the alkoxy group and the spacer length, can be incorporated into the PP chain in a small amount. The copolymer (PP-OTMS) was obtained without significant deactivation by controlling the TEA amount. When the amount of OTMS is sufficiently small, the tensile properties of PP-OTMS improved by *in-situ* formed long-chain branched structure without deteriorating the basic properties of PP.

Chapter 3 described the study of PP-OTMS/SiO_2 nanocomposites that can be grafted *in-situ* with SiO_2 nanoparticles during melt mixing using PP-OTMS having less than one OTMS groups per molecular chain. The melt mixing of PP-OTMS led to introduction of a LCB structure, as well as *in-situ* grafting to SiO_2 nanoparticles. These events dramatically promoted the crystallization as compared to pristine PP and its nanocomposites. The grafted chains also improved the dispersion of the SiO_2 nanoparticles, and strengthened the interfacial bonding with the matrix for the tensile reinforcement.

Chapter 4 described the study on the improvement of toughness by adding an elastomer for the purpose of balancing stiffness and toughness. The toughness of PP-OTMS/SiO_2 nanocomposites was dramatically improved by the addition of ethylene-octene

copolymer (EOC). The introduction of OTMS improved the dispersion of SiO_2 nanoparticles selectively present in the PP phase and enhanced yield strength and Young's modulus, whereas the toughness was sacrificed. In the impact test, not only the grafting but also the cross-linking point by the interchain reaction between PP-OTMS was very sensitive to applied impact.

In conclusion, the trace functionalization strategy of PP by means of copolymerization under suitable comonomer and polymerization conditions using a ZN catalyst has dramatically facilitated an access to functionalized PP. In particular, the development of side-functionalized PP with less than one side chain per molecular chain has proven useful as an alternative for end-functionalized PP. The graft-type nanocomposites prepared based on this strategy have drastically alleviated preparation difficulties compared to the previous methodologies. Although some of the remaining obstacles in terms of toughness still will be a challenge for the future, the characteristic properties of graft-type nanocomposites will continue to attract both academic and industrial interests. Based on these strategies, I hope that the usage of PP will further expand and contribute towards the betterment of the demanding necessities of materials for global community.

Achievements

＜Original paper＞

“Synthesis of polypropylene functionalized with a trace amount of reactive functional groups and its utilization in graft-type nanocomposites”

Eiji Kurahashi, Toru Wada, Takeshi Nagai, Patchanee Chammingkwan, Minoru Terano, Toshiaki Taniike, Polymer, 2018, 158, 46.

＜International conference＞

“Improvement of Properties of Polypropylene by Trace Functionalization and its Development to Nanocomposite Materials”

Asian Polyolefin Workshop 2017, Tianjin, China, Oct. 2017.

“Polypropylene with a Trace Amount of Silicon Methoxy Groups as Promising Matrix for Graft-type Nanocomposite”

5th Blue Sky Conference on Catalytic Olefin Polymerization, Sorrento, Italy, Jun. 2019.

＜Domestic conference＞

“極微量アルコキシ基を導入した PP ナノコンポジットの物性に関する検討”

マテリアルライフ学会 第 22 回春季研究発表会、横浜、2018 年 2 月

Acknowledgement

I would like to express my sincere regards to Associate Professor Dr. Toshiaki Taniike for his excellent guidance and encouragement. I am deeply grateful to Senior Lecturer Dr. Chammingkwan Patchanee for her helpful discussion and many suggestion about experiments.

I would like to thank Research Assistant Professor Dr. Toru Wada and Dr. Ashutosh Thakur for their quite valuable advice and comments. I would like to thank Professor Dr. Masayuki Yamaguchi for the assistance of my research, especially for rheological measurement. I would like to thank Dr. Akio Miyazato for his support and guidance regarding GC-MS measurement and analysis. Great acknowledgments are made to Professor Dr. Shin-ichi Kuroda and Assistant professor Dr. Takahiko Kawai in Gunma University provided valuable advices and helpful discussions for my minor research.

I would like to thank Dr. Priyank Mohan, Dr. Kalaivani Seenivasan, Dr. Bulbul Maira, Dr. Thi Tuyet Mai Le, Ms. Emi Sawade, Mr. Shunjiro Nagai, Ms. Hiroko Takemoto, Ms. Maki Tsushi, Mr. Koyuru Nakayama, Mr. Shin Yoshida, Ms. Thuy Tran Phuong Nhat, Ms. Nhan Ton Nu Thanh, Mr. Thanh Nhat Nguyen, Ms. Xi Zhang, Mr. Tomohiro Ikeda, Mr. Gentoku Takasao, Mr. Kai Togawa, Ms. Hui You, and other members in Taniike laboratory.

I also deeply appreciate all the members in Yamaguchi laboratory for their kind supporting my research.

I am deeply grateful to my company Senior Adviser Yoichiro Kojima, President Eiji Kojima, Director Atsushi Matsumoto, General Manager Hisanori Tsuchikawa, Deputy General Manager Tetsuya Tadano, Manager Tamotsu Araki and Assistant Manager Takeshi Nagai for encouragement and supports of my study. I also thank to all the

colleagues in Kojima Industries Corporation for their encouragement.

I highly appreciate my wife, child and our parents for their understanding my work and supports for my life.

Minor-research

Effect of long-chain branched structure formed by functionalized PP on fracture behavior during stretching

by

Eiji Kurahashi

Submitted to

Japan Advanced Institute of Science and Technology

Supervisor in Gunma University: Professor Dr. Shinichi Kuroda

Supervisor in JAIST: Professor Dr. Tatsuo Kaneko

September 2019

Introduction

Polypropylene (PP) is one of the most widely used plastics due to its low density, low cost, and well-balanced properties, whereas its melt tension is relatively low. It is well known that insertion of long-chain branched (LCB) structures into PP improves not only melt tension but also mechanical properties [1−3]. Improvement of melt tension helps processes such as blow molding and foam molding.

Although LCBPP can be generated *in situ* during polymerization by using specific catalysts [4−6], two post-treatment methods are mainly adopted in industry; one is electron beam irradiation under an inert atmosphere [7,8], and the other is reactive extrusion using peroxides [9−11]. These methods can easily produce LCBPP. However, electron beam or peroxides also generates radicals, and the physical properties of PP itself can deteriorate due to the simultaneous progress of β-scission [8,11]. In recent years, I have developed a unique functionalized PP by incorporating a trace amount of reactive silicon methoxy groups into PP by means of copolymerization with (7-octen-1-yl)trimethoxysilane (OTMS) using a general Ziegler-Natta catalyst (defined as PP-OTMS) [12]. The incorporation of 1.5–7.1 × 10^{-3} mol% of OTMS corresponded to the introduction of 0.02–0.12 side chains per main chain, hence sufficiently low to maintain the basic properties of PP. During melt mixing, PP-OTMS partially reacted with each other and formed a small amount of crosslinking points. In other words, it locally possesses LCB structure, which had improved tensile properties. In particular, the elongation at break showed a specific behavior against the amount of OTMS. Specifically, introduction of a trace amount of silicon methoxy groups (1.5 × 10^{-3} mol%) reduces the elongation at break as compared with homoPP. However, as the introduction amount of OTMS is increased (from 1.5 × 10^{-3} to 7.1 × 10^{-3} mol%), the

elongation at break tends to improve gradually. It is speculated that this specific behavior is due to the formation of a local LCB structure. However, the mechanism for how the local LCB structure affects the fracture behavior still has not been fully clarified yet. In order to get insight into the mechanism, *in-situ* structural analysis during physical destruction is indispensable. It is very interesting and important for both in industry and academia to investigate the effects of such a trace amount of LCB structure.

It is known that internal pores formed during deformation are closely related to fracture of polymers [13,14]. To observe the pores, direct observation with a microscope, gas adsorption, synchrotron X-ray, etc. are usually used. In order to analyze the structural change during rapid deformation, *in-situ* observation of non-destructive, short intervals with good sensitivity is required. In SPring-8, which can produce the highest brightness synchrotron radiation, it is possible to obtain good scattering with little noise in short exposure time, which is a suitable technique for this study. It is also an advantage to quantitatively evaluate the average structure of the sample.

The purpose of this study is to investigate the effect of a trace amount of LCB structure prepared thorough PP-OTMS on the fracture behavior during stretching based on internal structural changes. In-situ WAXD/SAXS simultaneous measurement was adopted to observe the internal structure during stretching. From SAXS measurements, the formation of voids generated during stretching and its amount (scattering intensity) was mainly evaluated, whereas a change in crystal structure was observed from the WAXD measurement. The relationship between the change of internal structure and the fracture behavior during stretching was discussed based on the amount of OTMS.

1. Experimental

The functionalized PP with reactive functional groups (defined as PP-OTMS: Scheme 1) was synthesized according to our previous study [12]. The properties of PP-OTMS quoted from our paper are summarized in Tables 1 and 2, and typical stress-strain (S-S) curves of PP-OTMS are shown in Fig. 1. The preparation conditions are described in the following sections 1.1–1.3.

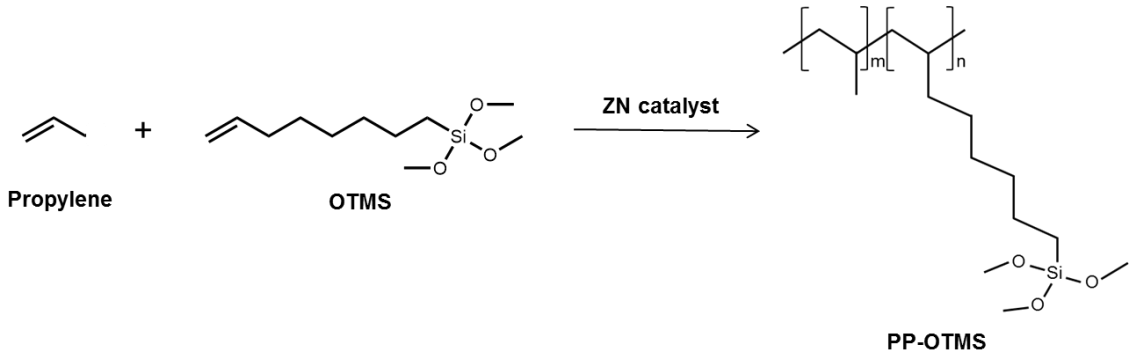

Scheme 1. Synthesis of PP-OTMS by means of copolymerization of propylene with (7-octen-1-yl)trimethoxysilane (OTMS).

Table 1. Catalytic activity and characterization of PP-OTMS [12].

Samples	OTMS [mmol]	Activity [kg-polymer /mol-Ti·h·atm]	*mmmm* [a] [mol%]	M_n [b]	M_w [b]	M_w/M_n [b]	OTMS content [$\times 10^{-3}$ mol%] [c]	OTMS content [Number per main chain] [d]
HomoPP	0	1030 ± 8	95	6.3×10^4	2.4×10^5	3.9	n.a.	0
PP-OTMS5	5	470 ± 5	97	6.3×10^4	2.4×10^5	3.8	1.5 ± 0.2	0.02
PP-OTMS10	10	230 ± 8	98	7.3×10^4	2.7×10^5	3.7	3.2 ± 0.2	0.06
PP-OTMS15	15	93	98	7.3×10^4	2.9×10^5	3.9	7.1	0.12

[a] Determined by ^{13}C NMR.

[b] Determined by GPC.

[c] Determined by ^{1}H NMR.

[d] Calculated using the OTMS content and M_n.

Table 2. Tensile properties and crystallinity of samples [12].

Samples	Yield strength [a] [MPa]	Young's modulus [a] [MPa]	Elongation at break [a] [%]	Crystallinity [b] [%]
HomoPP	31.1 ± 0.9	603 ± 24	26.9 ± 10.3	51
PP-OTMS5	33.3 ± 1.0	616 ± 43	21.6 ± 6.4	53
PP-OTMS10	34.2 ± 0.7	622 ± 40	32.5 ± 9.8	53
PP-OTMS15	35.0 ± 0.9	637 ± 20	48.0 ± 11.0	51

[a] Tensile test was performed on at least five specimens at room temperature.

[b] Measured by DSC.

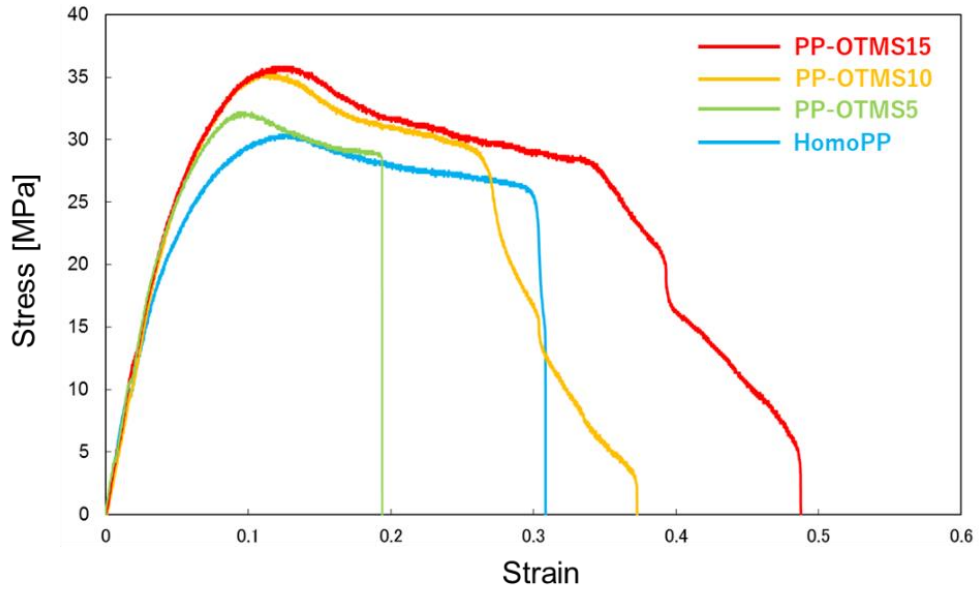

Fig. 1. Typical S-S curves for PP-OTMS measured at room temperature [12].

1.1. Materials

Propylene of a polymerization grade was donated by Japan Polypropylene Corporation and used as delivered. (7-octen-1-yl)trimethoxysilane (OTMS) was used as a comonomer without further purification. A $TiCl_4/MgCl_2$ Ziegler-Natta (ZN) catalyst containing diether as an internal donor was prepared based on our previous publication [15]. Triethylaluminum (TEA, donated by Tosoh Finechem Corporation) was used as an activator. *n*-Heptane as a polymerization solvent was dried over molecular sieve 4A. Octadecyl-3-(3,5-di-tert-butyl-4-hydroxyphenyl)propionate (AO-50, donated by ADEKA Corporation) was used as a stabilizer.

1.2. Synthesis of PP-OTMS

PP copolymer with OTMS (PP-OTMS) was synthesized by catalyzed propylene polymerization using OTMS as a comonomer. The polymerization was conducted in a 1 L stainless steel reactor using the ZN catalyst in a semi-batch mode. To the reactor that was sufficiently blanked by nitrogen, 500 mL of heptane, 5–20 mmol of TEA, and 0–15 mmol of OTMS were introduced in this order. Subsequently, the solution was saturated with 0.5 MPa of propylene at 50 °C for 30 min. Followed by the introduction of 16 mmol of hydrogen, 50 mg of the catalyst was injected to initiate the polymerization. The polymerization was continued for 60 min at 50 °C under the constant pressure of propylene, and terminated by depressurization. The supernatant of the reaction slurry was removed by decantation under nitrogen, and the remaining polymer powder was repetitively washed with ethanol and acetone. Thus obtained powder was finally purified by reprecipitation (xylene to acetone), followed by drying in *vacuo* at room temperature. Four samples were synthesized: HomoPP, PP-OTMS5, PP-OTMS10, and

PP-OTMS15, corresponding to the addition amount of OTMS of 0, 5, 10, and 15 mmol, respectively.

1.3. Preparation of films

PP-OTMS that was pre-impregnated with 1.0 wt% of AO-50 was melt-mixed using Micro Compounder MC5 (Xplore) at 185 °C and 100 rpm for 15 min under nitrogen atmosphere. After melt mixing, the extrudate was hot-pressed into films with a thickness of 200 μm at 230 °C under 20 MPa for 5 min, followed by quenching at 100 °C and subsequently at 0 °C. As a reference sample, homoPP was also melt-mixed and hot-pressed according to the same procedure.

1.4. Characterizations

The relaxation behavior was evaluated by dynamic mechanical analyzer (DMA, Toyoseiki RHEOLOGRAPH-SOLID) using a 4 mm × 20 mm × 200 μm strip-shaped specimen. The measurement was performed at a frequency of 1 Hz by heating from −120 °C to 150 °C at a heating rate of 2 °C/min under nitrogen atmosphere.

The structural changes of samples during stretching process were analyzed by *in-situ* simultaneous measurements of wide-angle X-ray diffraction (WAXD) and small-angle X-ray scattering (SAXS) at the BL05XU beamline in SPring-8 (Hyogo, Japan). The beam was irradiated for 0.35 seconds every 6 seconds during tensile test. The tensile test was performed using a tensile tester (Dip) at a crosshead speed of 1 mm/min at 100 °C. A notch-shaped specimen was cut out from a 200 μm-thick film (*cf*. Fig. 2). Only the center part of the specimen was heated by hot air. The relationship between load and elongation was recorded while being irradiated with X-rays. The specific conditions of

measurement are summarized in Fig. 2. The obtained image was denoised with dark and background data and edited in one dimension using Fit2d software. Note that the analyzes in the meridional direction and the equatorial direction were performed with a width of 10°.

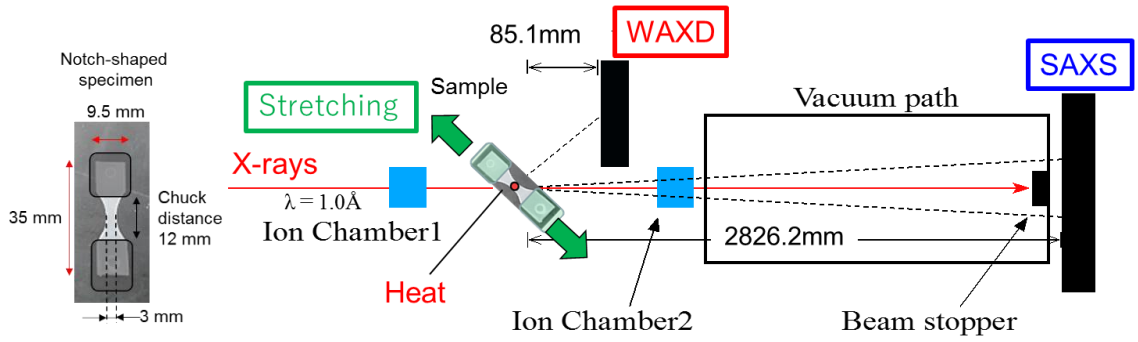

Fig. 2. Schematic diagram of tensile test/WAXD/SAXS simultaneous measurement.

Additional tensile tests at 100 °C atmosphere were performed a tensile tester (A&D Company TENSILON RTF-1350) equipped with a heating chamber in order to check the effect of temperature unevenness. A notch-shaped specimen was adopted as in the case of WAXD/SAXD simultaneous measurement during stretching.

2. Results and Discussion

The influence on relaxation behavior by incorporation a trace amount of OTMS into PP was evaluated by DMA measurement. Fig. 3 shows the temperature dependence of storage modulus (G') and tan δ obtained from DMA measurement. In all samples, a peak attributed to β relaxation was observed around 10 °C in tan δ, and G' significantly decreased at this temperature as a boundary. In addition, a broad peak was also observed around 50–130 °C attributed to α relaxation. β relaxation is known as relaxation based on the glass-rubber transition due to Brownian motion in the amorphous region, and α relaxation is known as relaxation involving the crystalline region [16,17]. The fact that the G' values of PP-OTMS are nearly equal at temperatures above the glass transition may indicate that the abundance of OTMS has a significant effect on the amorphous part. The results of the glass transition temperature (T_g) obtained from the peak top of the fitting curve of tan δ are summarized in Table 3. Note that the fitting was performed at a fixed temperature range between −30 °C and 50 °C. The T_g of homoPP was 9.5 °C, and that of PP-OTMS15 was 7.8 °C, showing no significant difference. In α relaxation region, it was difficult to fit the curve, and the difference of α relaxation by the incorporation OTMS could not be judged.

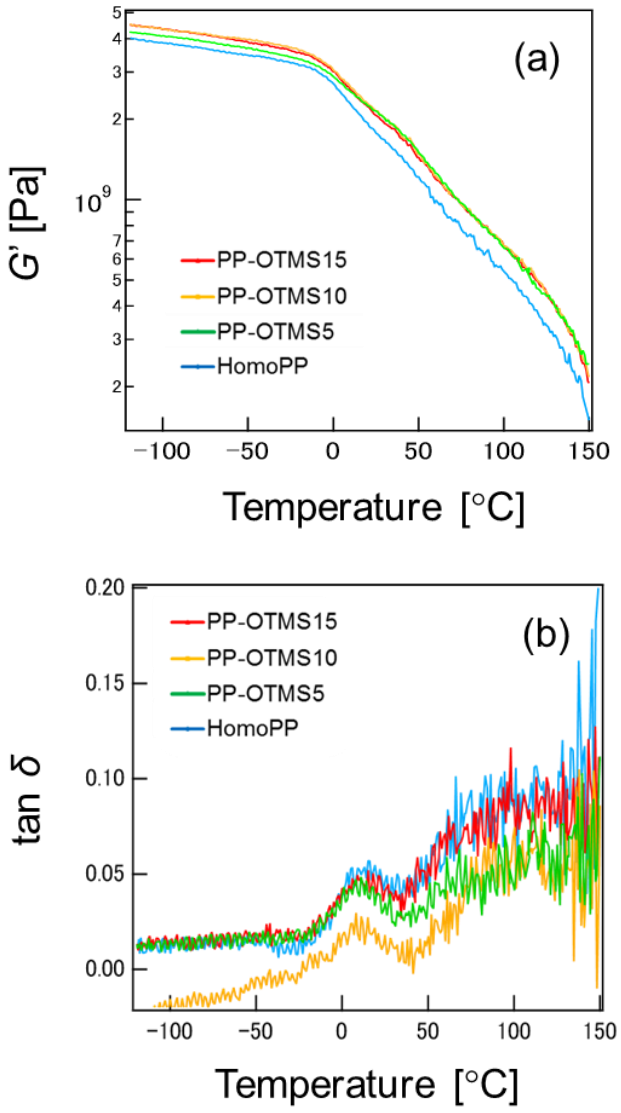

Fig. 3. (a) *G*' and (b) tan δ curves of PP-OTMS.

Table 3. Glass transition temperature of PP-OTMS.

Samples	Glass transition temperature (T_g) [a] [°C]
HomoPP	9.5
PP-OTMS5	8.6
PP-OTMS10	8.7
PP-OTMS15	7.8

[a] Analyzed by DMA.

Tensile test/WAXD/SAXS simultaneous measurement was performed at 100 °C in order to make the difference in the relaxation behavior and in the fracture behavior between samples more prominent. Fig. 4 shows typical S-S curves for PP-OTMS during the WAXD/SAXS simultaneous measurement. To reliably stretch the X-ray irradiated part, only the center part of a notch-shaped specimen was heated (*cf.* Fig. 2). It should be noted that the tensile test was performed on a notch-type specimen and therefore differs from the exact strength and elastic modulus values, because the heating area (and cross-sectional area) may change depending on the sample. In the 100 °C tensile test, the same fracture behavior as that measured at room temperature was obtained except for the unusually high strength of PP-OTMS5. Specifically, the introduction of a trace amount of OTMS into PP deteriorated the elongation at break (PP-OTMS5), and further increase in the amount of OTMS improved the elongation at break. In other words, toughening was induced by the introduction of an appropriate amount of OTMS.

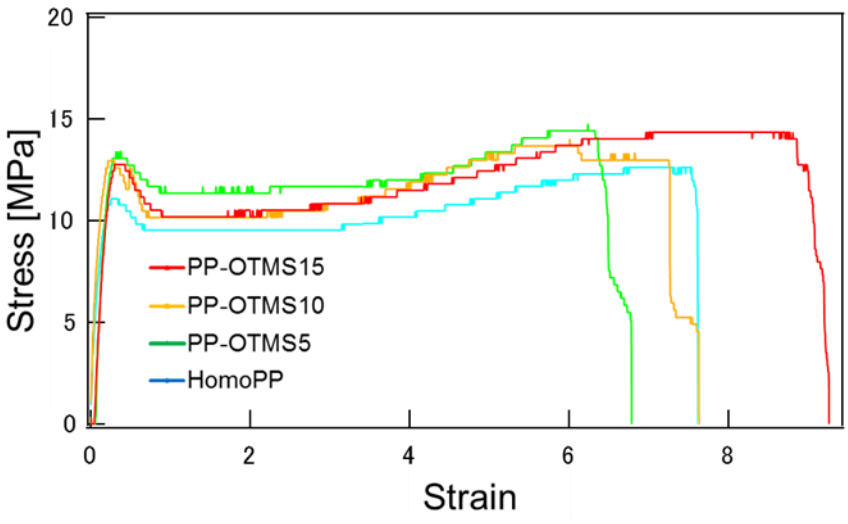

Fig. 4. S-S curves for PP-OTMS measured at 100 °C. Only the center part of the specimen was heated.

In terms of strength, in order to confirm the reproducibility of the tensile behavior at 100 °C and at room temperature, an additional tensile test was performed using a sample in which the entire specimen was heated in a heating chamber (Fig. 5). As shown in Fig. 5, the trend between OTMS amount and the strength was similar to that at room temperature, and PP-OTMS15 showed the highest strength.

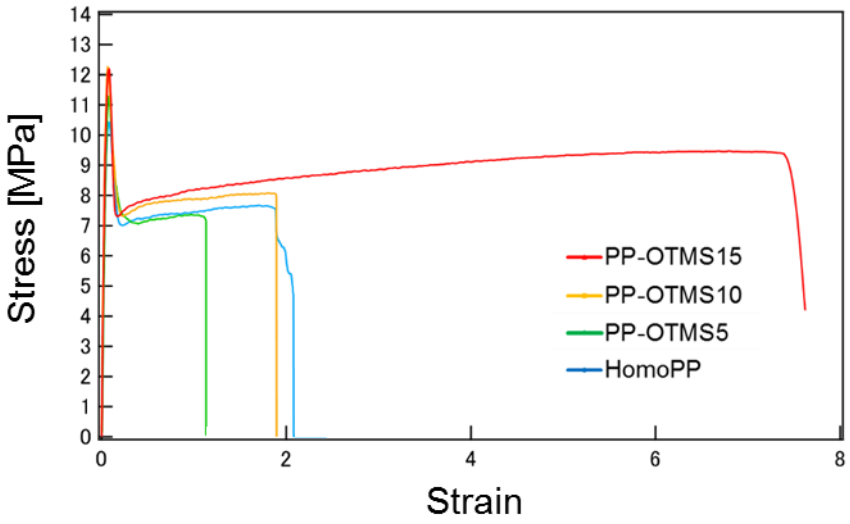

Fig. 5. S-S curves for PP-OTMS measured at 100 °C. The entire specimen was heated.

In order to elucidate the improvement of toughness by the introduction of OTMS, the internal structure change between nano and submicron range and the crystal structure change on Å range during stretching were evaluated by SAXS and WAXD, respectively. Fig. 6 shows SAXS profile of pristine films (before stretching). There is a peak around q = 0.4, which clarifies a long period ordered structure between lamellae interval. The scattering intensity except the peak area based on long period monotonically increased along with OTMS content. These increments of scattering intensity were estimated due to alkoxysilane possessing the large electron density element such as O and Si atoms.

Whereas, the intensity in long period area was the largest in homoPP and that of PP-OTMS was lower. Considering that the crystallinity in homoPP was the same or less than that of PP-OTMS series (*cf.* Table 2), the difference of density between crystalline phase and amorphous phase was reduced by the introduction of OTMS. Therefore, it was presumed that the density of the amorphous phase was increased by the presence of the alkoxysilane in the amorphous phase between lamellae.

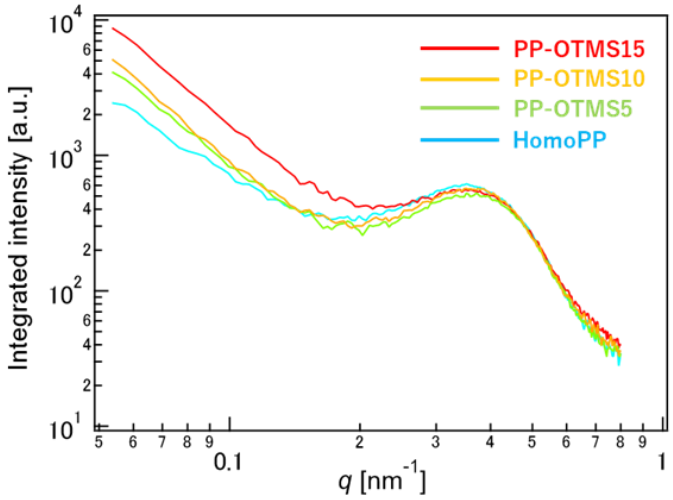

Fig. 6. SAXS profiles of PP-OTMS (represented by the equatorial direction).

Fig. 7 shows the changes in SAXS pattern of the samples at each strain (ε) during stretching. The yield point from tensile test was located at around $\varepsilon = 0.35$. It is known that the q dependence of the scattering intensity reflects the interfacial structure between the matrix and scatter, and the slope of the fourth power of q represents a sharp interface [13]. As the strain increased, strong scattering was detected in the equatorial direction before the yield point. Since this scattering intensity in the equatorial direction decreased with the slope of q^{-4} in the small angle region (Fig. 7a), (sub)micron-sized voids (craze) could be formed by dividing the lamellae existing parallel to the stretching

direction. From near the yield point, the scattering intensity in the meridional direction became gradually stronger. After passing the yield point, the scattering intensity in the meridional direction decreased with the slope of q^{-4} in the wide angle region (Fig. 7b). This result suggested that nano-sized voids were formed by slipping the lamellae existing (or rearranged) perpendicular to the stretching direction and became nanoblocks. When the stretching was further continued, the generated nanovoids were strongly oriented in the stretching direction and showed strong scattering in the meridional direction.

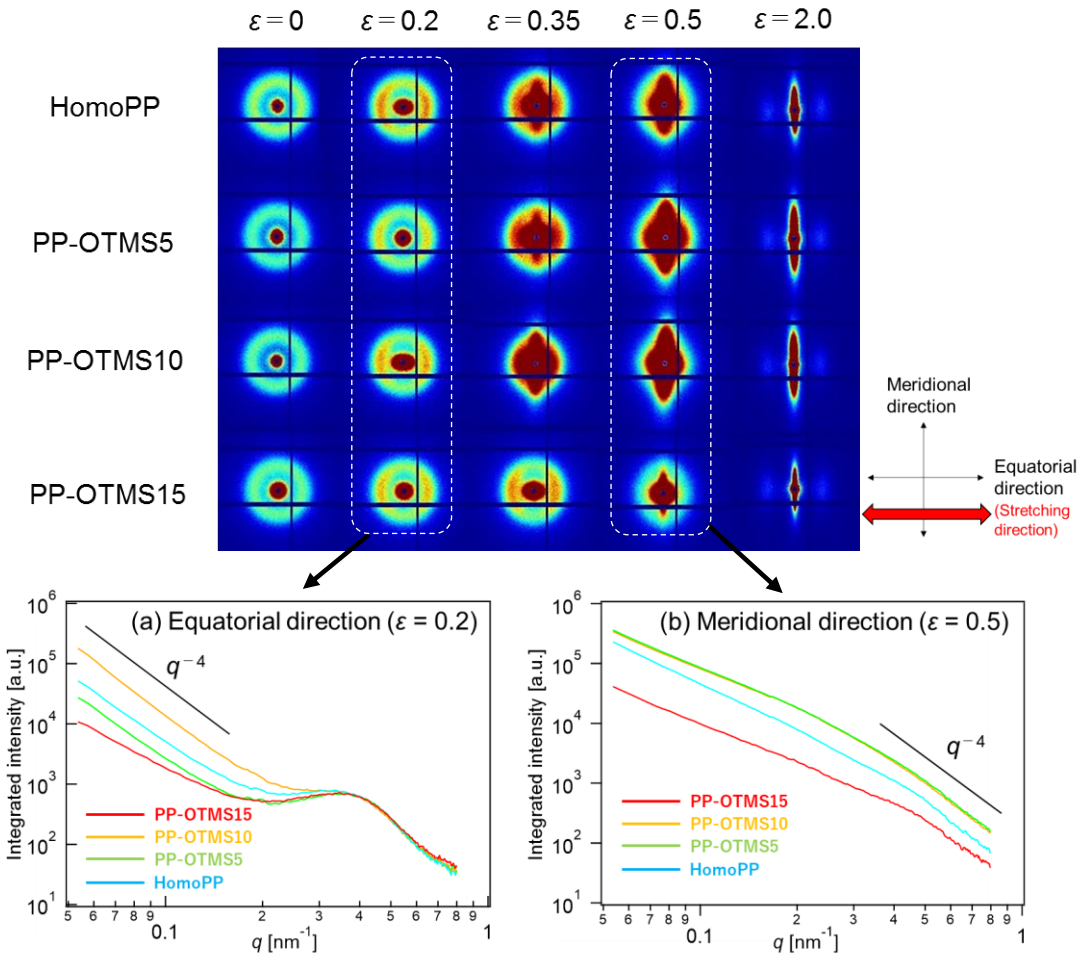

Fig. 7. SAXS patterns and profiles of PP-OTMS.

The integrated scattering intensities in the equatorial direction and the meridional direction during the stretching were plotted and compared among samples (Fig. 8). Note that the scattering intensity was normalized with the initial scattering intensity. It is noteworthy that the scattering intensity of PP-OTMS15 is very low. Otherwise, the intensity increased in the same directions along with the amount of OTMS. Therefore, in PP-OTMS15, it is believed that generation of (sub)micron-sized craze and nanovoids are suppressed as compared with other samples, which may lead to toughening. The discussion for these mechanisms are described later.

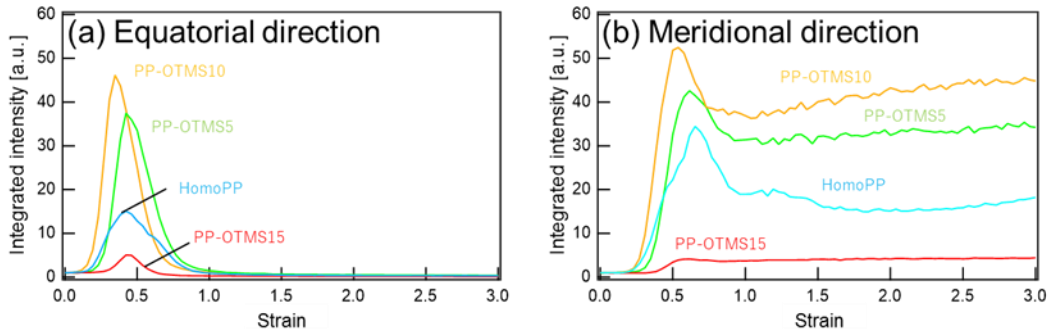

Fig. 8. Normalized integrated scattering intensity of PP-OTMS during stretching: (a) equatorial direction and (b) meridional direction.

Fig. 9 shows the WAXD patterns of PP-OTMS5 at $\varepsilon = 0$ (pristine) and $\varepsilon = 2$. In the pristine sample, isotropic scattering was observed, which means that the crystals are non-oriented. Regardless of the sample, there was no significant change in the WAXD pattern from the initial state until reaching the lower yield point (data not shown). On the other hand, when $\varepsilon = 2$, molecular chains were strongly oriented in the stretching direction so that strong scattering due to extended-chain crystal could be detected in the meridional direction. The scattering intensity of (1 3 0) plane (q = 12.5–13.8) at $\varepsilon = 2$

was plotted against angle, and the degree of crystalline orientation of each sample was calculated using obtained full width at half maximum (FWHM) by using the formula as shown below:

$$\text{Degree of orientation} = \frac{180 - \text{FWHM}}{180} \qquad \text{Eq. (1),}$$

The result is shown in Fig. 10. The degree of crystalline orientation increased monotonically along with the OTMS amount. These results indicated that the number of stress transmission point to lamella increased due to the presence of silicon methoxy groups in the amorphous phase. In other words, it is plausible that the crosslinking reaction between OTMS increased apparent density of tie molecules. Therefore, the enhancement of tensile strength observed in PP-OTMS system (*cf.* Table 2 and Fig. 5) should be due to the increase of the number density of this tie molecule.

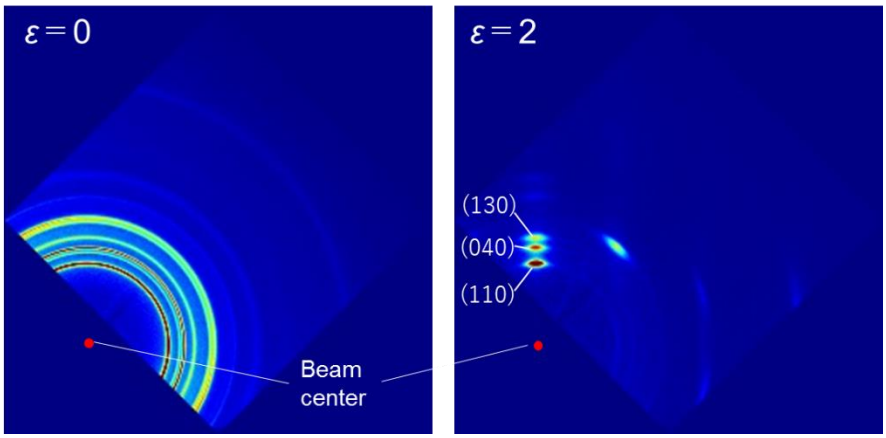

Fig. 9. WAXD patterns of PP-OTMS5 at ε = 0 and 2.

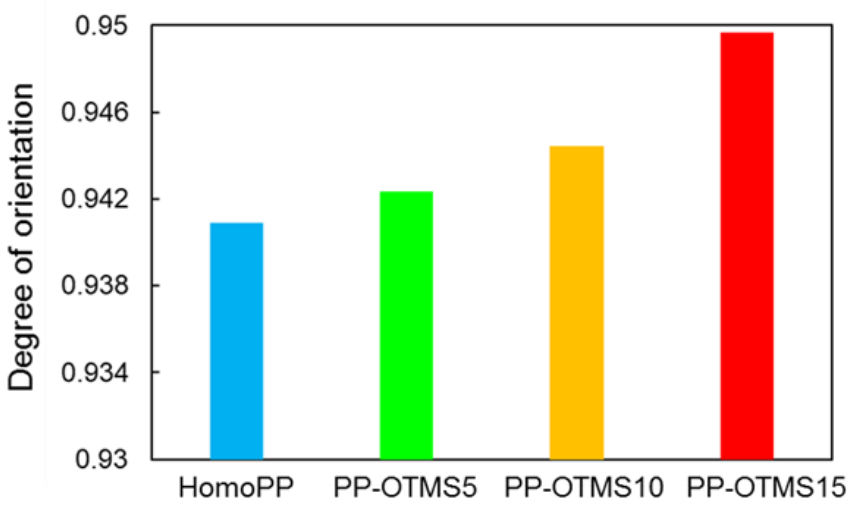

Fig. 10. Degree of orientation of PP-OTMS at $\varepsilon = 2$.

An estimated mechanism was proposed on the correlation between scattering intensity and toughening relative to the amount of OTMS (Fig. 11). As a premise, in our previous report, the results of the melt viscoelasticity measurement concluded that the incorporation of OTMS into PP increased the storage modulus (G') at lower frequencies and produced less relaxation components, especially in PP-OTMS15 (Fig. 12) [12]. In this report, I found that the less relaxation components exist in the amorphous phase and increase the apparent tie molecules (*cf.* Fig. 6). In the case where the amount of OTMS is extremely small, the slightly increased tie molecules could amplify stress concentration on the local lamellae (PP-OTMS5 and PP-OTMS10 in Fig. 11). As a result, the lamellae were easily divided at the early stage of stretching, and the scattering intensity for (sub)micron-sized craze increased (*cf.* Fig. 8). A further increase in the cross-linking point in the amorphous part not only increases the number density of the tie molecule but also the length of the tie molecule itself. It is presumed that a wide range of long-chain tie molecules not only suppress lamellae division by dispersing stress toward multiple lamellae (PP-OTMS15 in Fig. 11) but also behave

elastomerically by forming a network via lamellae. That is, OTMS makes the tie molecule tougher. As a result, it seems that scattering intensity was greatly reduced by suppressing the generation of nanovoids or propagation from voids to cracks, resulting the improvement of the elongation at break. In PP-OTMS10, since the scattering intensity is large and the elongation at break is larger than PP-OTMS5, so that the latter explanation is more plausible.

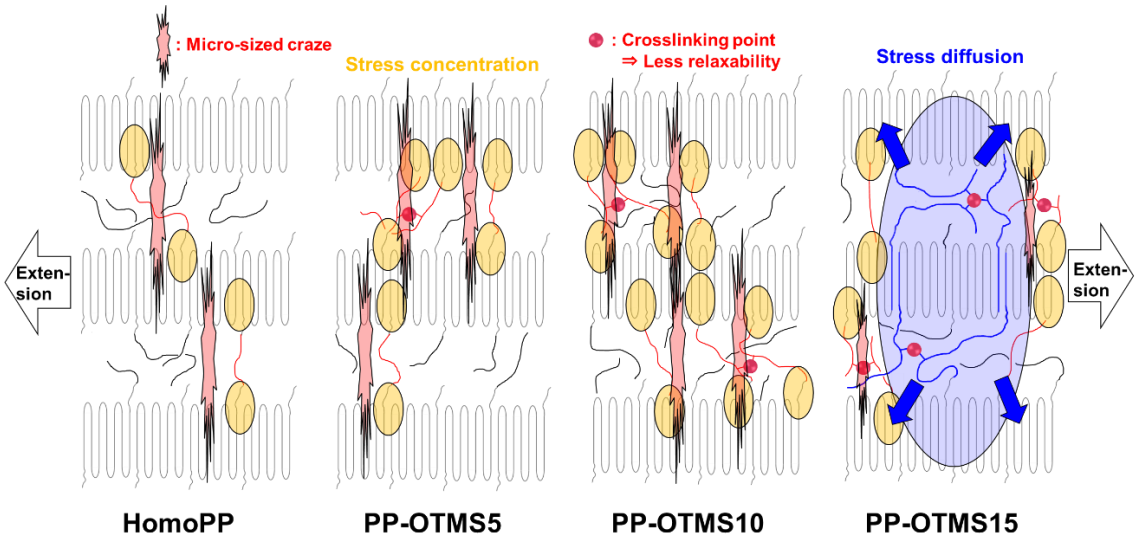

Fig. 11. Proposed toughening model for PP-OTMS.

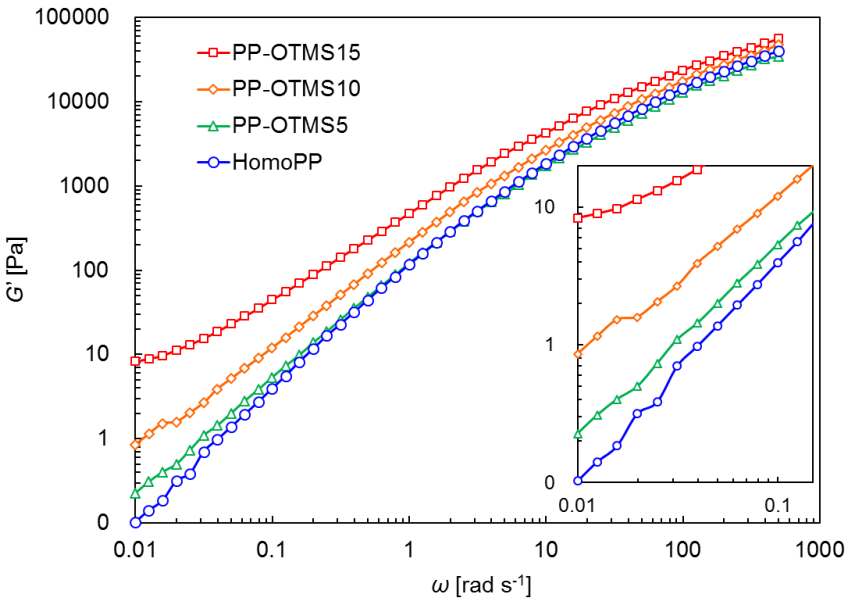

Fig. 12. Melt viscoelastic behavior of PP-OTMS [12].

3. Conclusions

PP-OTMS with a different trace amount of reactive functional groups was synthesized and intermolecularly reacted with them each other by melt mixing. Changes in the internal structure of PP-OTMS during stretching were observed by tensile test/WAXD/SAXS simultaneous measurements, and an estimated mechanism for PP-OTMS fracture was proposed. Incorporating of a trace amount of OTMS into PP increased the apparent density of the tie molecules and improved the tensile strength. However, too small amounts of cross-linking points also became stress concentration points, which promoted lamellar division at the initial stage of stretching (PP-OTMS5 and PP-OTMS10). On the other hand, further increased cross-linking points in the amorphous part (PP-OTMS15) dispersed the stress toward lamellae and made the tie molecule tougher. As a result, the elongation at break improved and the material became tougher. In conclusion, it was found that the proper amount of long-chain branched structures is effective way to improve toughness in addition to increasing tensile strength by suppressing void formation and its propagation to cracks. In this study, it was achieved by introducing 0.12 OTMS per PP main chain and intermolecular reaction by melt mixing. These results will lead to new promising materials with high strength and toughness.

Acknowledgement

The preliminary experiments utilizing synchrotron radiation were performed at the BL40B2 of SPring-8 with the approval of the Japan Synchrotron Radiation Research Institute (JASRI) (Proposal No. 2016A1005).

I would like to express my sincere gratitude to Professor Kuroda and Assistant professor Kawai in Gunma University. This work would never have been achieved without their kind helps. I wish to express my gratitude to the laboratory members for their kind advice and cooperation. Especially, I deeply appreciate Mr. Tsuchiya for his helps and suggestions on all the experiments and analysis. Finally, I am deeply grateful for the kind suggestions to Associate Professor Toshiaki Taniike and Professor Kaneko, and for giving me valuable experience to JAIST.

References

[1] W. Zhao, Y. Huang, X. Liao, Q. Yang, Polymer 54 (2013) 1455–1462.

[2] J. Cao, Y. Zheng, T. Lin, Polym. Test. 55 (2016) 318–327.

[3] S. Zhou, W. Wang, Z. Xin, S. Zhao, Y. Shi, J. Mater. Sci. 51 (2016) 5598–5608.

[4] W. Weng, W. Hu, A. H. Dekmezian, C. J. Ruff, Macromolecules 35 (2002) 3838–3843.

[5] P. K. Agarwal, R. H. Somani, W. Weng, A. Mehta, L. Yang, S. Ran, L. Liu, B. S. Hsiao, Macromolecules 36 (2003) 5226–5235.

[6] J. A. Langsten, R. H. Colby, T. C. M. Chung, F. Shimizu, T. Suzuki, M. Aoki, Macromolecules 40 (2007) 2712–2720.

[7] D. Auhl, J. Stange, H. Münstedt, B. Krause, D. Voigt, A. Lederer, U. Lappan, K. Lunkwitz, Macromolecules 37 (2004) 9465–9472.

[8] B. Krause, M. Stephan, S. Volkland, D. Voigt, L. Häußler, H. Dorschner, J. Appl. Polym. Sci. 99 (2006) 260–265.

[9] F. Yu, H. Zhang, R. Liao, H. Zheng, W. Yu, C. Zhou, Eur. Polym. J. 45 (2009) 2110–2118.

[10] J. Tian, W. Yu, C. Zhou, Polymer 47 (2006) 7962–7969.

[11] F. H. Su, H. X. Huang, Polym. Eng. Sci. 50 (2010) 342–351.

[12] E. Kurahashi, T. Wada, T. Nagai, P. Chammingkwan, M. Terano, T. Taniike, Polymer 158 (2018) 46–52.

[13] T. Kawai, S. Soeno, S. Kuroda, S. Koido, T. Nemoto, M. Tamada, Polymer 178 (2019) 121523.

[14] B. Chang, K. Schneider, F. Xiang, R. Vogel, S. Roth, G. Heinrich, Macromolecules 51 (2018) 6276–6290.

[15] Y. Hiraoka, S. Y. Kim, A. Dashti, T. Taniike, M. Terano, Macromol. React. Eng. 4 (2010) 510–515.

[16] R. H. Boyd, Polymer 26 (1985) 1123–1133.

[17] K. Prashantha, M. F. Lacrampe, P. Krawczak, Express Polym. Lett. 5 (2011) 295–307.

Eiji Kurahashi

Taniike Laboratory,

Graduate School of Advanced Science and Technology,

Japan Advanced Institute of Science and Technology